UNIVERSITI KEBANGSAAN MALAYSIA
The National University of Malaysia

3rd VIRTUAL CONFERENCE ON COMPUTATIONAL AND EXPERIMENTAL MECHANICS (VCCEM 2024)

VIRTUAL CONFERENCE ON COMPUTATIONAL & EXPERIMENTAL MECHANICS

EDITED BY:
MUHAMAD ALIAS MD JEDI
T PRAKASH G THAMBURAJA
SHAHRUM ABDULLAH
CHIN CHUIN HAO

ORGANISED BY:
COMPUTATIONAL AND EXPERIMENTAL MECHANICS RESEARCH GROUP (CEM), UKM
INSTITUT TEKNOLOGI BANDUNG (ITB)

Proceedings of the

3rd Virtual Conference on Computational and Experimental Mechanics

(VCCEM 2024)

2-3 July 2024

Organised by:

Universiti Kebangsaan Malaysia (UKM) & Institut teknologi bandung (ITB)

In collaboration with
Computational and Experimental Mechanics (CEM) Research Group, UKM

Printed in Malaysia

Computational and Experimental Mechanics (CEM) Research Group, Department of Mechanical and Manufacturing Engineering, Faculty of Engineering and Built Environment Universiti Kebangsaan Malaysia 43600 UKM Bangi, Selangor, Malaysia

Edited by:
Muhamad Alias Md Jedi
T Prakash G Thamburaja
Chin Chuin Hao
Shahrum Abdullah

Publish by:

Fakulti Kejuruteraan & Alam Bina
Universiti Kebangsaan Malaysia
43600 Bangi, Selangor

PREFACE

It is with great pleasure that we present the proceedings of the 3rd Virtual Conference on Computational and Experimental Mechanics, held on 2-3 July in an entirely virtual format. This compilation brings together a diverse range of research papers and presentations that reflect the innovative and interdisciplinary nature of the work presented at this year's conference.

The 3rd Virtual Conference on Computational and Experimental Mechanics has long been a forum for the exchange of ideas and advancements in the fields of computational and experimental mechanics, providing a platform for researchers, practitioners, and students to share their latest findings, discuss emerging trends, and foster collaborations. This year's conference was no exception, featuring an impressive array of contributions from both established experts and emerging scholars.

The topics covered in these proceedings encompass a broad spectrum, including fatigue, material modeling, applied mechanics, manufacturing, and numerous other areas. This demonstrates the extensive breadth and depth of current research in the field.. Each paper included in this volume has undergone a rigorous peer-review process, ensuring that the highest standards of scholarship and scientific integrity are upheld.

We extend our gratitude to all the authors for their valuable contributions and to the reviewers for their diligent work in evaluating the submissions. We also wish to thank the members of the organizing committee, whose dedication and hard work made this conference possible. Special thanks go to our sponsors and partners, whose support has been instrumental in the success of this event.

It is our hope that the papers contained in this volume will inspire further research and innovation, fostering new ideas and collaborations that will advance the fields of computational and experimental mechanics and contribute to the broader scientific community. We are confident that readers will find the proceedings to be a valuable resource and a testament to the vibrant and dynamic nature of contemporary research.

We look forward to welcoming you to future editions of the 3rd Virtual Conference on Computational and Experimental Mechanics and continuing the tradition of excellence in research and scholarship.

Sincerely,

T Prakash G Thamburaja
Chair, VCCEM2024

No	Content	Page
1	Experimental Investigation of Fatigue Crack Growth Behavior in Cracked Structure. *Mohd Adham bin Adnan, Muhamad Husnain Bin Mohd Noh, Mohd Akramin Bin Mohd Romlay*. Mohd Shamil Bin Shaari*	1
2	Machine Learning Aided Probabilistic Fractal Dimension Analysis in Crack Propagation Using the Box Counting Method *Saeed Hossein Moghtaderi, Muhamad Alias Md Jedi , Ahmad Kamal Ariffin Mohd Ihsan , Prakash Thamburaja*	3
3	Moisture-dependent Mode II Delamination Behaviour of Unidirectional Carbon/Epoxy Composites *King Jye Wong , Mastura Nabilah Mohd Fua'ad, Haris Ahmad Israr*	5
4	Delamination Resistance for Sandwich Panel using Data Analysis of Fuzzy AHP-TOPSIS *Mohd Khairul Faidzi, Shahrum Abdullah, Mohamad Faizal Abdullah, Salvinder Singh Karam Singh, Abdul Hadi Azman*	7
5	Forecasting the Airborne Droplet Nuclei Traveled Length in a Cafeteria Using Discrete Phase Modeling Simulations *Zulkarnaini Abdullah*	9
6	Probabilistic Characterisation for Fatigue Reliability Assessment under Various Road Loads Strain-based *Lennie Abdullah, Salvinder Singh Karam Singh, Ahmad Kamal Ariffin Mohd Ihsan, Shahrum Abdullah*	11
7	Nonlinear Material Properties with Parameter Uncertainty for Structural Analysis *Zhi Hao Bon, Ahmad Kamal Ariffin Mohd Ihsan*	13
8	Prediction of Mechanical Behaviour of Polymer Composites Using Machine Learning Algorithm *Woei Jie Lee*	15
9	Comparison Study of Radial Basis Function and Reaction-Diffusion Equation based on Level Set Topology Optimization method *Loc Le, Tatacipta Dirgantara, Lavi Rizki Zuhal, Annisa Jusuf*	17
10	An implicit plasticity model with an application to fatigue prediction of metals *Prakash Thamburaja*	19

No	Content	Page
11	Numerical Approaches of Wave Height Estimation of Friction Force on Submerged Permeable Breakwater *Tulus Tulus, Jonathan Marpaung, Suriati Suriati*	21
12	Analysis of Brachial Artery Blood Flow Model Output Using the Casson Fluid Model *Tulus Tulus, Freddy Sutanto*	23
13	Prediction of Elastic Moduli of Polymer Composites using 3D RVE modelling *Fajwa Kamar Shah, Sarah Kamaludin, Norwahida Yusoff*	25
14	Mechanical Properties of Gigantochloa scortechinii Bamboo Fiber/Epoxy Composites *Khalid Mohammed, Rozli Zulkifli, Mohd Faizal Mat Tahir, Tayser Sumer Gaaz*	27
15	Application of Contrastive Learning in rotating machinery fault diagnosis *Jicai Wang, Shahrum Abdullah, Azli Arifin, Salvinder Singh Karam Singh*	29
16	Thermal shock behaviour of ceramics - description using constitutively informed particle dynamics *Mahendaran Uchimali, Srikanth Vedantam, Venkatesh Ananchaperumal*	31
17	Miter Gate Inspired Structure for Anti-Intrusion Beam in Side Collisions *Wan Fathul Hakim W. Zamri,Fauziana Lamin, Jia Chyn Kho*	33
18	K-Means Clustering of Road Surface Conditions using Wavelet-based Vibration Parameters *Chuin Hao Chin, Shahrum Abdullah, Ahmad Kamal Ariffin Mohd Ihsan, Salvinder Singh Karam Singh*	35
19	Numerical study of back-to-back gapped built-up cold-formed steel of C-channel with long bolted connection in trusses system *Muhammad Khairuddin Zulkifli, Shahrizan Baharom*	37
20	Experimental and Modeling of Tribological Behavior of Rare Earth Oxide Mediated Mg nanocomposites *Surja Deka, Farzin Mozafari, Ashis Mallick*	39
21	Comparison on axial compressive behavior of different types of cementitious mortars incorporated with silica fume *S M Priok Rashid, Hassan Amer Algaifi, Shahrizan Baharom, A.B.M.A. Kaish*	41

No	Content	Page
22	Numerical Simulation and Experimental Study of Mechanical Properties of Aluminum Foam at High Strain Rate Using Split Hopkinson Pressure Bar *Afdhal Afdhal*, Leonardo Gunawan, Sigit Santosa*	43
23	Finite Element Analysis on Residual Compression Strength After Various Low-Velocity Impact Loading of Composite Sandwich Laminate *Muhamad Giri Suada, Hendri Syamsudin, Afdhal Afdhal**	45
24	Bone Implant Design with Lattice Structures for Additive Manufacturing *Abdul Hadi Azman*	47
	ACKNOWLEDGEMENT	49

Experimental Investigation of Fatigue Crack Growth Behaviour in Cracked Structure

M.A.Adham[1], M.N.M. Husnain[1], M.R.M Akramin[1*], M.S. Shamil[1], Akiyuki Takahashi[2]
[1]*SUPREME Focus Group, University Malaysia Pahang Al-Sultan Abdullah, 26600 Pekan, Pahang*
[2]*Tokyo University of Science, 2641 Yamazaki, Noda, Chiba, 278-8510, Japan*
Tel: +60145147687 Email: husnainoh94@gmail.com

ABSTRACT

This study examines the fatigue crack growth behaviour of AlSi10Mg, an aluminium alloy renowned for its excellent castability, high strength, and good corrosion resistance. It is ideal for additive manufacturing and lightweight applications. Through cyclic loading experiments, the testing aims to understand its fracture mechanics and durability. Based on Linear Elastic Fracture Mechanics theory, crack growth is validated with the S-version Finite Element Method. The results show that the crack growth from the experiment and simulation technique agrees well. These findings enhance the material design and predictive maintenance strategies, ensuring safer use of AlSi10Mg in critical applications.
Keywords: Fatigue life, Additive manufacturing, Crack growth

INTRODUCTION

The study of fatigue crack growth behavior in AlSi10Mg, a widely used aluminum alloy in additive manufacturing, is vital for improving the performance and reliability of structural components. This investigation examines how AlSi10Mg responds to cyclic loading, providing critical insights into its durability and fracture mechanics (Suresh, 2006). AlSi10Mg is known for its lightweight and high-strength properties, which make it an ideal candidate for applications in aerospace, automotive, and engineering sectors where high fatigue resistance is crucial. The alloy's performance under cyclic stress is a key factor in predicting the lifespan and ensuring the structural integrity of components made from this material.

Despite extensive research, the behaviour of fatigue cracks, particularly in advanced materials like AlSi10Mg, remains inadequately understood, posing significant risks in the aerospace, automotive, and structural engineering industries. The structural integrity of these materials under cyclic loading is a major concern, as failure can lead to catastrophic outcomes. AlSi10Mg combines aluminium with silicon and magnesium, providing a balance of ductility and strength crucial for applications where reducing weight without compromising mechanical performance is essential. However, the lack of comprehensive understanding of its fatigue crack growth behaviour hinders the development of effective design and maintenance strategies, necessitating further investigation to improve the performance and reliability of components made from this alloy. Thus, it is essential to analyse fatigue parameters for crack growth analysis based on linear elastic fracture mechanics (LEFM).

The findings from these studies aim to enhance material design and predictive maintenance strategies, ensuring safer and more efficient use of AlSi10Mg in critical structures. Predictive maintenance, guided by a thorough understanding of fatigue crack growth, can significantly reduce the risk of unexpected failures in service. Ultimately, the integration of advanced materials like AlSi10Mg with precise fatigue analysis contributes to the development of more durable and reliable structural components across various industries.

METHODOLOGY

A three-point bending specimen of AlSi10Mg was prepared. Fatigue testing was conducted based on two types of stress ratios for beachmark and crack growth. Iteration of the two stress ratios created a series of beachmark on the crack surface. Validation of the experimental result was compared with the S-version finite element method.

RESULTS AND DISCUSSION

Experimental results revealed insights into AlSi10Mg's fracture mechanics under various loading conditions. Crack initiation sites exhibited radial propagation patterns, indicative of tensile load and cyclical loading. Three-point bending experiment was conducted as shown in Fig.1. Fig. 2 shows the crack depth versus crack length of the beachmark’s fatigue crack. The beachmark was compared with the S-version Finite Element Method (S-FEM).

Fig. 1 Specimen breakpoint

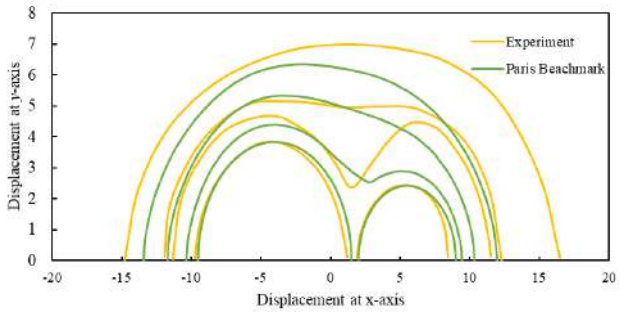

Fig. 2 Beachmark result

CONCLUSION

This study provides a comprehensive analysis of fatigue crack growth in AlSi10Mg through experimental investigation and S-FEM. The fatigue crack growth shows good agreement with the S-FEM. The findings enhance material design and predictive maintenance strategies, ensuring long-term structural reliability.

REFERENCES

- Suresh, S. (2006). Fatigue of Materials. Cambridge University Press.
- Paris, P. C., & Erdogan, F. (1963). A critical analysis of crack propagation laws. Journal of Basic Engineering, 85(4), 528-534.
- Zhang, X., Liu, Y., Lu, X., & Wang, Y. (2021). Fatigue crack growth behaviour of AlSi10Mg fabricated by additive manufacturing. Journal of Materials Science, 56(18), 11052-11065.
- Zhou, Y., Chen, X., Wang, Z., & Li, Q. (2022). Microstructural characterization and fatigue performance of AlSi10Mg produced by selective laser melting. Materials & Design, 213, 110358.
- Gong, J., Liu, Q., Sun, Q., & Li, S. (2023). Fatigue behavior of additively manufactured Ti-6Al-4V: Effects of surface roughness and heat treatment. International Journal of Fatigue, 166, 107244.
- Kim, T., Lee, S., Kim, D., & Kim, H. (2022). Fatigue performance of 3D printed metallic materials: A review. Metals, 12(1), 88.
- Li, S., Wei, Y., Chen, J., & Zhang, X. (2021). Investigation on the fatigue crack growth behavior of laser powder bed fused Inconel 718. Materials Science and Engineering: A, 804, 140773.
- • Ren, X., Tan, X., & Lyu, H. (2020). Effect of microstructure on fatigue crack growth behavior in selective laser melted stainless steel. Additive Manufacturing, 36, 101502.
- • Wu, W., Zhao, J., Zhang, L., & Cheng, X. (2023). Influence of heat treatment on fatigue performance of additive manufactured AlSi10Mg. Materials, 16(2), 472.
- • Yang, Y., Li, Y., Han, J., & Xu, F. (2022). Fatigue life prediction of 3D printed AlSi10Mg under variable amplitude loading. Engineering Fracture Mechanics, 262, 108256.
- • Zhang, M., Wang, X., Liu, Z., & Zhang, H. (2021). Influence of build orientation on fatigue crack growth behavior of additive manufactured Inconel 718. Journal of Alloys and Compounds, 862, 158451.

ACKNOWLEDGEMENT

This study was funded by RDU220367 and RDU230134 from University Malaysia Pahang (UMP) and Fundamental Research Grant Scheme (FRGS/1/2023/TK10/UMP/02/26) from Kementerian Pendidikan Tinggi (KPT) Malaysia.

Machine Learning Aided Probabilistic Fractal Dimension Analysis in Crack Propagation Using the Box Counting Method

Saeed H. Moghtaderi, Alias Jedi, Ahamd Kamal Ariffin, Prakash Thamburaja

Department of Mechanical and Manufacturing Engineering, Faculty of Engineering and Built Environment, Universiti Kebangsaan Malaysia, 43600 Bangi, Selangor, Malaysia
Tel: +60183592390 Email: p116028@siswa.ukm.edu.my

ABSTRACT

Fractal dimension calculation plays and important role for crack propagation examinations, yet determining the appropriate amount of fractal dimension remains challenging due to factors such as number of steps and size of boxes which is used in the box counting method. This paper presents a unique technique to probabilistic fractal dimension analysis that combines the box counting method along with machine learning. This method uses machine learning algorithms to calculate fractal dimension values from binary images of cracks. Following probabilistic analysis, using techniques such as normal distribution, aids in the selection of the best fractal dimension. By addressing the fundamental variability in fractal dimension determination, our technique provides a solid foundation for improving fracture characterization accuracy.

Keywords: Probabilistic analysis, Fractal fracture analysis, Machine learning model, Box counting method.

INTRODUCTION

Crack propagation analysis plays a pivotal role in understanding the behavior of materials and structures subjected to mechanical stress, serving as a cornerstone in various disciplines including material science, and engineering. One of the key challenges in crack propagation analysis is accurately characterizing the intricate patterns formed by fractures. Fractal geometry has emerged as a powerful tool for quantifying the irregularity and self-similarity inherent in these patterns, providing valuable insights into the underlying mechanisms of crack propagation (Moghtaderi et al. 2023).

The box counting method (BCM) stands out as a widely used technique for estimating fractal dimensions in crack networks. By systematically partitioning an image of a crack pattern into increasingly smaller boxes and counting the number of boxes containing part of the pattern, the fractal dimension can be calculated (Tello-Cifuentes et al. 2024). However, determining the optimal fractal dimension for a given crack pattern remains a complex task, influenced by variables such as the number of steps and size of boxes.

In recent years, machine learning has garnered significant attention for its ability to automate and optimize complex tasks in various domains. In the context of crack propagation analysis, machine learning models offer the potential to streamline the process of fractal dimension calculation and selection (Moghtaderi et al. 2024). By training models on a dataset of crack images with known properties, these models can learn to predict the most appropriate fractal dimension for new crack patterns.

In this study, we propose a novel approach that integrates machine learning modeling with probabilistic analysis to address the challenge of fractal dimension selection in crack propagation analysis. Leveraging the box counting method and machine learning techniques, our framework automates the calculation of fractal dimensions from binary crack images and employs probabilistic methods, such as normal distribution, to determine the most suitable dimension. Through experimentation and validation on diverse crack propagation scenarios, we demonstrate the effectiveness of our approach in enhancing the accuracy and efficiency of crack characterization.

RESULTS AND DISCUSSION

One way to express the BCM formula was introduced by the pioneer work of Mandelbrot (1983) as follows:

$$N = M / S^D \tag{1}$$

where N, S, D, and M, respectively, demonstrate the number of boxes required to cover the object, the size of the boxes, the fractal dimension, and a constant value relating to the scale and resolution of the measurement.

By putting Eq. (1) into logarithmic form, the following equation is obtained which is the equation of a line whose absolute slope value is the fractal dimension.

$$\log N = -D \log S + \log M \tag{2}$$

For probabilistic analysis of fractal dimension, one stage of crack propagation considered as shown in Fig. 1 with an image resolution of 1920x480 pixels. To

calculate fractal dimension based on the algorithm of BCM, box sizes of 1 to 10 pixels considered and different number of points from 2 to 10 points considered which lead to different values of fractal dimensions. These values are illustrated completely in Table 1.

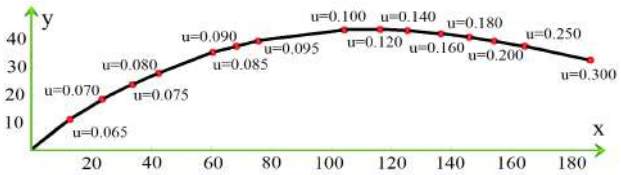

Fig. 1 Crack path under different stages of displacement load

No. of steps	Size of Boxes (Pixel(s))								
	Fractal Dimensions								
2	1,2	2,3	3,4	4,5	5,6	6,7	7,8	8,9	9,10
	1.8	1.7	1.6	1.5	1.6	1.4	1.4	1.4	1.3
3	1-3	2-4	3-5	4-6	5-7	6-8	7-9	8-10	
	1.8	1.7	1.5	1.5	1.5	1.4	1.4	1.4	
4	1-4	2-5	3-6	4-7	5-8	6-9	7-10		
	1.7	1.6	1.6	1.5	1.5	1.4	1.4		
5	1-5	2-6	3-7	4-8	5-9	6-10			
	1.7	1.6	1.5	1.5	1.5	1.4			
6	1-6	2-7	3-8	4-9	5-10				
	1.7	1.6	1.5	1.5	1.4				
7	1-7	2-8	3-9	4-10					
	1.7	1.6	1.5	1.5					
8	1-8	2-9	3-10						
	1.6	1.6	1.5						
9	1-9	2-10							
	1.6	1.5							
10	1-10								
	1.6								

Table 1. Fractal dimension values with different number of steps in BCM and different pixel sizes

These values were analyzed using probability density function (PDF) with a normal distribution to check the probability of best fractal dimension value to be choose for fractal fracture analysis.

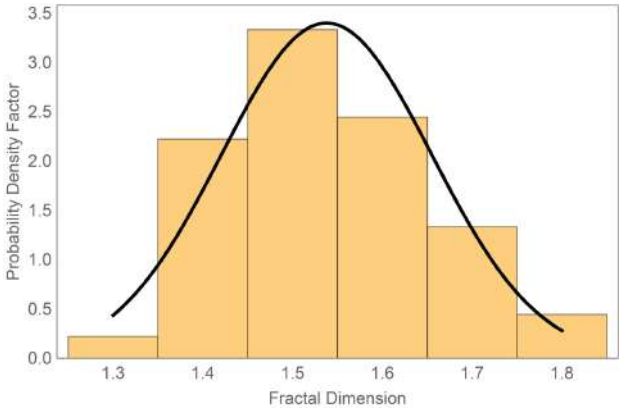

Fig. 3 Normal distribution of fractal dimension values

The algorithm applied to determine the optimal fractal dimension value is illustrated schematically in Figure 4. Initially, the input image is converted to a binary format, which organizes the pixels into black and white or binary (0 and 1) values. The algorithm proceeds to employ the BCM to compute all possible values of fractal dimension. Finally, using a probabilistic analysis that includes approaches such as normal distribution, the machine learning model determines the best appropriate fractal dimension value.

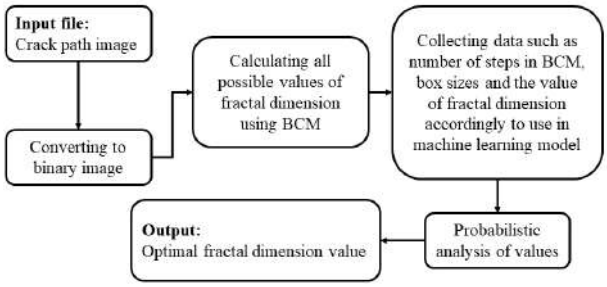

Fig. 4 Algorithm of optimizing fractal dimension value

CONCLUSION

In conclusion, integrating machine learning with the box counting method offers a promising approach for probabilistic fractal dimension analysis in crack propagation studies. This framework automates dimension calculation and selection, leading to significant improvements in accuracy and efficiency. Probabilistically determining the most suitable fractal dimension enhances understanding of crack propagation mechanisms and aids in developing more reliable fracture prediction models. Further research in this direction has the potential to refine crack propagation analysis methodologies, benefiting material science, engineering, and related fields dependent on fracture mechanics.

REFERENCES

Mandelbrot, B.B. 1983. The fractal geometry of nature. W.H. Freeman and Co., New York.

Moghtaderi S.H., Jedi A. & Ariffin A.K. 2023. A Review on Nonlocal Theories in Fatigue Assessment of Solids. *Materials* 16.

Moghtaderi, S.H., Jedi, A., Ariffin, A.K. & Thamburaja, P. 2024. Application of machine learning in fracture analysis of edge crack semi-infinite elastic plate. *Frattura ed Integrità Strutturale* 68:197-208.

Tello-Cifuentes, L., Marulanda, J. & Thomson, P. 2024. Detection and classification of pavement damages using wavelet scattering transform, fractal dimension by box-counting method and machine learning algorithms. *Road Materials and Pavement Design* 25(3):566–584.

ACKNOWLEDGEMENT

Fundamental Research Grant Scheme Ministry of Higher Education Malaysia under the Institution of Universiti Kebangsaan Malaysia funded this research, grant number FRGS/1/2022/TK10/UKM/02/30.

Moisture-dependent Mode II Delamination Behaviour of Unidirectional Carbon/Epoxy Composites

K.J. Wong [a,*], M.N. Mohd Fua'ad [b] and H.A. Israr [b]

[a] Department of Mechanical, Materials and Manufacturing Engineering, Faculty of Science and Engineering, University of Nottingham Malaysia, Jalan Broga, 43500 Semenyih, Selangor, Malaysia.
[b] Faculty of Mechanical Engineering, Universiti Teknologi Malaysia, 81310 UTM Skudai, Johor, Malaysia.

Tel: +60167826700 Email: KingJye.Wong@nottingham.edu.my

ABSTRACT

The cohesive zone model (CZM) is widely employed for simulating delamination and debonding behaviour in engineering structures. However, the choice of CZM shape significantly impacts the accuracy of simulation results. Therefore, the selection of a suitable Traction-Separation Law (TSL) with appropriate cohesive parameters is crucial. This study focuses on simulating the mode II delamination of unidirectional carbon/epoxy composites under varying moisture content levels (0%, 2.2%, 3.8%, and 5.3%) using the end notched flexure (ENF) test. Two TSLs, namely the trapezoidal TSL (TTSL) and bilinear TSL (BTSL), were implemented and compared. The results indicate that TTSL yields a more accurate force-displacement response compared to BTSL.

Keywords: Carbon/epoxy composite, Moisture absorption, Mode II delamination, Cohesive zone model, Residual property model.

INTRODUCTION

The Cohesive Zone Model (CZM) has become a prominent tool for simulating delamination behaviour in composite laminates and adhesive joints in recent decades. Finite element simulations utilising CZM offer valuable insights into stress states, damage initiation, and growth, providing an alternative to extensive and complex experimental setups. The choice of CZM shape, which is described by the traction-separation law (TSL), significantly influences simulation accuracy (Zhang et al., 2018). The bilinear traction-separation law (BTSL) is widely adopted for its simplicity and accuracy, especially in modelling brittle and moderately ductile materials (Chaves et al., 2014). However, its applicability is not universal. On the other hand, trapezoidal TSL (TTSL) has proven successful in simulating delamination behaviour, particularly in interfaces exhibiting non-linear fracture behaviour (Moreira et al. 2022) and elastic-plastic behaviour, where ductility was to be considered (Noruzi & Khoramishad, 2023).

In this study, finite element (FE) modelling was employed to investigate mode II delamination in unidirectional carbon/epoxy composite laminates with varying moisture content. The cohesive zone model (CZM) was adopted, incorporating two traction-separation laws (TSLs): BTSL and TTSL. Numerical force-displacement curves were generated for different moisture content levels (M = 0, 2.2, 3.8, and 5.3%), and these were compared with experimental data published by Johar et al. (2019).

RESULTS AND DISCUSSION

Fig. 1 shows the finite element model of the ENF specimen. Fig. 1(a) illustrates that the composite laminate was modelled using continuum shell elements (SC8R). The mid-plane interface was modelled using cohesive elements (COH3D8) with a cohesive layer thickness set at 10 μm. In the thickness direction (z-axis) of the composite, a total of four elements were discretised. For the imposition of boundary conditions, a roller condition was applied at the bottom-left end, while the right end was fixed with a pinned condition. To emulate the experimental setup, a vertical displacement was introduced at the specimen's midpoint, serving as the designated loading condition. Along the length of the specimen, Fig. 1(b) shows that the delamination zone of interest was discretised with fine mesh at 0.1 mm. The elements outside the delamination zone of interest were coarser at 2 mm. In the width direction, the specimen was discretised at 0.5-mm mesh.

In Fig. 2(a)-(d), the force-displacement curves present a comprehensive comparison between experimental and numerical results at varying moisture content levels. Notably, following the attainment of peak force, a distinct drop is observed, indicating a sudden crack jump at the specimen's interface. The numerical simulations, employing the TTSL, demonstrate a close alignment with experimental data in terms of peak force, slope, and displacement at failure. The maximum difference, approximately 13%, is noted, with an exception for one specimen at M = 3.8%. Given the

singular occurrence of this deviation, it can reasonably be attributed to experimental scatter.

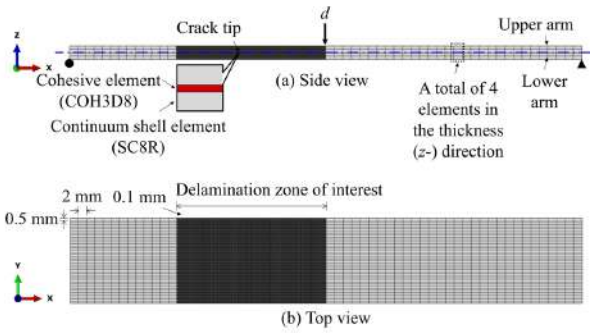

Fig. 1 Finite element model for mode II delamination under end-notched flexure loading: (a) side and (b) top view.

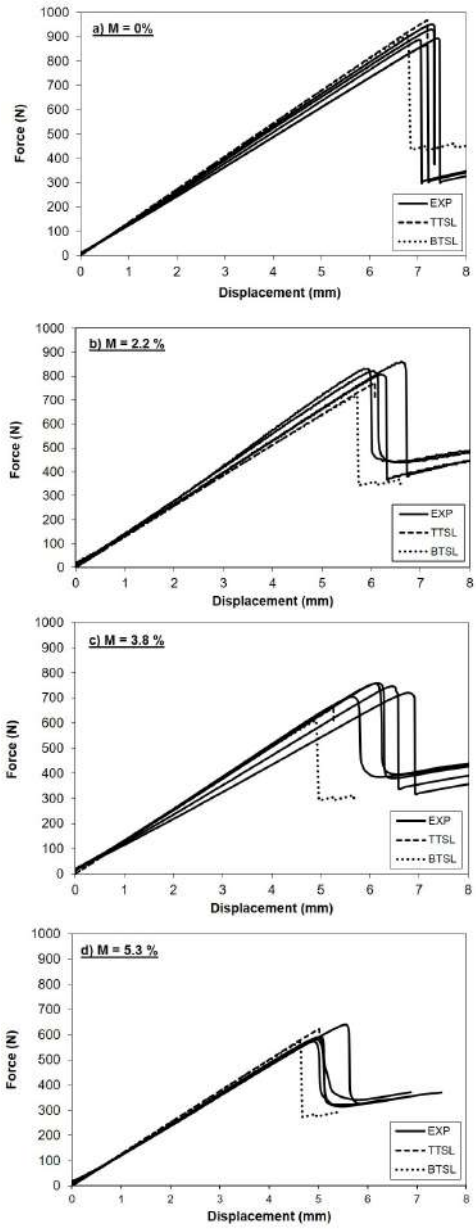

Fig. 2 Experimental and numerical force-displacement curves at moisture content levels of (a) M = 0 %, (b) M = 2.2 %, (c) M = 3.8 %, and (d) M = 5.3 %.

CONCLUSION

In this study, the cohesive zone model (CZM) was employed to simulate the mode II delamination behaviour in unidirectional carbon/epoxy composite laminates across moisture content levels of 0, 2.2, 3.8, and 5.3 %. Two traction-separation laws (TSL) were implemented for the CZM, which were bilinear (BTSL) and trapezoidal (TTSL). Finite element models were constructed based on the experimental setup of end notched flexure (ENF) test specimens. Results showed that TTSL consistently outperformed BTSL in predicting force-displacement responses across all moisture conditions, encompassing the initial slope, peak force, and displacement at failure.

REFERENCES

Chaves, F.J.P., da Silva, L.F.M., de Moura, M.F.S.F. Dillard, D.A. & Esteves, V.H.C. 2014. Fracture mechanics tests in adhesively bonded joints: A literature review. *The Journal of Adhesion* 90(12): 955-992.

Johar, M., Chong, W.W.F., Kang, H.S. & Wong, K.J. 2019. Effects of moisture absorption on the different modes of carbon/epoxy composites delamination. *Polymer Degradation and Stability* 165: 117-125.

Moreira, R.D.F., de Moura, M., Rocha, R.J.B. & Oliveira, C.F.M. 2022. Mode II fracture characterisation of a honeycomb/carbon-epoxy sandwich panel using the asymmetric end-notched flexure test. *Journal of Sandwich Structures & Materials* 24(7): 2030-2046.

Noruzi, M. & Khoramishad, H. 2023. An equivalent cohesive zone model for a wide range of ductile and brittle adhesives. *Fatigue & Fracture of Engineering Materials & Structures* 46(10): 3939-3952.

Zhang, J., Wang, J., Yuan, Z. & Jia, H. 2018. Effect of the cohesive law shape on the modelling of adhesive joints bonded with brittle and ductile adhesives. *International Journal of Adhesion and Adhesives* 85: 37-43.

ACKNOWLEDGEMENT

This work was supported by Ministry of Higher Education Malaysia and Universiti Teknologi Malaysia through Fundamental Research Grant Scheme (FRGS) No. R.J130000.7851.5F517 and UTM Fundamental Research (UTMFR) Grant No. Q.J130000.3851.21H92.

Delamination Resistance for Sandwich Panel using Data Analysis of Fuzzy AHP-TOPSIS

M.K. Faidzi[2], S. Abdullah[1], M.F. Abdullah[2], S.S.K. Singh[1] and A.H. Azman[1]
[1]Department of Mechanical and Manufacturing Engineering, Faculty of Engineering and Built Environment, Universiti Kebangsaan Malaysia, 43600 UKM Bangi, Selangor, MALAYSIA
[2]Department of Mechanical Engineering, Faculty of Engineering, Universiti Pertahanan Nasional Malaysia, Kem Perdana Sg. Besi, 57000 W.P Kuala Lumpur, MALAYSIA
Email: shahrum@ukm.edu.my

ABSTRACT

This paper presents a combination of data analysis approach to improve the delamination resistance and better decision in core selection for sandwich panel. An additional improvement on the core surface layer were vital to be analyse. The output from finite element analysis were further analysed with data analytic of decision making and verified with experimental results and statistically using 95% of confidence intervals analysis. It showed that a dimple configuration of 6.0 mm diameter and 3.0 mm depth (known as A1) tend to have better fatigue life (40% - 60% difference) and lowest maximum delamination value with 38% difference compared to the dimple configuration of 8.0 mm diameter and 4.0 mm depth (known as A2). The combination uses of various data analysis have proved the results accuracy and allow the reduction costs and time required in the design process.

Keywords: Core selection, Data analytic, Delamination, Dimple configuration, Decision making.

INTRODUCTION

The delamination resistance for metal sandwich panel were crucial, especially under severe loading conditions such as cyclic loading. The structural integrity between the layer of the panel plays significant role in determining the holding strength and preserved the functionality of the panel (Yang et al. 2024). Hence, additional modification on the layer of the panel based on the irregular / regular core surface layer were vital to enhance the delamination resistance of the panel.

The process of modification involved various methodology to obtain a reliable data analysis. The finite element analysis (FEA) become one of the valuable tools to give an early examination regarding the performance of sandwich panel with various irregular / regular core surface layer. A bunch of information related to the delamination by FEA with various core specification were crucial to be analyses with multi criteria decision making analysis (MCDA). These steps are important to establish a robust design solution without bias perception on the data analysis (Abishini & Karthikeyan 2023). In addition, an examination of fatigue life on the specimens through testing and statistical analysis also important to justify the FEA and MCDA results and proved the reliability of the data analysis. This would allow a suitable core surface design specification to be determine and improved the structural integrity of sandwich panel (Faidzi et al. 2021).

The sandwich panel were modelled and examined using FEA under 50% and 70% of maximum cyclic loads. Then the results were validated using data analytic and experimental procedure. The statistical analysis was done to obtain the high precision and reliable data analysis. Fig.1 shows the workflow of the study.

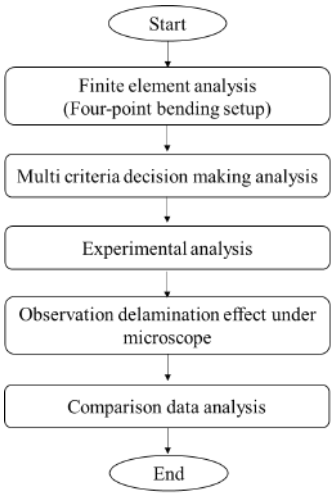

Fig. 1 The workflow of the study

RESULTS AND DISCUSSION

The results from FEA were analysed using the MCDA with fuzzy element. This is to ensure the best determination of dimple configuration for sandwich panels. Fig. 2 shows that dimple configuration with 6.0 mm diameter and 3.0 mm depth (known as A1) was the best whilst 8.0 mm diameter and 4.0 mm depth (known as A2) was the least suitable, in terms of delamination resistance. Further analysis was done using experimental setup. Table 1 shows that under 50% and 70% of maximum cyclic loading conditions, the fatigue life for A1 specimen was higher (ranging from 40% - 60%) compared to A2 specimen.

Fig. 3 shows the maximum delamination of A1 specimens also lower 38% with higher fatigue life compared to the A2 specimens. This indicated that sandwich panel with A1 configuration tend to have

better delamination resistance and validated the data analytic and FEA results.

Table 1 Data from the fatigue life of experimental process and finite element analysis

Type of loading conditions	Dimple configuration	Fatigue life of experimental (Cycle)	Fatigue life of FEA (Cycle)
50% of $\sigma_{x-x,maximum}$	6.0 ; 3.0 mm	55,426	53,265
70% of $\sigma_{x-x,maximum}$	6.0 ; 3.0 mm	37,852	23,654
50% of $\sigma_{x-x,maximum}$	8.0 ; 4.0 mm	28,542	25,469
70% of $\sigma_{x-x,maximum}$	8.0 ; 4.0 mm	14,568	9,877

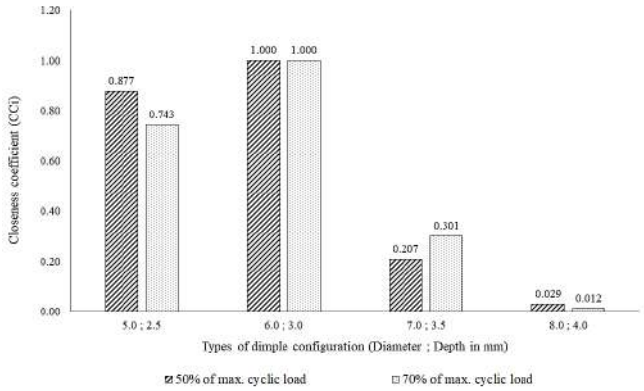

Fig. 2 Closeness coefficient for each dimple configuration under 50% and 70% of maximum cyclic loading

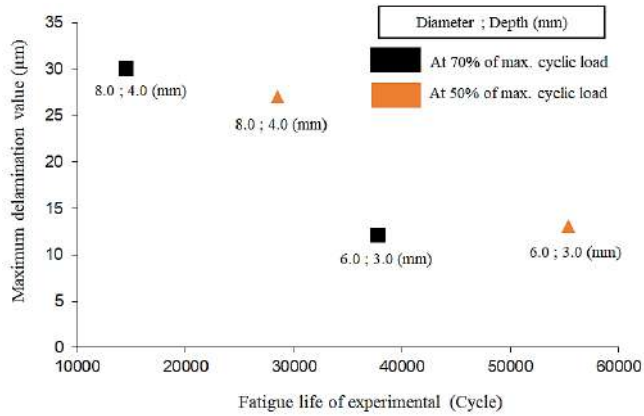

Fig. 3 Maximum delamination over fatigue life of experimental under 50% and 70% of maximum cyclic loading

Extended analysis using statistic as shown in Fig. 4 indicated that the data distribution between experimental and FEA was within the 95% of confidence intervals and no outliers data point. It shows that the distribution of data analysis was good and high efficiency. This indicated that A1 configuration has potential to enhance holding strength between layer and less damage occurrence compared to the A2 configuration.

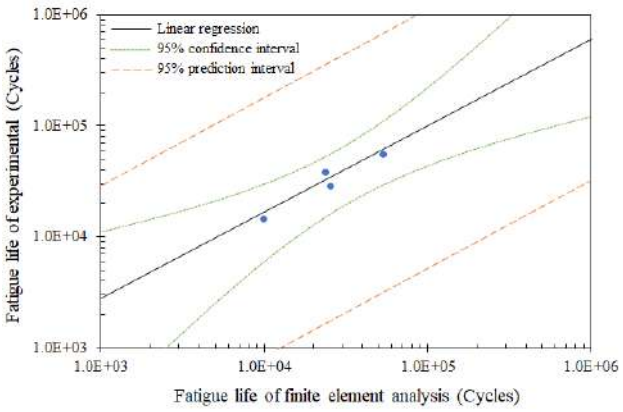

Fig. 4 95% confidence intervals analysis between experimental and finite element analysis fatigue life cycle

CONCLUSION

The delamination resistance of sandwich panels were measured under the 50% and 70% of maximum cyclic loads, using combination analysis of FEA, data analytic (MCDA) and experimental. The sandwich panel with A1 dimple configuration tend to have improvements on delamination resistance by 38% compared to the A2 dimple configuration. The data survivability analysis with 95% of confidence intervals shows that the data distribution was 100% within the intervals, with no outliers data point. This study proved a good correlation between the experimental and FEA findings and revealed the potential of A1 dimple configuration to prolong the sandwich panel life and preserved the better delamination resistance.

REFERENCES

Abishini, A. H., and Karthikeyan, K. M. B. 2023. Application of MCDM and Taguchi super ranking concept for materials selection problem. *Materials Today: Proceedings* 72: 2480-2487.

Faidzi, M.K., Abdullah, S., Abdullah, M.F., Azman, A.H., Hui, D. and Singh, S.S.K., 2021. Review of current trends for metal-based sandwich panel: Failure mechanisms and their contribution factors. *Engineering Failure Analysis* 123: 105302.

Yang, S., Luo, H., Wang, L., Mu, Y. and Wu, L. 2024. Effect of core structure on the quasi-static bending behaviors and failure mechanisms of aluminum foam sandwiches at elevated temperatures. *Materials Characterization* 208: 113638.

ACKNOWLEDGEMENT

The authors would like to express their gratitude to Universiti Kebangsaan Malaysia (GUP-2021-016) for funding.

Forecasting the Airborne Droplet Nuclei Traveled Length in a Cafeteria Using Discrete Phase Modeling Simulations

Zulkarnaini Abdullah, Zakaria Jusoh, Siti Muzahidah
Universiti Kuala Lumpur Malaysia France Institute, Section 14, Jalan Teras Jernang, Bandar Baru Bangi, 43650 Selangor, Malaysia
Tel: +60389132800 Email: zulkarnaini@unikl.edu.my

ABSTRACT

Airborne respiratory illnesses are known to be transmitted by droplet nuclei that extend in the air with the airflow. Human breathing, sneezing, coughing, and even sweating all naturally produce water-liquid droplets that include cells, electrolytes, and occasionally infectious germs and viruses. The core of droplets with a diameter larger than 6 μm tends to fall to the earth due to gravity whereas the droplets smaller than 5 μm stay suspended in the air. A discrete phase modelling computational fluid dynamic software analyzes the transmission distance of 5 to 6 μm diameter droplet nuclei in a cafeteria of 15 m (L) x 3.5 m (H) with exhaust chimneys. A natural ventilation airflow of 1 m/s is applied to the room. The particle's travel time-distance duration of 15 seconds is measured. Droplet nuclei concentration of 0.0976 kg/m^3 is measured from the source to the person at 2 m whereas the concentration of a person at 5 m and 10 m is 0.0893 kg/m^3 and 0.0401 kg/m^3 respectively. The droplet nuclei are dispersed to the end of the cafeteria and the exhaust chimneys lower the droplet nuclei-person contact from 0.0797 kg/m^3 to 0.0402 kg/m^3.

Keywords: Computational Fluid Dynamics, Discrete Phase Modelling, Droplets Nuclei

INTRODUCTION

The cafeteria, bistro and bar environment has been at the heart of debates concerning the balance between social activities, and health and safety protocols. The American Society of Heating, Refrigerating and Air-Conditioning Engineers (ASHRAE) Guidelines during the COVID-19 Pandemic [1] outlined that the recommended distance to maintain social distancing is 1 to 2 meters, along with various other cleanliness measures. Following the era of post-pandemic, cafe outlets continue to enforce a distance between coffee goers, although the social distance, mask and other cleanliness protocols have been relaxed, to accommodate the business and financial needs. The study examined the movement of airborne droplet particles in a small cafeteria room with airflows of 1m/s, to count and visualize the flow patterns. The flow simulation tool employed in these studies comes from the ANSYS Fluent software suite. Since the cores of water-based droplets are influenced by their weight, the trajectory of droplets in the atmosphere is significantly affected by gravity. The size and weight of the droplet cores are influenced by the surrounding air's evaporation, which in turn is affected by the airflow's direction and intensity, temperature, and relative humidity [2, 3, 4, 5].

MODELLING AND COMPUTATION

In a standard event and gathering environment, an air conditioner is typically mounted on the ceiling of the room. Without the air conditioner, the reliance on natural air flow is at a rate of 1 m/s [7, 8, 9, 10,]. The primary means of dispersing droplet nuclei in the air is through air movement, and the actions of people can influence the mixing of air within various areas. Fig. 1 depicts the dimensions of a cafeteria and the people arrangement, measuring 15 m (L) x 3.5 m (H). The origin of droplet nuclei is marked by the position of the man standing.

RESEARCH METHODOLOGY

Computational Fluid Dynamics

In this study, the airflow patterns are simulated using ANSYS Workbench-Fluent CFD modelling. The Eulerian discrete phase model determines the time step-travelling of the droplet nuclei. The size of the injected droplet ranges from 5 to 6 μm.

Mesh and Boundary Condition

The boundary conditions and the mesh setup are displayed in Table 1 and Fig. 2.

Table 1. The set-up for the simulation study of distance throw and airflow in a cafeteria.

	Items
Mesh Nodes	24548
Mesh Elements	23652
Solver	Pressure, Transient, Gravity Y-axis -9.81 m/s^2
Model	Multiphase (Eulerian), Viscous (Laminar), Mixture, Discrete Phase (On), Min dia. 5 μm, Max dia. 6 μm, Mean dia. 5 μm.
Materials	Fluid – air, Inert Particle – Water-liquid
Boundary Conditions	Inlet – air, 1 m/s, 300K, Inlet – droplet, Granular 0.0001 m^2/s^2
Methods	Scheme - Phase Coupled Simple, Gradient – Least Squares Cell-Based, Pressure – PRESTO! Momentum – First Order Upwind

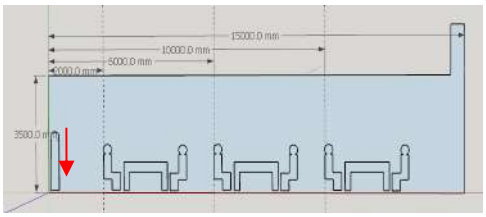

Fig. 1 Modeling of the simulations. The inlet air is at 1 m/s. The droplet injection point is indicated to the standing person. The nearest seated person from the particle source is 2 m.

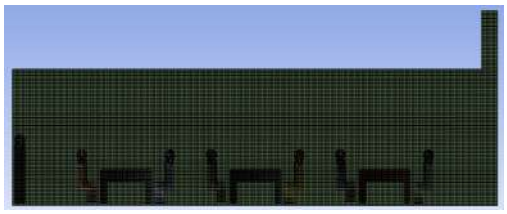

Fig.2 Mesh for the simulation, nodes 24548 and elements 23652.

CONCLUSION

Simulations Analysis

The particle measurement of the cafeteria simulation results shows that the focus point is between Line 1 and Line 2 region. Table 2 shows the droplet nuclei concentration at the line region.

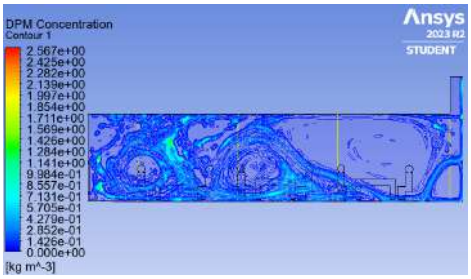

Fig. 4 The particle diameter distribution simulation shows that the inlet air flow moved most of the droplet nuclei at 2 to 5 m. With less density, the droplet nuclei with a size of 5 µm are freely moving to 10 m.

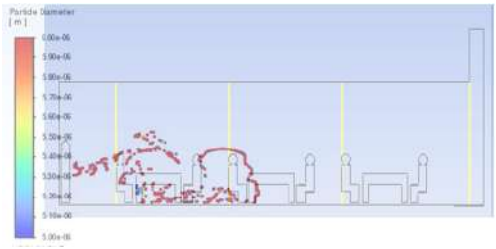

Fig.5a

Fig.5b

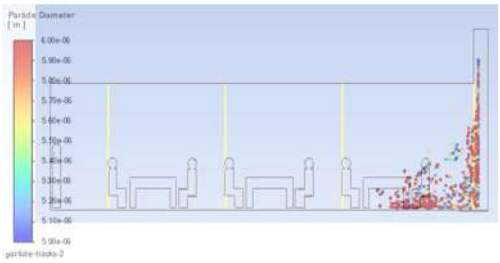

Fig.5c

Fig.5 The number of concentrations and the travel length at a. 5 seconds b. 10 seconds c. 15 seconds

Table 2: The concentration of the droplet nuclei at the line region in a cafeteria after 15 seconds.

Line	Concentration kg/m^3
1	0.0976
2	0.0893
3	0.0401
4	0.0402
Streamline	0.0797

REFERENCES

Lawrence, J.S. 2020, Guidance for Building Operations During the COVID-19 Pandemic. ASHRAE Journal. https://www.ashrae.org/

Wells, W.F. 1955, Airborne contagion, and Air Hygiene. Cambridge, MA. Harvard University Press.

Stetzenbach, L.D., Buttner, M.P., Cruz P. 2004. Detection and Enumeration of Airborne Bio contaminants, Current Opinion in Biotechnology., 15(3)170–174.

Wong, N.H., Feriadi, H., Lim, P.Y., Tham, K.W., Sekhar, C., & Cheong, K.W. 2002, Thermal Comfort Evaluation of Naturally Ventilated Public Housing in Singapore, Building and Environment., 37 1267-1277.

Tang, J.W., et al. 2006, Factors Involved in the Aerosol Transmission of Infection and Control of Ventilation in Healthcare Premises, Journal of Hospital Infection., 64(2) 100-114.

Wells, W.F. 1955, Airborne contagion, and Air Hygiene. Cambridge, MA. Harvard University Press.

Jamaluddin, A.A., Hussein, H., Mohd Ariffin, A.R., & Keumala, N. 2014, A Study on Different Natural Ventilation Approaches at a Residential College Building with the Internal Courtyard Arrangement, Energy and Buildings., 72, 340-352.

Nicol, J.F., & Humphreys, M.A. 2002, Adaptive Thermal Comfort and Sustainable Thermal Standards for Buildings, Energy and Buildings., 34 563-572.

Wong, K.C., Leung, K.S. 2004, Transmission and Prevention of Occupational Infections in Orthopedic Surgeons, Journal of Bone and Joint Surgery America., 86-A (5) 1065–1076.

Priyadumkol, J., & Kittichaikarn, C. 2014, Application of the Combined Air-Conditioning Systems for Energy Conservation in Data Centre, Energy and Buildings., 68 Part A 580-586.

Probabilistic Characterisation for Fatigue Reliability Assessment under Various Road Loads Strain-based

L. Abdullah, S.S.K. Singh, A.K. Ariffin, S. Abdullah
Department of Mechanical and Manufacturing Engineering, Faculty of Engineering and Built Environment, Universiti Kebangsaan Malaysia, 43600 UKM Bangi, Malaysia
Tel: +60389216508 Email: salvinder@ukm.edu.my

ABSTRACT

This study aims to characterise the probabilistic durability under random loads strain-based for fatigue reliability assessment of a leaf spring. Characterising random data involving a probabilistic approach needs to be addressed in terms of defining applicable distribution as the strain data are random cyclic loading that leads to fatigue failure. A random strain loads were extracted repetitively at a sampling rate of 500 Hz for 300 s per block for various road load profiles. The load sequence effects computed the highest fatigue life with an estimated range of 1.66×10^4–3.16×10^4 cycles/block. The probabilistic analysis shows the Gumbel distribution is the most appropriate distribution to be used based on the captured strain signals. The highest probability of fatigue failure was identified for the highway data in the range of 1.06×10^6–1.71×10^7 cycles/block with the probability of 0.72–0.99 since a smooth road surface produced low amplitudes in the strain data. The reliability assessment obtained a mean cycle to failure is in the range of 3.07×10^7–3.57×10^7 cycles/block. Hence, the probabilistic approach using the Gumbel probability plot for analysing fatigue failure under random strain loads provides better probabilistic characterisation in terms of the mean cycle to failure in reliability assessment.

Keywords: Leaf Spring; Random Strain Load; Fatigue Life; Gumbel Distribution, Reliability.

INTRODUCTION

A leaf spring is broadly used in heavy vehicles with non-independent suspension. It is normally connected to a vehicle axle and a bus rim to transfer vibration through the axle and the wheel. A leaf spring is an elastic component that can reduce the impact from a road surface to ensure a comfortable ride (Cheng et al. 2022). Road conditions with various loadings can lead to severe damage to a leaf spring, due to cyclic fatigue loading during service life. Hence, a fatigue life prediction is an essential tool in engineering for quality and reliability assessment.

Probabilistic modelling is suitable to predict the reliability assessment of structural failure due to random road loads for different vehicle structures (Li et al. 2023). The prediction of extreme events is important to determine the probability of failure accurately, depends on the reliability design and risk assessment. The stochastic method of Monte Carlo simulation is applicable to extreme events. This study aims to use a Gumbel probability plot for predicting the probability of failure for random data. This proposed method provides the capabilities of modelling fatigue reliability data under extreme conditions.

RESULTS AND DISCUSSION

The process flow of fatigue reliability assessment for random strain data associated with the reliability assessment of a leaf spring is illustrated in Fig. 1. Finite element analysis was performed on static load to identify the stress concentration of a leaf spring. A 25.914 kN preload of a commercial bus, representing the quarter weight of the test vehicle, was applied on the leaf spring. The material properties of SAE 5160 carbon steel were used in the static load analysis. The geometric model of a leaf spring was meshed using isoparametric tetrahedron elements in three dimensions using 2 mm mesh size, as illustrated in Fig. 2. The maximum von-Mises stress at the eye's region is 1,697.97 MPa.

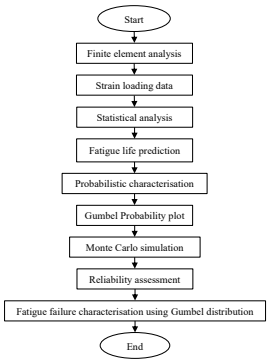

Fig. 1 Process flow of fatigue reliability assessment using the Gumbel distribution

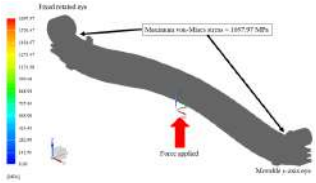

Fig. 2 Finite element analysis of leaf spring

Various strain data were captured using strain gauge on a leaf spring of a commercial bus. Data were extracted in three road conditions; a highway, a rural, and a campus road for 4 days repetitively. The random strain loads were extracted in a period of 100 s with a 500 Hz sampling rate, which resulted in 50,000 discrete data points. Fig. 3 shows the time history for a highway (H), a rural (R), and a campus (C). Fig. 4 illustrates the fatigue life prediction for each road condition, that shows the fatigue life is in the range of 9.43×10^3–3.16×10^4 cycles/block. The highway data recorded the highest fatigue life prediction as the data contained less significant amplitude in the random strain data.

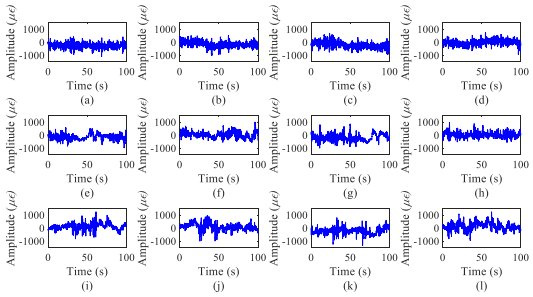

Fig. 3 Time history plot for (a) H1, (b) H2, (c) H3, (d) H4, (e) R1, (f) R2, (g) R3, (h) R4, (i) C1, (j) C2, (k) C3, (l) C4

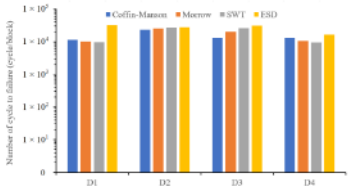

Fig. 4 Fatigue life prediction of leaf spring

In probabilistic analysis, the Gumbel distribution was chosen to be used for random strain loads. In predicting a fatigue failure of a leaf spring, the Gumbel probability plot was illustrated in Fig. 5. The damage occurred at 2×10^6 cycles/block with 50% probability of failure and more than 70% will occur at 3.23×10^6 cycles/block. In reliability assessment, the estimation of the mean cycle to failure (McTF) is used to predict a failure in terms of cycle unit. The highway, rural, and campus data produced the McTF in the ranges of 3.070×10^7–3.571×10^7 cycles/block, 3.070×10^7–3.114×10^7 cycles/block, and 3.003×10^7–3.005×10^7 cycles/block, respectively.

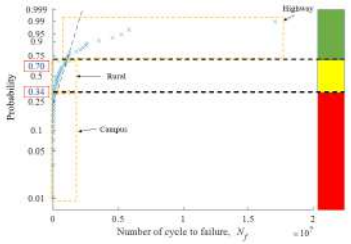

Fig. 5 Gumbel probability plot of fatigue life prediction

The Monte Carlo simulation was performed to obtain more data and it was determined that the overall difference was less than 0.10%. Fig. 6 displays the reliability plots in determining the probability of failure of a leaf spring, which can lead to the risk of fatigue damage. Campus data produced narrow curves due to the data contained mostly high-amplitude range, especially when the vehicle travelled on a bumpy road.

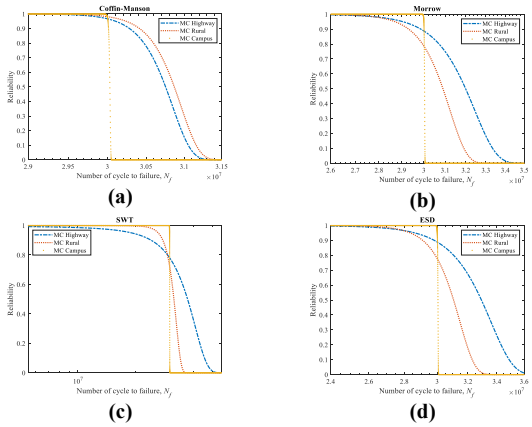

Fig. 6 Reliability based on Monte Carlo simulation for: (a)Coffin-Manson, (b) Morrow, (c) SWT, (d) ESD models

CONCLUSION

This study presents the probabilistic characterisation in the reliability assessment of fatigue life for various road strain loads of a heavy vehicle leaf spring. The random strain data mostly contained high-amplitude excitation due to bumps and potholes, with the maximum kurtosis at 3.93 $\mu\varepsilon$ that is significantly to high amplitudes. In the durability analysis, the fatigue life of various road conditions is in the range of 1.66×10^4–3.16×10^4 cycles/block, based on the ESD model. The probabilistic analysis shows the Gumbel distribution is suitable for most random strain data. The Gumbel probability plot indicated a higher probability of leaf spring failure in the range of 3×10^6–7×10^6 cycles/block with a probability of 0.70–0.96. Thus, the Gumbel distribution can be used in analysing various road strain loads for fatigue reliability assessment as it provides better statistical characterisation using the probabilistic approach.

REFERENCES

Cheng, G., Chen, K., Zhang, Y. & Chen, Y. 2022. The fracture of two-layer leaf spring: Experiments and simulation. *Engineering Failure Analysis* 133: 105971.

Li, H., Wang, P., Hu, H., Su, Z., Li, L. & Yue, Z. 2023. Data-driven reliability assessment with scarce samples considering multidimensional dependence. *Probabilistic Engineering Mechanics* 72: 103440.

ACKNOWLEDGEMENT

The authors would like to express their gratitude to Universiti Kebangsaan Malaysia (Research funding: GUP-2022-013 & innovation program under the Marie Sklodowska-Cuire grant agreement (No 730888)) for supporting this research.

NONLINEAR MATERIAL PROPERTIES WITH PARAMETER UNCERTAINTY FOR STRUCTURAL ANALYSIS

Bon, Z. H., Kamil, S. (USK), Suffian, M. S. Z. M. (UNIMAS) & Ihsan, A. K. A. M.
Department of Mechanical and Manufacturing Engineering,
Faculty of Engineering and Built Environment, Universiti Kebangsaan Malaysia
Tel: +601155059626 Email: bonzhihao@gmail.com

ABSTRACT

Finite Element Analysis (FEA) plays a pivotal role in understanding and predicting structural behaviour, particularly when dealing with material nonlinearities and complex stress-strain relationships. This study aims to develop a computational model for bar elements, incorporating uncertain nonlinear material properties using Fuzzy Random Variables (FRV) within Excel Visual Basic Applications (VBA). Focusing on one-dimensional bar element modelling, we utilise the kinematic bilinear model for the stress-strain curve of Wire Arc Additive Manufacturing High Strength Steel (WAAM HSS). The results demonstrate that FRV provides a more precise depiction of material behaviour in the nonlinear domain, effectively accounting for uncertainties in material properties and nonlinear stress-strain relationships. The findings reveal a nonlinear stress-strain correlation with yield deviations surpassing the yield strength at random intervals. Analysing failure percentage trends with increasing membership numbers via the FRV approach shows consistency and convergence of the findings, in contrast to the randomness approach, which lacks specific trends. Consequently, FRV holds promise for enhancing structural risk assessment, thereby improving material safety, efficiency and longevity.

Keywords: Structural Behaviour, Material Nonlinearities, Uncertainties, Stress-Strain Relationships, Risk Assessment.

INTRODUCTION

FEA is an important tool for modelling and evaluating structural and component behaviour, forecasting design performance under different loading circumstances, improving performance, and assuring structural integrity. Advances in Finite Element (FE) modelling approaches have made it possible to simulate complicated structural reactions (Liu, Li and Park, 2022). However, higher computational power and more efficient techniques have resulted in increasingly complicated FE models. This complexity, together with the requirement for comprehensive geometry and mechanical characteristics, renders extremely detailed FE models impracticable for large and complex structures, particularly when considering uncertainties in structural factors such as mechanical properties.

Nonlinear material analysis with uncertainty is critical in structural engineering. Nonlinear analysis considers significant deformations, material and geometric nonlinearities, resulting in a more realistic perspective of structure reactions (Luu, Bui and Kim, 2023). Nonlinear material analysis and stress-strain interactions present substantial modelling and analytical issues for linear systems, necessitating sophisticated approaches. Material and geometric nonlinearities have practical ramifications because they increase uncertainty and unpredictability in structure reactions, making performance prediction and control more difficult. Uncertainty analysis in complex structural systems is critical for risk assessment and decision-making since it provides useful insights into model output uncertainties and identifies potential risks (Hong and Zhongmin, 2023).

The purpose of this study is to create a computational model for one-dimensional bar components using Excel VBA. The existing code is changed to accommodate fuzzy and random theories, as well as FRV representation in FEA. The model looks at nonlinear stress and strain under hybrid uncertainty settings. This study focuses on the application of FEA to structural models with nonlinear material characteristics, with a particular emphasis on the link between stiffness and nonlinear behaviour. The significance of this study stems from the fact that many engineering applications cannot be accurately modelled using a linear framework. It alters design and analytical methodologies for structures susceptible to nonlinear material behaviours and uncertainties, resulting in safer and more efficient designs in sectors where unpredictability is prevalent.

RESULTS AND DISCUSSION

The bilinear kinematic model technique (Huang, Kyvelou and Gardner, 2023) shown in equation (1) served as the primary guidance for further investigation of nonlinear material characteristics. The measured material properties of WAAM HSS (Huang *et al.*, 2022) shown in Table 1 are taken for use of uncertainty propagation in the structural analysis of nonlinear material behaviour by randomness as well as FRV.

$$\varepsilon = \begin{cases} \dfrac{f}{E} + 0.002\left(\dfrac{f}{\sigma_y}\right)^n & \text{for } f \le \sigma_y \\ \dfrac{f-\sigma_y}{E_{0.2}} + \varepsilon_u\left(\dfrac{f-\sigma_y}{\sigma_u-\sigma_y}\right)^m + \varepsilon_{0.2} & \text{for } \sigma_y < f \le \sigma_u \end{cases} \quad (1)$$

Table 1. Measured material properties of WAAM HSS coupons (M = Machined; AB = As-built) used for comparison with predicted stress-strain curves

Label	Surface	Feedstock wire	t_{nom} (mm)	θ (°)	E (MPa)	f_y (MPa)	f_u (MPa)	n	m
HS-M-2-90	M	E120C-GH4	2	90	204000	842	1004	33.1	2.3
HS-M-3-90		ER110S-1	3	90	223800	705	841	7.1	1.9
HS-M-5-90		800 MPa	5	90	206388	776	846	17.7	3.0
HS-AB-8-0	AB	ER110S-G	3	0	220800	671	731	14.5	1.5
HS-AB-3-45		ER110S-G	8	45	214200	633	721	12.2	2.0
HS-AB-3-90		ER90S-B91	3	90	190600	671	754	12.7	3.0

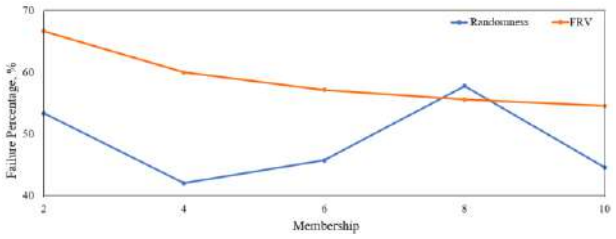

(a)

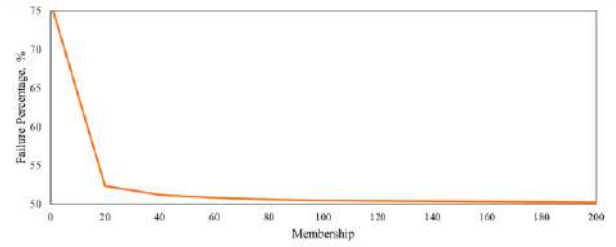

(b)

Figure 1 Graph of failure percentage against membership: (a) randomness versus FRV, (b) FRV

Failure trend is studied using two distinct input load techniques, randomness and FRV, with failure percentage computed for outputs surpassing mean yield strength of WAAM HSS (737.5 MPa). Figure 1 (a) demonstrates considerable changes in how the input data structure influences failure results. Random input behaves in a wave-like manner, with a variable failure percentage as the alpha segment grows, emphasising the difficulty in anticipating failure patterns.

In contrast, FRV input results in a constant drop in failure percentage from 66.67% to 54.55% with increasing membership, illustrating the effectiveness of a structured approach in lowering failure risk under uncertainty. Figure 1 (b) shows a constant fall in FRV failure percentage from 66.67% (alpha cut = 2) to 50.24% (alpha cut = 200), with limited additional reduction up to 1000 alpha, resulting in a value of about 50%. This situation can be related with the nature of FRV of mixing fuzziness and randomness, in which rising alpha reduces uncertainty and failure, reaching a critical equilibrium point of roughly 50% and optimising risk assessment in material structures.

CONCLUSION

The findings of study underline the importance of input data structure on failure rates. Random input data poses difficulties in predicting failure patterns owing to its variable failure percentage with increasing membership. This unpredictability highlights the difficulties of minimising failure risk through random inputs. The findings indicate that employing FRV input is a more organised and dependable strategy to decreasing failure risk at various uncertainty levels. The capacity of FRV to continuously lower the failure percentage and achieve a critical equilibrium point optimises risk assessment in material structures, making it a better technique than random input.

REFERENCES

Hong, G. and Zhongmin, D. (2023) 'Dynamic response analysis of nonlinear structures with hybrid uncertainties', *Applied Mathematical Modelling*, 119. doi: 10.1016/j.apm.2023.02.029.

Huang, C. *et al.* (2022) 'Mechanical testing and microstructural analysis of wire arc additively manufactured steels', *Materials and Design*, 216. doi: 10.1016/j.matdes.2022.110544.

Huang, C., Kyvelou, P. and Gardner, L. (2023) 'Stress-strain curves for wire arc additively manufactured steels', *Engineering Structures*, 279. doi: 10.1016/j.engstruct.2023.115628.

Liu, W. K., Li, S. and Park, H. S. (2022) 'Eighty Years of the Finite Element Method: Birth, Evolution, and Future', *Archives of Computational Methods in Engineering*. doi: 10.1007/s11831-022-09740-9.

Luu, V. T., Bui, V. T. and Kim, S. E. (2023) 'An advanced computational method for nonlinear inelastic thermo-mechanical analysis of spatial steel frames in fires', *Engineering Structures*, 275. doi: 10.1016/j.engstruct.2022.115329.

ACKNOWLEDGEMENT

The authors would like to acknowledge the financial support from Ministry of Higher Education Malaysia and Universiti Kebangsaan Malaysia through the European Unions' Horizon 2020 research and innovation programme under the Marie Sklodowska-Curie grant agreement No 730888.

PREDICTION OF MECHANICAL BEHAVIOUR OF POLYMER COMPOSITES USING MACHINE LEARNING ALGORITHM

Lee Woei Jie, Sarah Binti Kamaludin, Muhammad Razi Abdul Rahman
School of Mechanical Engineering,
Engineering Campus, Universiti Sains Malaysia,
14300 Nibong Tebal, Seberang Perai Selatan,
Penang, Malaysia.
Tel: +6016-3136 315 Email: leeweijie@student.usm.my

ABSTRACT

This study develops a Machine Learning (ML) algorithm to predict the mechanical behavior of fiber reinforced polymer composites using Python. Random Forest Regressor (RF) from Scikit-Learn library was selected as the ML model used due to its high interpretability and relatively simple architecture while still being robust enough to capture the non-linear relationship of the target values. The training dataset consisting of 11 features was obtained through literature review, a collection of experimental data was compiled and processed before they are used to train the RF model. The target values predicted by the algorithm are tensile modulus, tensile strength, flexural modulus and flexural strength of FRPC. The RF model can predict all four properties accurately with R^2 score above 0.9.

Keywords: Machine Learning, Random Forest Regressor, Mechanical Properties Prediction, Fiber Reinforced Polymer Composite (FRPC)

INTRODUCTION

Fiber-reinforced polymer composites (FRPC) are commonly used in aerospace, automotive, construction, and defense applications due to their high strength-to-weight ratio, corrosion resistance, and ease of manufacturing complex shapes. Fibers, having excellent tensile properties along their length, enable high tensile strength in FRPC compared to other classes of composites such as particulate reinforced composites and laminated composites.(Hashin, 1983) There are several factors affecting the mechanical properties of an FRPC. The conditions of the fiber, which includes fiber type, fiber size (length and diameter), fiber orientation. Besides, the properties of matrix, fiber-matrix interface and manufacturing process could affect the mechanical properties of the FRPC. Introduction of additives into matrix (Thomason,2002) or fiber surface coating(Rahmanian et al., 2013) could improve interfacial strength of the FRPC, improving load transfer to achieve better mechanical properties.

On the other hand, data driven method like machine learning have shown great potential in predicting the mechanical properties of FRPC as they are capable of handling complex relationships between variables. In past researches, several machine learning algorithms were attempted to predict the mechanical properties of FRPC including linear regression (LR) (Khademi et al., 2017), support vector machine (SVM)(Liu et al., 2022), decision tree(Almohammed & Soni, 2023; Guo et al., 2021; Qi et al., 2019; Shang et al., 2022), ensemble method (random forest, adabost, XGboost), artificial neural network (ANN) etc. Within these methods, linear algorithms including LR, SVM with a linear kernel, Bayesian Ridge regression and Elastic net performed poorly while other non-linear algorithms could reach an R^2 score above 0.9. (Yin & Liew, 2021) This proves that the relationships between the specification of the FRPC and its mechanical properties are non-linear. A suitable ML algorithm could predict multiple mechanical properties including tensile modulus, tensile strength, shear strength, compressive strength etc. However, independent models need to be trained to predict every single mechanical property.

In this study, Random Forest Regressor was used to predict the tensile modulus, tensile strength, flexural modulus and flexural strength of FRPC.

RESULTS AND DISCUSSION

The trained model was evaluated through calculation of R^2 for the training and testing set shown in table 1. High R^2 with training set indicates that the RF model was able to capture the underlying trend within the training data. High R^2 with testing set indicates that the model could generalize well and is able to predict unfamiliar data that it was not trained with.

Figure 3 depict the performance plot of the RF model in testing set. Generally, the models can predict the target values accurately. Ideally, the datapoints should be close to the diagonal line. However, there are a few datapoints that are far from the diagonal line. For instance, 3286MPa was predicted as 2779MPa in figure 3 and 39MPa was predicted as 55.8MPa in figure 4. Thus, we can conclude that the model did well generally, but is not capturing the underlying pattern properly for some outliers across the

whole dataset. This cause abrupt drop in accuracy for a few datapoints. The significant mispredictions likely result from the model's sensitivity to certain data points, indicating areas for potential refinement.

Mechanical Property	Train Set R^2	Test set R^2
Tensile Modulus	0.9595	0.9380
Tensile Strength	0.9856	0.9733
Flexural Modulus	0.9616	0.9671
Flexural Strength	0.9834	0.9657

Table 1. Performance of RF Model

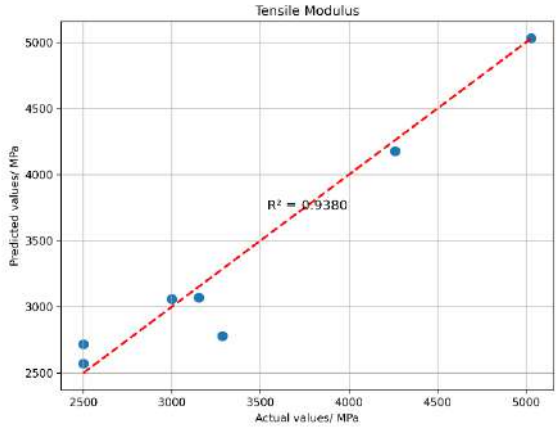

Fig. 1 Performance Plot for Tensile Modulus

CONCLUSION

The trained Random Forest model is capable of accurately capturing the trend of the learning dataset with $R^2 > 0.95$ when predicting the training dataset and at establishing new trend with $R^2 > 0.93$ when predicting testing dataset. Although the prediction of a few points was further from its actual values, the general performance of the model was good. While the model performs well, future work will focus on increasing the dataset size and exploring advanced hyperparameter tuning methods to further enhance model accuracy and robustness.

REFERENCES

Almohammed, F., & Soni, J. (2023). Using Random Forest and Random Tree model to Predict the splitting tensile strength for the concrete with basalt fiber reinforced concrete. *IOP Conference Series: Earth and Environmental Science*, *1110*(1), 012072. https://iopscience.iop.org/article/10.1088/1755-1315/1110/1/012072

Guo, P., Meng, W., Xu, M., Li, V. C., & Bao, Y. (2021). Predicting mechanical properties of high-performance fiber-reinforced cementitious composites by integrating micromechanics and machine learning. *Materials*, *14*(12). https://doi.org/10.3390/ma14123143

Hashin, Z. (1983). Analysis of composite materials: A survey. *Journal of Applied Mechanics, Transactions ASME*, *50*(3). https://doi.org/10.1115/1.3167081

Khademi, F., Akbari, M., Jamal, S. M., & Nikoo, M. (2017). Multiple linear regression, artificial neural network, and fuzzy logic prediction of 28 days compressive strength of concrete. *Frontiers of Structural and Civil Engineering*, *11*(1). https://doi.org/10.1007/s11709-016-0363-9

Liu, J., Zhang, Y., Zhang, Y., Kitipornchai, S., & Yang, J. (2022). Machine learning assisted prediction of mechanical properties of graphene/aluminium nanocomposite based on molecular dynamics simulation. *Materials & Design*, *213*, 110334. https://doi.org/10.1016/j.matdes.2021.110334

Qi, Z., Zhang, N., Liu, Y., & Chen, W. (2019). Prediction of mechanical properties of carbon fiber based on cross-scale FEM and machine learning. *Composite Structures*, *212*. https://doi.org/10.1016/j.compstruct.2019.01.042

Rahmanian, S., Thean, K. S., Suraya, A. R., Shazed, M. A., Mohd Salleh, M. A., & Yusoff, H. M. (2013). Carbon and glass hierarchical fibers: Influence of carbon nanotubes on tensile, flexural and impact properties of short fiber reinforced composites. *Materials and Design*, *43*. https://doi.org/10.1016/j.matdes.2012.06.025

Shang, M., Li, H., Ahmad, A., Ahmad, W., Ostrowski, K. A., Aslam, F., Joyklad, P., & Majka, T. M. (2022). Predicting the Mechanical Properties of RCA-Based Concrete Using Supervised Machine Learning Algorithms. *Materials*, *15*(2). https://doi.org/10.3390/ma15020647

Thomason, J. L. (2002). Micromechanical parameters from macromechanical measurements on glass reinforced polypropylene. *Composites Science and Technology*, *62*(10–11), 1455–1468. https://doi.org/10.1016/S0266-3538(02)00097-0

Yin, B. B., & Liew, K. M. (2021). Machine learning and materials informatics approaches for evaluating the interfacial properties of fiber-reinforced composites. *Composite Structures*, *273*, 114328. https://doi.org/10.1016/j.compstruct.2021.114328

ACKNOWLEDGEMENT

The work is financially supported by the Ministry of Higher Education (MOHE) Malaysia under the Fundamental Research Grant Scheme, FRGS (Grant number: FRGS/1/2023/TK10/USM/02/8). The authors would also like to thank Universiti Sains Malaysia for providing technical support

Comparison Study of Radial Basis Function and Reaction-Diffusion Equation based on Level Set Topology Optimization method

Le Tan Loc[1], Tatacipta Dirgantara[1*], Lavi Rizki Zuhal[1], Annisa Jusuf[1]
Faculty of Mechanical and Aerospace Engineering, Institute Technology of Bandung
Tel: +6222 2504243 Email: tdirgantara@itb.ac.id

ABSTRACT

Topology optimization is a mathematical approach that allows for generated efficient and lightweight structure designs. Level set topology optimization are computational techniques that are used to optimize the layout of material within a given design domain to achieve desired structural performance or other objectives, which have emerged as a popular approach to refine a component's design and increasing its performance. In this study, two different existing approaches for level set-based topology optimization: the Radial Basis Function (RBF) method and the Reaction-Diffusion Equation (RDE) method are compared. Numerical results on benchmark problems involving a total of five size elements in a specific design domain are conducted to compare the performance of the RBF and RDE methods, during which we evaluate geometrical accuracy, convergence behaviour, and computational efficiency. The results show that, overall, the Reaction-Diffusion Equation is much superior in dealing with high design domain size and low computation time. The work demonstrates that not only finds the advantages of algorithms based on design domain sizes to solve problems but also selects the proper method which drastically reduced computational cost.

Keywords: Topology Optimization, Radial Basis Function, Reaction-Diffusion Equation, Level Set Method.

INTRODUCTION

Topology optimization is a computational design approach used in engineering and design fields to determine the optimal layout or distribution of material within a given design space to achieve desired performance objectives.

The direct approach to level set based on topology optimization methods (Wang, Wang and Guo, 2003; Allaire, Jouve and Toader, 2004), and the traditional (Sethian, 2001), aim at tracking the motion of interfaces and updating the implicit function using a velocity function derived from shape sensitivity, but often lack of do not inherently facilitate the establishment of new apertures, and resolutions may rely on the original configuration (Dunning and Alicia Kim, 2013), at least for 2D problems. In addition, the quantity of iterations may result in a gradual convergence and/or suboptimal solutions, lead to take long time for computation and use more computational cost.

Holes are important in topology optimization because increasing the number of holes in a design, without changing its volume, generally improves the values of the objective functional (Otomori *et al.*, 2015). To overcome these limitations, this work studies the viability and characteristics of the extended methods in combination with the Level Set Method, RBF (Wei *et al.*, 2018) and RDE (Yamada et al., 2010; Yamada et al., 2010).

METHODOLOGY

In this work, we compared two variants of the Level Set method topology optimization algorithm, RDE and RBF, from (Otomori *et al.*, 2015) and (Wei *et al.*, 2018) works. The open-source codes have been proposed and allowed to study and compare to different topology optimization methods in aspects not presented in the original article.

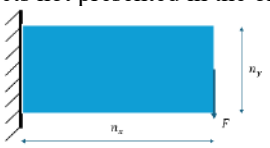

Fig. 1 The design domain and boundary conditions of the short cantilever beam

A rectangular design domain for short cantilever beam is assumed and discretized by square finite element mesh defined by five design domains of size $60x30, 80x64, 120x60, 160x128, and\ 240x120$, which volume fraction is set to 50%. The design domain and boundary conditions are shown in Fig. 1. Finally, the Reaction-Diffusion Equation method is used to calculate more higher design domain of size, up to $1920x960$ to evaluate the impact of computation time and RAM usage on increasing domain size using this method.

RESULTS AND DISCUSSION

The iteration numbers of the RDE method had a higher value compared to the RBF method, but the values are also very stable until convergence. According to

(a) (b)

Fig. 2a, the RDE method had faster convergence at each mesh parameters. Therefore, it is observed that although

the RDE gives a higher number of iterations, but it takes less computation time per iteration.

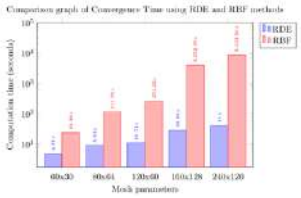

(a) (b)

Fig. 2 (a) The convergence time of RDE and RBF methods; (b) Time calculated due to the design domain (RDE)

The results in Table **1** show that the optimized configuration of RDE depends on the number of mesh elements. The mesh parameters value increases, which significantly increases the computation time, and the geometry boundaries get smoother. Fig. 2b provides a detailed time calculation of the RDE method for various mesh parameters, which achieved impressive good computation times for large design domain and predictable.

In conclusion, due to the computation time and RAM cost, the Reaction Diffusion Equation (RDE) is superior to Radial Basis Function (RBF). However, the RBF results are smoother in geometry than RDE results, especially at sparse number of elements. Both RDE and RBF can generate the number of holes in a given design while keeping its volume constant.

Table 1 Optimization result comparison between the RBF method, the RDE method

2D Numerical Examples		Design Domain Size Elements 60x30	80x64	120x60	160x128	240x120
Radial Basis Function	**Volume Fraction constraints**	0.49	0.49	0.5	0.5	0.5
	Iterations	100	94	100	91	79
	Optimized Configuration	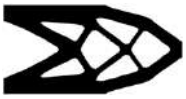				
Reaction-Diffusion Equation	**Volume Fraction constraints**	0.5	0.5	0.5	0.5	0.5
	Iterations	107	112	109	111	111
	Optimized Configuration				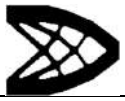	

REFERENCES

Allaire, G., Jouve, F. and Toader, A.M. (2004) 'Structural optimization using sensitivity analysis and a level-set method', *Journal of Computational Physics*, 194(1), pp. 363–393. Available at: https://doi.org/10.1016/j.jcp.2003.09.032.

Dunning, P.D. and Alicia Kim, H. (2013) 'A new hole insertion method for level set based structural topology optimization', *International Journal for Numerical Methods in Engineering*, 93(1), pp. 118–134. Available at: https://doi.org/10.1002/nme.4384.

Otomori, M. *et al.* (2015) 'Matlab code for a level set-based topology optimization method using a reaction diffusion equation', *Structural and Multidisciplinary Optimization*, 51(5), pp. 1159–1172. Available at: https://doi.org/10.1007/s00158-014-1190-z.

Sethian, J.A. (2001) 'Evolution, Implementation, and Application of Level Set and Fast Marching Methods for Advancing Fronts', *Journal of Computational Physics*, 169(2), pp. 503–555. Available at: https://doi.org/10.1006/jcph.2000.6657.

Wang, M.Y., Wang, X. and Guo, D. (2003) *A level set method for structural topology optimization*. Available at: www.elsevier.com/locate/cma.

Wei, P. *et al.* (2018) 'An 88-line MATLAB code for the parameterized level set method based topology optimization using radial basis functions', *Structural and Multidisciplinary Optimization*, 58(2), pp. 831–849. Available at: https://doi.org/10.1007/s00158-018-1904-8.

Yamada, T. *et al.* (2010) 'A topology optimization method based on the level set method incorporating a fictitious interface energy', *Computer Methods in Applied Mechanics and Engineering*, 199(45–48), pp. 2876–2891. Available at: https://doi.org/10.1016/j.cma.2010.05.013.

ACKNOWLEDGEMENT

This work was carried out with the support of Ganesha Talent Assistantship - International Fellowship (GT-IF) program by Institut Teknologi Bandung which is greatly acknowledged.

An implicit plasticity model with an application to fatigue prediction of metals

F Mozafari[1], P Thamburaja[2,3], A Srinivasa[3]

[1]*Department of Mechanical Engineering, Abdullah Gül University, Kayseri, Turkey*
[2]*Department of Mechanical and Manufacturing Engineering, Universiti Kebangsaan Malaysia, Bangi, Selangor 43600, Malaysia*
[3]*Department of Mechanical Engineering, Texas A&M University, College Station, TX 77843, USA*

ABSTRACT

A multi-dimensional, small-strain, rate-independent inelastic constitutive model has been developed to characterize the fatigue behavior of metals across a spectrum of cycles, from low to high. This characterization relies solely on the monotonic stress-strain curve and a limited number of initial cyclic tests (less than 1000 cycles). The model's innovative aspect lies in its treatment of the "microplastic response" occurring prior to full yield, utilizing a novel approach to inelastic modeling while maintaining a rate-independent characteristic. The model has been computationally implemented into a finite element code. The criterion adopted to predict fatigue life is based on total inelastic work dissipation, which correlates with the configurational entropy generated by damage. This model and its finite element algorithm effectively predict experimental strain-life responses.

Keywords: Plasticity Modeling, Computational Implementation, Experimental Investigation, Fatigue Analysis

INTRODUCTION

Fatigue failure, arising from alternating stresses in machinery components during operation, stands as the primary cause of failure in the industry. Despite stresses often falling below the material's macroscopic yield strength, they progressively accumulate microscopic defects, leading to eventual failure (Wang and Xiao 2017). Extensive research has delved into understanding how material microstructural features influence fatigue life behavior, with models like those by McDowell et al. (2003) focusing on elements such as carbides, inclusions, and grains to predict high cycle fatigue response. While these models advance our understanding of fatigue damage, their application is limited by the need for detailed microstructural knowledge.

Moreover, studies have explored metal fatigue life by incorporating microplastic deformation at a continuum-level scale, with notable theories like Mroz's multisurface plasticity theory (1967) and research by Dafalias and Popov (1976). Building upon these, a rate-type, rate-independent model has been proposed, emphasizing the hysteretic response without relying on a yield point. This model highlights the variation in tangent moduli during loading and unloading, offering a more adaptable and straightforward way to include the microplastic effect within a thermodynamically consistent framework.

The primary focus lies in demonstrating the advantages of a newly developed method for modeling hysteretic response and microplastic hysteresis, which modifies Rajagopal and Srinivasa's (2015) approach. This method aims to accurately predict high-cycle fatigue life based on the response of only a few cycles. By striving to develop a constitutive theory capable of reliably predicting fatigue life behavior across both low-cycle and high-cycle regimes, significant benefits are envisioned for experimental and practical applications within the automotive sector.

RESULTS AND DISCUSSION

The key constitutive equations of the present approach can be represented in the form of classical J2-type plasticity theory such that the Cauchy stress-strain relation can be written in the following rate form:

$$\dot{\boldsymbol{\sigma}} = \mathbb{C}: (\dot{\boldsymbol{\varepsilon}} - \dot{\boldsymbol{\varepsilon}}^{\boldsymbol{p}}) \tag{1}$$

with

$$\mathbb{C} = 2G\left(\mathbb{I} - \frac{1}{3}\mathbf{I}\otimes\mathbf{I}\right) + K(\mathbf{I}\otimes\mathbf{I}) \tag{2}$$

where G and K are the elastic shear and bulk moduli, respectively. Additionally, $\mathbb{I}$ and $\mathbf{I}$ represent the rank-four symmetric identity tensor and the second-order identity operator, respectively. The inelastic flow rate is defined as

$$\dot{\varepsilon}^p = \beta < \mathrm{sgn}(\sigma)\dot{\varepsilon} > \mathrm{sgn}(\sigma), \quad \mathrm{sgn}(\sigma) = \frac{\sigma}{|\sigma|} \tag{3}$$

here the Macaulay Bracket notation $< x >= (1/2)(x + |x|)$, sign function notation $\mathrm{sgn}(*)$ and the dimensionless function $\beta \geq 0$. The microplasticity can be capture by utilizing the following constitutive equation for β:

$$\beta = \frac{\widehat{\mathcal{H}}\left(|\boldsymbol{\sigma}| - s_\mu\right)\{1 + \tanh((|\sigma| - s_m)/\alpha)\}}{E(h_0/E)(1 - (s_m/s_m^*))^b + 1} \tag{4}$$

with $\widehat{\mathcal{H}}(x)$ is the step (or indicator) function defined by $\widehat{\mathcal{H}}(x) = 0$ if $x < 0$ and $\widehat{\mathcal{H}}(x) = 1$ if $x \geq 0$, and 0 controlling the transition from microplastic to macroplastic behavior. The macroplastic flow resistance, s_m evolves as follows:

$$\dot{s}_m = E(h_0/E)(1 - (s_m/s_m^*))^b |\dot{\boldsymbol{\varepsilon}}^p| \qquad (5)$$

with $s_m^* > s_m^0$, $h_0 \geq 0$ and $b > 0$ denoting the saturation value for the macroplastic flow resistance, the hardening modulus and the power-law coefficient, respectively. The fatigue life of a material is taken to be the number of cycles until the total entropy production due to plastic deformation, $\eta_p = \int \left(\frac{\delta}{\theta_0}\right) dt$, reaches a critical value $\eta_f > 0$ represents the (configurational) fatigue fracture entropy (FFE) production and θ_0 denotes the reference temperature.

Fig. 1 compares the reproduced stress-strain curve from the calibrated constitutive model with the data obtained from a simple compression test on SS304L.

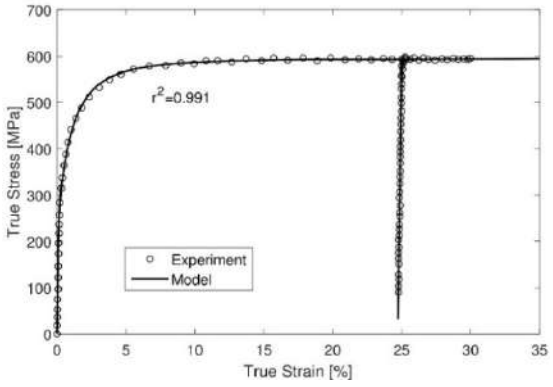

Fig. 1 The stress-strain response in simple compression for SS304L.

Fig. 2 shows the micro-hysteresis effect in SS304L that can be used to calibrate microplastic flow resistance, s_μ as the minimum value of the maximum stress, σ_{max} at which unloading from σ_{max} to zero stress results in a residual strain. Fig. 3 depicts fatigue life prediction derived from numerical simulations, confirming the accuracy of the developed constitutive theory in predicting strain-controlled fatigue life for SS304L material. The filled symbols represent low-cycle fatigue experimental data used to fit the FFE.

CONCLUSION

This study presents a multi-dimensional thermodynamically consistent rate-independent constitutive theory, designed to achieve smooth plastic transition in metals. The developed model has been computationally implemented into a finite element code. By utilizing well-calibrated constitutive parameters, the fatigue response of a steel alloy is predicted. By comparing to the experimental fatigue data, it is evident that both the constitutive theory and its numerical implementation can accurately predict fatigue life data across experiments spanning from low-cycle to high-cycle regimes for the steel alloy.

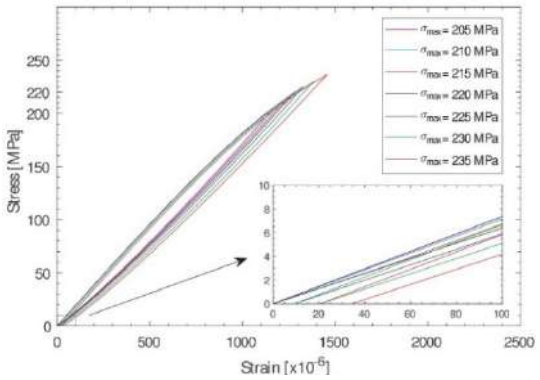

Fig. 2 Cyclic quasi-static compression stress-strain curves for cold-worked SS304L.

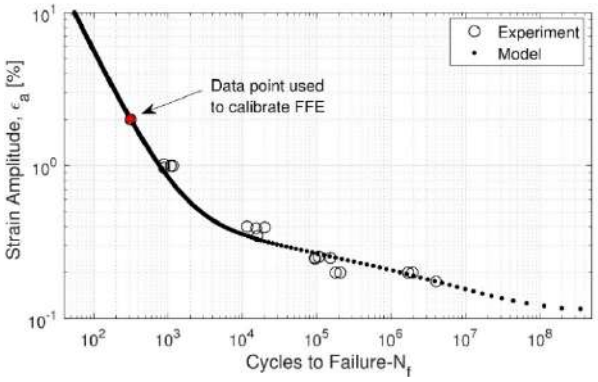

Fig. 3 Fatigue life data for SS304L under constant amplitude strain control with R = -1.

REFERENCES

Wang, Z.L. and Xiao, H., 2017. Direct modeling of multi-axial fatigue failure for metals. *International Journal of Solids and Structures*, 125, pp.216-231.

McDowell, D.L., Gall, K., Horstemeyer, M.F. and Fan, J., 2003. Microstructure-based fatigue modeling of cast A356-T6 alloy. *Engineering Fracture Mechanics*, 70(1), pp.49-80.

Mroz, Z., 1967. On the description of anisotropic workhardening. *Journal of the Mechanics and Physics of Solids*, 15(3), pp.163-175.

Dafalias, Y.F. and Popov, E.P., 1976. Plastic internal variables formalism of cyclic plasticity. *Journal of applied mechanics*, 43(4), pp.645-651.

Rajagopal, K.R. and Srinivasa, A.R., 2015. Inelastic response of solids described by implicit constitutive relations with nonlinear small strain elastic response. *International Journal of Plasticity*, 71, pp.1-9.

ACKNOWLEDGEMENT

F.M. acknowledges the partial support provided by the AGÜ Foundation.

Numerical Approaches of Wave Height Estimation of Friction Force on Submerged Permeable Breakwater

Tulus[1*], J.L. Marpaung[1], Suriati[2]
[1*,1]*Mathematics Department, Universitas Sumatera Utara, Medan, Indonesia*
[2]*Informatics Department, Universitas Harapan Medan, Medan, Indonesia*
Tel: +62 81375094001 Email: tulus@usu.ac.id

ABSTRACT

Coastal engineering, which uses wave breakwaters to reduce the impact of powerful waves, is important because it helps safeguard coastal areas. Coastal engineering reduces energy inflow from numerous sources. The study examines how fluid friction affects subsurface wave breakwater efficiency to improve coastal engineering. We numerically simulated numerous fluid friction scenarios on a submerged breakwater model. A numerical model that accurately simulates fluid-breakwater interaction was created using computational fluid dynamics (CFD) software in this work. The study found that fluid friction coefficients greatly impact submerged breakwater performance. More friction helps the wave breakwater reduce wave energy, lowering wave height behind it. However, increased friction increases force on the breakwater construction, which may affect its long-term stability and endurance. Less friction reduces the ability to suppress waves, but it also reduces structure stress. The study concludes that fluid friction calibration is necessary to balance breakwater efficacy and construction quality. The findings can help coastal engineers design more efficient and durable sink wave breakwaters based on their coastal environment.
Keywords: Breakwater, Simulation, Coastal, Computational Fluids Dynamics, Finite Element Methods

1. INTRODUCTION

Environmental sustainability, infrastructural protection, and natural catastrophe resilience depend on coastal protection engineering. Coastal engineering uses wave breakwaters, bars, and shelters to reduce seawater erosion, abrasion, and intrusion. To reduce the impact of natural calamities like tsunamis and tropical storms. By protecting ports, harbors, and tourism facilities from sea waves, coastal protection engineering helps ensure economic and social sustainability. This immediately benefits coastal communities(Tulus *et al.*, 2023). A complete, eco-friendly approach to coastal protection engineering promotes sustainable development that meets future generations' environmental, social, and economic needs. Energy-carrying waves make coastal damage more likely without coastal protection engineering(Peng *et al.*, 2017). The beachfront is vulnerable to erosion, abrasion, seawater intrusion, and ecological damage from strong waves and fast slopes without protective infrastructure. The effects include coastal territory loss, depletion of indigenous plant and animal ecosystems, damage to coastal infrastructure like dams and villages, and saltwater infiltration that depletes coastal freshwater resources(Romya *et al.*, 2022). Coastline tourism, agriculture, and fishing can suffer economically. Wave breakwaters defend coastlines from marine damage. Breakwaters reduce wave height, wavelength, and horizontal velocity before reaching the shoreline. Wave breakwater can protect coasts and infrastructure from massive ocean waves if designed and optimized for local environmental circumstances. For artificial seas and ports, breakwaters help. Main discoveries include spur dike scour depth estimation, vertical caisson dependability analysis, design challenges for overtopped mound breakwaters, run-up and overtopping in impermeable dikes, and using submerged breakwaters as artificial coral reefs. The principal vertical caisson failure modes are sliding and overturning. Traditional deterministic design has uncertainty safety(Shao and Luo, 2016). However, dependability design methodologies now prevail because they quantify uncertainty, although their drawbacks hinder widespread implementation. Design variable sensitivity of vertical caisson limit state function is determined via reliability analysis. For reliability index computation, this method offered design variable partial safety factors and load resistance factor(Zhang, Guo and Zhang, 2012).

RESULTS AND DISCUSSION

To simulate wave propagation approaching a breakwater, the wave model must be initialized by establishing its geometry. Figure 1 shows how COMSOL Multiphysics 5.6 will create a 2D wave model. The wave model defines the inlet and outflow sides with domain boundary constraints.

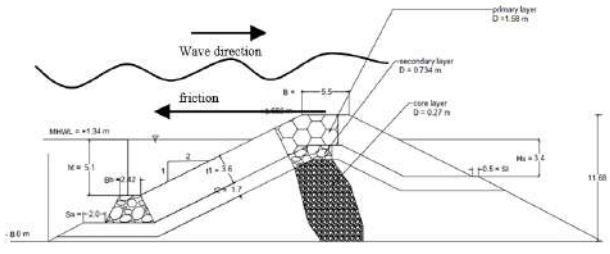

Figure 1. Breakwater simulation

The amount of the elements generated when meshing the model using finite elements was 185,845 with 1,772 edges, requiring computing in the wave model iteration to produce a considerable change in wave propagation over time. The simulation will examine how speed affects wave velocity distribution following wave attenuation at 1m/s, 1.5m/s, and 2m/s. Figure 2 shows the wave breaking process with a submerged breakwater model that has permeable properties and propagates in shallow water.

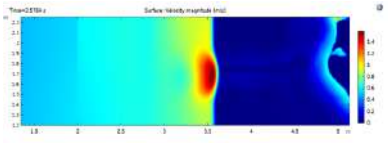

(a) t = 2,5s

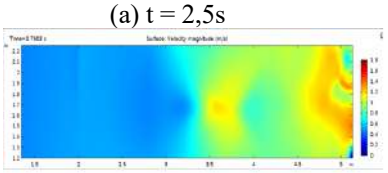

(b) t = 3,7s

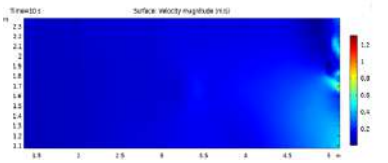

(c) t = 10s

Figure 2. Simulation of the velocity of the breakwater breaking process

The magnitude of the velocity fraction each time is shown in Figure 5 shows the propagation of waves that propagate after a break occurs using a porous submerged breakwater. The amplitude is generated against time and oscillates up to the outlet of the propagation area. The convergence of the wave amplitudes shows that the waves resulting from the wave splitting process show significant results, with as many as 4,836 iterations during $t = [0,10]$.

Table 1. Amplitude magnitude to variety of position

$u(x,t)$	h_b=1,196	h_b=1,696	h_b=2,196
x=9,52	0.13439	0.13438	0.13097
x=14,52	0.13988	0.13859	0.13161
x=19,52	0.043203	0.12468	0.12515

Table 1 shows the magnitude of the wave height that occurs in the interval $t(0,15)$, which gives the result that for a breakwater that is 19,52m, it gives a large wave height on the surface that is equal to 0,12515m, which is the minimum wave height value from a variation of 9,52m, which is 0,13097m, and a distance of 14,52m produces a wave height of 0,13161m.

CONCLUSION

This study shows that ocean wave sedimentation is significantly affected by the sinking wave breaker's frictional properties. Friction that absorbs and uses incoming wave kinetic energy reduces wave energy. Thus, it reduces coastal wave height and power. The modified Navier-Stokes equation, which accounts for friction, shows that increasing fluid viscosity and wave breaker surface rigidity improves wave detection. Thus, including these friction variables in the design of a sinking wave breaker improves its ability to protect the beach and provide calm sea conditions behind it. This study suggests that varied friction patterns can improve coastal infrastructure stability and safeguard delicate marine habitats from violent wave dynamics. This can be achieved by optimizing wave breaker designs.

ACKNOWLEDGMENT

The authors would like to express their gratitude and thanks to Universitas Sumatera Utara for funding this research under the International Collaboration Grant: 367/UN5.2.3.1/PPM/KP-TALENTA/2022.

REFERENCES

Peng, W. et al. (2017) 'Numerical analysis and performance optimization of a submerged wave energy converting device based on the floating breakwater', Journal of Renewable and Sustainable Energy, 9(4). doi: 10.1063/1.4997505.

Romya, A. A. et al. (2022) 'Performance assessment of corrugated semi-circular breakwaters for coastal protection', Alexandria Engineering Journal, 61(5), pp. 3587–3598. doi: 10.1016/j.aej.2021.08.086.

Shao, L. and Luo, J. (2016) 'Numerical investigation of the interaction between linear/nonlinear waves and breakwater', International Journal of Computational Methods and Experimental Measurements, 4(2), pp. 153–164. doi: 10.2495/CMEM-V4-N2-153-164.

Tulus et al. (2023) 'Computational Assessment of Wave Stability Against Submerged Permeable Breakwaters: A Hybrid Finite Element Method Approach', Mathematical Modelling of Engineering Problems, 10(6), pp. 1977–1986. doi: 10.18280/mmep.100607.

Zhang, N., Guo, K. and Zhang, W. Z. (2012) 'Two-dimensional numerical wave simulation for port with submerged breakwater', Applied Mechanics and Materials, 226–228, pp. 1343–1347. doi: 10.4028/www.scientific.net/AMM.226-228.1343.

Analysis of Brachial Artery Blood Flow Model Output Using the Casson Fluid Model

Freddy Sutanto[1], Tulus[2*]
[1] *Student of Mathematics, Universitas Sumatera Utara, Medan, Indonesia*
[2*] *Mathematics Department, Universitas Sumatera Utara, Medan, Indonesia*

Tel: +6281375094001 Email: tulus@usu.ac.id

ABSTRACT

Blood flow modeling is a crucial area of research in medicine and biomedical engineering. This study aims to analyze the output of a blood flow model in the brachial artery, specifically using the Casson fluid model. Parameters such as flow velocity, pressure distribution, velocity gradient, and external forces will be evaluated to understand the characteristics of blood flow under normal conditions. This research is expected to provide valuable insights into the behavior of arterial blood flow, particularly in the brachial artery. The blood flow model employed includes three equations: the continuity equation, the momentum equation, and the Casson fluid model. The finite volume method (FVM) will be used to implement these equations in the software.

Keywords: Blood flow model, Casson fluid model, Brachial artery, Finite Volume Method.

INTRODUCTION

Blood is a fluid in the human body that circulates through the heart, arteries, capillaries, and veins. The process of blood circulation is influenced by several factors, including blood velocity, vessel cross-sectional area, blood pressure, and the work of the muscles found in the heart and blood vessels. Evidence shows that fluid dynamics within blood vessels plays a major role in the development and progression of arterial diseases (Srivastava, 1985; Tu & Deville, 1996).

The brachial artery, one of the major blood vessels in the body, plays an important role in circulating blood to the lower arm and hand. Disturbances in blood flow in this artery can indicate various cardiovascular problems, such as atherosclerosis, hypertension, and peripheral artery disease. An in-depth analysis of blood flow characteristics in the brachial artery is crucial as it can aid in developing more accurate diagnostic methods and more effective treatments.According to the World Health Organization (WHO), stroke is a condition with a high risk of mortality. Stroke patients may experience loss of vision and speech, paralysis, and confusion. The risk of subsequent strokes increases significantly in individuals who have previously suffered a stroke. This condition underscores the urgency of thoroughly understanding and analyzing the dynamics of blood flow in arteries such as the brachial artery, as a better understanding of this can be key in preventing and managing cardiovascular diseases, including the risk of stroke. In the fields of medicine and biomedical science, modeling arterial blood flow is a crucial research topic. One model used to describe realistic blood flow is the Casson fluid model. This model considers the non-Newtonian nature of blood, which is actually a mixture of red blood cells and plasma. The Casson fluid model is one of the non-Newtonian models often used to describe blood flow. This model accounts for the fact that blood has a minimum shear stress that must be reached before flow can begin, known as yield stress. Once this stress is exceeded, blood flows with behavior more resembling a non-Newtonian fluid. This makes the Casson model suitable for depicting blood viscosity, which varies depending on the shear stress experienced. According to Donald R. Peterson and Joseph D. Bronzino in the book “Biomechanics: Principles and Applications” (R. Peterson & D. Bronzino, 2008), the Casson fluid model is suitable for presenting basic concepts of blood flow.Another fluid model often used for pseudoplastic fluids, where viscosity decreases with increased shear rate, is the Power-Law fluid model. Research by Jung et al. (2006) used the Power-Law model to analyze blood flow in arteries with varying diameters, providing insights into how structural changes in arteries affect flow distribution and pressure.

This study will use a computational simulation approach to analyze blood flow in the brachial artery. A mathematical model based on the Casson fluid will be developed and implemented using fluid simulation software with the Finite Volume Method (FVM) approach. The finite volume method is a method for representing and evaluating partial differential equations in the form of integral equations (LeVeque, 2004). The finite volume method has been used in several studies, such as the journal titled “A Finite Volume Approach for Blood Flow Modeling in Arteries” in 2014 by Karabulut Y, Aksoy S, and Secer A. (Karabulut Y et al., 2014).

RESULTS AND DISCUSSION

In this study, we use a couple of equation for the models. Here are the equation :

1.Momentum Equation: For incompressible flow and 1D, the momentum equation is :

$$\rho\left(\frac{\partial v}{\partial t}+v\frac{\partial v}{\partial x}\right)=-\frac{\partial p}{\partial x}+\mu\frac{\partial^2 v}{\partial x^2}+\tau_y \quad (1)$$

Using the discretized momentum equation, the velocity is updated based on the current pressure :

$$v(i)=v(i)-\Delta t\left(v(i)\frac{v(i+1)-v(i-1)}{2\Delta x}+\frac{p(i)-p(i-1)}{\rho\Delta x}-\frac{\mu\left(v(i+1)-2v(i)+v(i-1)\right)}{\rho(\Delta x)^2}-\frac{\tau_y}{\rho}\right) \quad (2)$$

2.Continuity Equation

For incompressible flow and 1D, the continuity equation is :

$$\frac{\partial v}{\partial x}=0 \quad (3)$$

And the descrete form of the continuity equation is :

$$\frac{v_{i+1}-v_i}{\Delta x}=0 \quad (4)$$

After the velocity is updated, the pressure is updated using the continuity equation in its discrete form :

$$p(i)=p(i)-\Delta t\rho\frac{v(i+1)-v(i)}{\Delta x} \quad (5)$$

3. Casson Model

There are 3 main equation for Casson model, such as

a. Viscosity

$$\mu=\frac{\tau_y}{\sqrt{\gamma}}+\eta_\infty \quad \text{, when } \gamma\neq 0 \quad (6)$$

b. Shear rate

$$\gamma\approx\left|\frac{v_{i+1}-v_{i-1}}{2\Delta x}\right| \quad (7)$$

c. Shear stress

$$\tau=\mu\cdot\gamma \quad (8)$$

Table 1. Parameters

Parameters	Values
L (length)	0.23 meters
R (radius)	0.004 meters
ρ (density)	1060 kg/m^3
τ (yield stress)	0.05 Pa
η_∞ (Infinite shear viscosity)	0.0035
v_0 (initial velocity)	0.2m/s
p_0 (initial pressure)	13.000 Pa
Blokage 25%	0.1035-0.1265 meter

CONCLUSION

The simulation results offer valuable insights into the hemodynamics of arterial blood flow, providing a detailed understanding of velocity, pressure, and viscosity profiles along the artery. The velocity profile illustrates the flow behavior, revealing regions of acceleration and deceleration within the artery, while variations in pressure along the artery reflect changes in resistance or the presence of blockages. Additionally, the viscosity profile sheds light on the fluid's resistance to flow, indicating potential pathological conditions or variations in hematocrit levels. The simulation allows for the study of how arterial occlusion affects flow patterns and pressure gradients, providing critical information about the severity of stenosis and the risk of complications such as thrombosis or ischemia. Overall, computational modeling plays a crucial role in advancing our understanding of cardiovascular physiology and improving patient care in healthcare research and clinical practice.

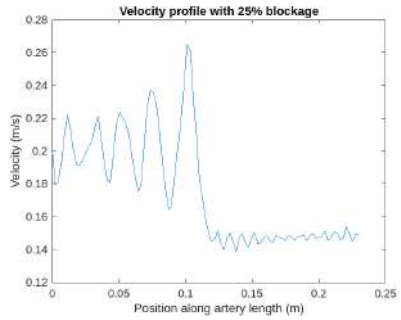

Fig. 1 Velocity of blood flow in artery brachialis

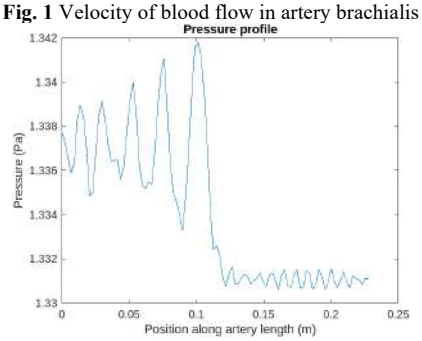

Fig. 2 Pressure of blood flow in artery brachialis

REFERENCES

Karabulut Y, Aksoy S, & Secer A. (2014). *A Finite Volume Approach for Blood Flow Modeling in Arteries*.

LeVeque, R. J. (2004). *Finite-Volume Methods for Hyperbolic Problems*.

R. Peterson, D., & D. Bronzino, J. (2008). *Biomechanics Principles and Applications* (2 ed.).

Srivastava, L. (1985). *Flow of Couple Stress Fluid Through Stenotic Blood Vessels*. J. Biomech.

T. Ishikawa, L.F.R. Guimaraes, S. Oshima, & R. Yamone. (1998). *Effect of Non-Newtonian Property of Blood on Flow Through a Stenosed Tube*. *Fluid Dynamic Research 22* , 251–264.

Tu, C., & Deville, M. (1996). *Pulsatile Flow of Non-Newtonian Fluids Through Arterial Stenosis*. J. Biomech

Prediction of Elastic Moduli of Polymer Composites using 3D RVE modeling

Fajwa Kamar Shah, Norwahida Yusoff, Sarah Kamaludin*
School of Mechanical Engineering, Universiti Sains Malaysia,
Transkrian, Nibong Tebal, 14300, Penang, Malaysia
Email: sarahkamaludin@usm.my

ABSTRACT

Polymer composite materials (PCMs) are increasingly used in engineering because of their excellent mechanical properties. However, accurately determining the properties of these materials remains a challenge. Traditional experimental methods are resource-intensive, encouraging interest in more efficient modelling. This work generates 3D random fiber distributions inside Representative Volume Elements (RVEs) for PCM microstructural characterization utilizing the Random Sequential Expansion (RSE) technique for more efficient modelling. Finite element analysis (FEM) is utilized to validate the model by assessing Young's modulus in both the X and Y directions through transverse tensile testing. Fiber-reinforced polymer composites (FRPC) are accurately represented by the RVE model, which matches reference and experimental data.

Keywords: Finite Element Method (FEM), Random Fiber Distribution, Representative Volume Element (RVE), Composite, Elastic

1.0 INTRODUCTION

PCMs' outstanding mechanical properties make them essential in aerospace, automotive, and industrial applications (Hsissou et al. 2021). Affordable methods that precisely identify the properties of these materials are vital for their maximum utilization. Previously, resource-intensive experimental procedures were used. Alternatively, a computational model is more efficient. To analyze composites' microscale behavior and upscale it to the macroscale, computer modelling uses the Representative Volume Element (RVE). Multiple studies have explored methods to model fiber distribution in RVE. Traditional hard-core models often result in larger than actual inter-fiber distances, limiting the maximum achievable fiber volume fraction that do not fully capture the stochastic nature of real-world composites. These limitations highlight the need for more sophisticated techniques to generate random fiber distributions accurately. Thus, Yang et al. (2013) develop the random sequential expansion (RSE) approach, which is used in this work to create a 3D random fibre distribution with higher fibre percentages or volume fractions. To evaluate the model's accuracy, the generated RVE model undergoes finite element analysis and is compared to findings from experiments.

2.0 METHODOLOGY

2.1 Algorithm Description

The RSE model ensures controlled inter-fiber distances, allowing for higher and more accurate fiber volume fractions. The process starts with defining input parameters (RVE dimensions, fiber properties, minimal inter-fiber distances, *lmin* and maximal inter-fiber distances, *lmax*) and generating the initial random point for the first fiber center. New fiber coordinates are iteratively generated, ensuring no overlap and adherence to inter-fiber distance constraints, until the desired fiber volume fraction is achieved. The final fiber coordinates are then used to model the fibers in ABAQUS, facilitating realistic simulations of microstructural properties.

2.2 Finite Element Model

FEM examines the elastic behavior of the PCM and validate the effectiveness of the algorithm presented by Yang et al. (2013). Based on Melro et. al. (2008), the input variables for the analysis are: r_f=2.6 μm, δ=50, l_{min}=0.182 μm, l_{max}=0.8 μm, and V_f=60%. Both the fiber and matrix are considered isotropic materials, with Young's modulus and Poisson's ratio values of E_f =74 GPa, ν_f =0.2, and E_m =3.35 GPa, ν_m =0.35, respectively. The model is created in ABAQUS 6.13 (Hibbitt, Karlsson & Sorensen 1995) in which Python scripts are employed to generate the model of the RVEs in ABAQUS. Figure 2 shows the RVE model generated with fiber volume, *Vf=60%* and the boundary conditions. The 3D RVE models of composites are meshed mainly with eight-node linear solid elements that use reduced integration, called C3D8R elements.

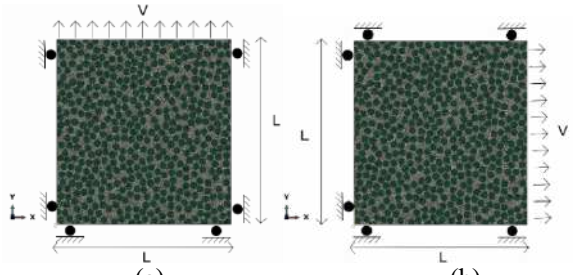

Fig. 2 3D RVE Generated with Fiber Volume Fraction of 60% with Boundary Conditions: (a) Transverse Tensile in Direction-Y (b) Transverse Tensile in Direction-X.

3.0 RESULTS AND DISCUSSION

From the FEM simulation, nominal stress-strain data of RVE is obtained as shown in Figures 4. The predicted Young's Modulus in transverse tensile of Y-direction (E_2) and X-direction (E_3), is determined from the stress-strain data by determining the gradient (slope) of the linear portion. The gradient is the Young's modulus. From Table 1, E_2 and E_3 show good agreement with theoretical references but a larger discrepancy with experimental data, likely due to the absence of interphase in the model. The equal modulus values in X and Y directions indicate transverse isotropy, suggesting uniform fiber distribution and consistent matrix properties.

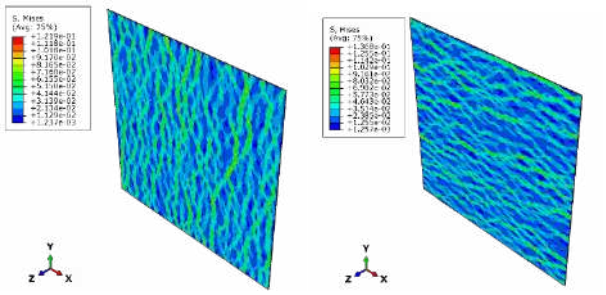

(a) (b)

Fig. 3 Von Mises Stress Contour for: (a) Transverse Tensile Direction-Y (b) Transverse Tensile Direction-X

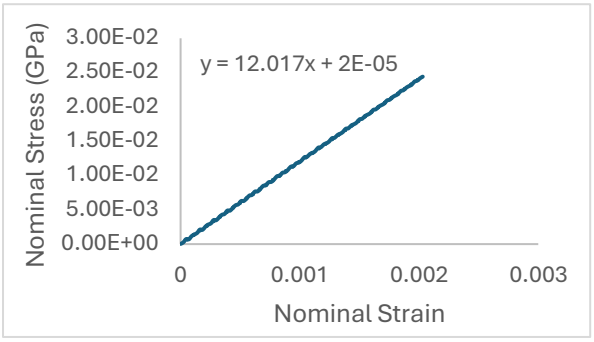

(a)

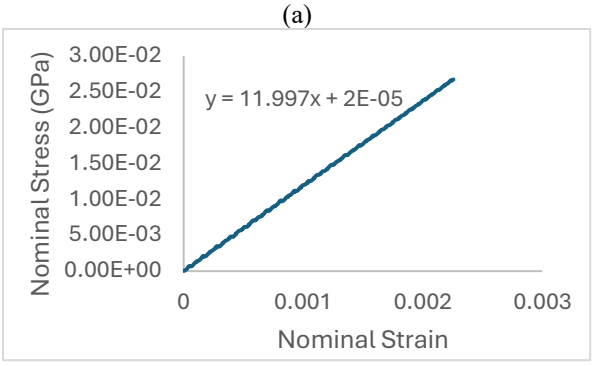

(b)

Fig. 4 Nominal Stress-Strain Curve for: (a) Transverse Tensile in Direction-Y (b) Transverse Tensile in Direction-X.

	E_2 (GPa)	E_3(GPa)
Stress-Strain Curve	12.017	11.997
References (Yang et al. 2013)	13.047	13.086
Experimental (Soden et. al. 1998)	16.2	16.2
Errors with References (%)	7.89%	8.32%
Errors with Experimental (%)	25.82%	25.94%

Table 1. Elastic Properties Predicted

4.0 CONCLUSION

This study demonstrates that employing the RSE algorithm to model random fiber distributions within RVE effectively simulates PCMs behavior. The model's accuracy in predicting Young's Modulus values confirms its reliability for real-world applications in composite material design.

REFERENCES

Hibbitt, Karlsson & Sorensen. 1995. ABAQUS_Theory_Manual.

Hsissou, R., Seghiri, R., Benzekri, Z., Hilali, M., Rafik, M. & Elharfi, A. 2021. Polymer composite materials: A comprehensive review. *Composite Structures* 262: 113640.

Melro, A.R., Camanho, P.P. & Pinho, S.T. 2008. Generation of random distribution of fibres in long-fibre reinforced composites. *Composites Science and Technology* 68(9): 2092–2102.

Soden, P. 1998. Lamina properties, lay-up configurations and loading conditions for a range of fibre-reinforced composite laminates. Composites science and technology 58(7): 1011–1022.

Yang, L., Yan, Y., Ran, Z. & Liu, Y. 2013. A new method for generating random fibre distributions for fibre reinforced composites. *Composites Science and Technology* 76: 14–20.

ACKNOWLEDGEMENT

This work was supported by a Universiti Sains Malaysia, Short-term Grant with Project No: 304/PMEKANIK/6315686.

Mechanical Properties of Gigantochloa scortechinii Bamboo Fiber/Epoxy Composites

Khalid Mohammed[1], Rozli Zulkifli[1],*, Mohd Faizal Mat Tahir[1], Tayser Sumer Gaaz[2]

[1]Department of Mechanical and Manufacturing Engineering, Faculty of Engineering and Built Environment, Universiti Kebangsaan Malaysia, 43600, UKM Bangi, Selangor, Malaysia
[2]Prosthetics and Orthotics Engineering Department, College of Engineering and Technologies, Al-Mustaqbal University, Babylon 51001, Iraq
*Corresponding author: rozlizulkifli@ukm.edu.my

ABSTRACT

Bamboo has attracted researchers' attention due to its renewability, environmental friendliness, non-toxicity, cost-effectiveness, non-abrasiveness, and biodegradability. This study investigates the mechanical properties of bamboo fiber-reinforced epoxy composites using G. scortechinii (Buluh Semantan) at 9, 13, and 18 wt.% fiber content, cured at 26°C, 38°C, and 50°C. Results show that at 26°C, composites with 0.52 μm particles at 13 wt.% loading achieved a tensile strength of 41.6 MPa and Young's modulus of 2.84 GPa. However, as curing temperature increased, tensile strength decreased, with 1.5 μm particles at 18 wt.% loading showing tensile strengths of 21.2 MPa and 6.15 MPa, and Young's moduli of 3.27 GPa and 4.51 GPa at 38°C and 50°C, respectively. Improved tensile strength at lower temperatures is attributed to better fiber-matrix adhesion. Flexural strength peaked at 105 MPa for 1.5 μm particles at 13 wt.% loading, and impact strength reached 5593 J/m² for 1.5 μm particles at 18 wt.% loading. SEM analysis confirmed good fiber-matrix interfaces and minimal filler clumping at 13 wt.% loading. This study presents a new method for creating lightweight, high-strength composites from natural fibers and polymers.

Keywords: Bamboo, Fiber-reinforced composite, Epoxy resin, Mechanical properties.

INTRODUCTION

Fiber-reinforced polymer (FRP) composites commonly incorporate synthetic fibers like aramid, glass, and carbon due to their strength and availability. These materials find extensive use in civil engineering, architecture, and aerospace industries [1, 2]. However, synthetic fibers pose environmental challenges, as glass and carbon fibers are difficult to biodegrade, leading to pollution [3]. Additionally, the energy-intensive production of synthetic fibers [4] increases material costs, reducing the affordability of FRP materials for construction and architectural applications. Natural fibers present a solution to these issues, offering high strength and elasticity modulus, abundant availability, low cost, low energy requirements, renewability, and biodegradability [5, 6, 7]. Commonly studied plant fibers include kenaf, jute, flax, sisal, coir, and bamboo [8]. Despite the potential of bamboo fiber, there is limited research on bamboo fiber composites, which this study aims to address. Bamboo fiber is of particular interest due to its low density, high stiffness, high strength, and rapid growth, leading to ample availability [9].

This study explores the mechanical properties of G. scortechinii (Buluh Semantan), a bamboo species widely distributed in Southeast Asia. Bamboo fibers require extensive treatment before use, including retting, steam explosion, alkali treatment, degumming, grinding, and crushing, which affect their quality and strength [10, 11, 12, 13]. Numerous studies have shown improvements in the mechanical characteristics of alkali-treated natural fibers [14]. For example, [15] reported that Malaysia hosts around 70 bamboo species, with significant distributions in Peninsular Malaysia, Sabah, and Sarawak. Additionally, [16] identified ten major bamboo genera, including Bambusa, Dinochloa, Yushania, Chusquea, Gigantochloa, Phyllostachys, Dendrocalamus, Racemobambos, Thyrsostachys, and Schizostachyum. Previous research by [17] on continuous bamboo fiber-reinforced epoxy treated with 0.1N NaOH at 100°C for 12 hours showed improved adhesion between bamboo fiber and epoxy polymer but did not investigate the effect of fiber volume percentage. Similarly, [19] found that bamboo fiber treated with 6% NaOH had the best tensile strength, with failure primarily due to fiber-matrix debonding, fiber pull-out, fiber breakage, and matrix cracking. These studies did not specify the bamboo species, limiting their applicability to other species like Gigantochloa scortechinii, commonly used in construction in Malaysia, Indonesia, and Thailand.

Research by [20] comparing five bamboo species revealed tensile strengths ranging from 144.93 N/mm² to 233.98 N/mm². This study seeks to investigate the impact of fiber loading and treatment conditions on the mechanical properties of bamboo fiber composites at different temperatures. Few studies have examined the

effects of treatment duration and alkali concentration on Gigantochloa scortechinii fibers [21]. Most research focuses on epoxy as the matrix due to its superior properties, with less attention to alternative polymers [22, 25].

The novelty of this research lies in reinforcing bamboo fiber with epoxy resin to evaluate the mechanical properties. This study addresses gaps in existing literature by varying bamboo fiber and composite materials and examining different treatment settings to enhance composite strength and morphology. The goal is to ascertain the optimal conditions for reinforcing thermoset resin epoxy composites with bamboo fiber, contributing to the development of high-performance, natural fiber-reinforced materials.

RESULTS AND DISCUSSION

Figure 1 shows the tensile test setup. Table 1 presents the experimental findings for the tensile strength and Young's modulus of epoxy-based composites (a, b). The results indicate that the tensile properties of the epoxy resin composite were enhanced when reinforced with bamboo fiber. The tensile characteristics of the composites were significantly influenced by the curing temperature. At a curing temperature of 26°C, the tensile strength and Young's modulus of the bamboo fiber/epoxy composites increased to 41.6 MPa and 2.84 GPa, respectively, for a particle size of 0.52 μm at 13% weight loading (Figure 9). According to [29], as the curing temperature increased to 38°C and 50°C, the tensile strength decreased to 21.2 MPa and 6.15 MPa for a particle size of 1.5 μm at 18% weight loading, with Young's modulus of 3.27 GPa and 4.51 GPa for the same particle size and weight loading, respectively, as shown in Figures 10(b) and 11(c). The improvement in tensile strength is attributed to superior fiber-matrix interface adhesion. Additionally, it is believed that the epoxy resin treatment of the bamboo fibers created new mechanical interlocking sites, enhancing resin/fiber interpenetration and tensile strength [30]. The uneven orientation of the bamboo fibers results in unequal stress distribution on each fiber. As the temperature rises, the resin becomes softer and more pliable, weakening the overall structure. Shear failure between fibers and debonding of fibers from the matrix were observed at 50°C. This gradual degradation indicates that the fibers, rather than the epoxy resin, withstand the tensile force. Similarly, under tensile stress, the fiber and matrix gradually separate due to the degradation of fiber/matrix adhesion at 50°C.

Fig. 1 Tensile testing of composites specimen

Table 1. Results of the tensile properties of bamboo fibers reinforced epoxy composites at different temperatures.

Materials	Tensile strength (GPa)			Tensile modulus (MPa)		
	$T26^{\circ}$	$T38^{\circ}$	$T50^{\circ}$	$T26^{\circ}$	$T38^{\circ}$	$T50^{\circ}$
(Epoxy+hardener)+ bamboo fiber 9%	38.7	26.2	6.15	2.54	2.42	4.38
(Epoxy +hardener)+bamboo fiber 13%	41.6	21.2	7.01	2.84	2.25	3.75
(Epoxy +hardener)+bamboo fiber 18%	36.1	27.4	7.49	2.76	3.27	4.51

CONCLUSION

This study investigates the tensile performance and mechanical properties of epoxy composites reinforced with bamboo fibers at curing temperatures of 26°C, 38°C, and 50°C. Key failure modes included fiber breaking, matrix cracking, debonding, and fiber pull-out, analyzed via SEM. The bamboo fibers treated with epoxy resin improved the mechanical properties of the composites. Epoxy composites with bamboo fibers were successfully fabricated, showing enhanced adherence. Optimal tensile performance was at 26°C with 13% weight loading and 0.52 μm particle size. Flexural characteristics improved with increased particle size, peaking at 1.5 μm. Maximum impact strength of 5593 J/m² was at 18 wt.% loading and 1.5 μm particle size.

REFERENCES

[1] M. Abd-El Salam, "Mechanical properties of bamboo powder reinforced ethylene propylene diene monomer (EPDM) composites: effect of filler loading and particle size," Journal of Advances in Physics, vol. 6, 2014.

[2] T. S. Gaaz, A. B. Sulong, and A. A. H. Kadhum, "Influence of sulfuric acid on the tensile properties of halloysite reinforced polyurethane composite," Journal of Mechanical Engineering, vol. 7, pp. 1-10, 2017.

[3] A. A. Salih, R. Zulkifli, and C. H. Azhari, "Mechanical and morphological properties of bamboo mesoparticle/nylon 6 composites," International Journal of Materials Research, vol. 110, pp. 130-136, 2019.

[4] A. Mohan Kumar, R. Rajasekar, P. Manoj Kumar, R. Parameshwaran, A. Karthick, and M. Muhibbullah, "Comparative analysis of drilling behaviour of synthetic and natural fiber-based composites," Advances in Materials Science and Engineering, vol. 2021, pp. 1-13, 2021.

ACKNOWLEDGEMENT

The authors would like to express their gratitude and thanks to The Ministry of Higher Education Malaysia and Universiti Kebangsaan Malaysia for funding this research.

Application of Contrastive Learning in rotating machinery fault diagnosis

Wang Jicai, Shahrum Abdullah, Azli Arifin, Salvinder Singh Karam Singh
Department of Mechanical and Manufacturing Engineering, Faculty of Engineering and Built Environment, Universiti Kebangsaan Malaysia,436000 UKM Bangi, Selangor MALAYSIA
Tel: +8615857369615 Email: P126827@siswa.ukm.edu.my

ABSTRACT

To address the low proportion of labeled samples in practical industrial scenarios, this study proposes a semi-supervised learning framework based on a contrastive learning pre-training model. This framework introduces three methods for diagnosing faults in rotating machinery: contrastive learning, modified Gramian Angular Field, and Multi-scale Permutation Entropy. These methods will be tested and validated for their classification performance in experiments involving tool wear image recognition, bearing fault diagnosis, tool condition monitoring and gearbox fault detection.

Keywords: contrastive learning, rotating machinery, fault diagnosis, semi supervised learning, data expansion.

INTRODUCTION

Mechanical equipment is gradually shifting towards largescale, complex, integrated, and intelligent directions. As mechanical equipment becomes increasingly complex and precise, it also increases greater uncertainty and randomness. Mechanical equipment failures, will affect production, cause damage to the equipment and economic losses.

Rotating machinery, as an important part of mechanical equipment, is widely used in the fields of transportation, manufacturing, metallurgy, aviation and other fields(Cheng et al. 2021). Many failures in mechanical equipment are attributed to malfunctions in their rotating machinery. According to statistics, Bearing failures in induction motors account for 42% of the total number of failures(Song et al. 2020).Therefore, Intelligent fault diagnosis of rotating machinery can extend machine operation safety and enhance work efficiency.

In recent years, various machine learning-based methods have been developed for intelligent fault diagnosis, particularly using deep learning (DL) techniques, which have shown significant achievements in diagnosing faults in rotating machinery(Li X et al. 2021). However, these DL-based methods require sufficient labeled training samples to learn the model, which is challenging in many practical industrial scenarios due to the need for extensive experimentation(Wang et al. 2023).

There is a need to develop a classification method capable of learning from limited labeled samples and a large amount of unlabeled samples to enhance the identification accuracy of rotating machinery fault diagnosis under such circumstances.

METHODS

When monitoring of tool wear state in the laboratory, the experimental cost is high, the obtained samples are small and each category accounts for uneven proportion. This study determines a fault image classification based on Contrastive Learning(CL) mothod.

The overall framework of CL is illustrated in Figure 1. It mainly includes four modules: data augmentation module, feature extraction module, multilayer perceptron module, and contrastive loss function module.

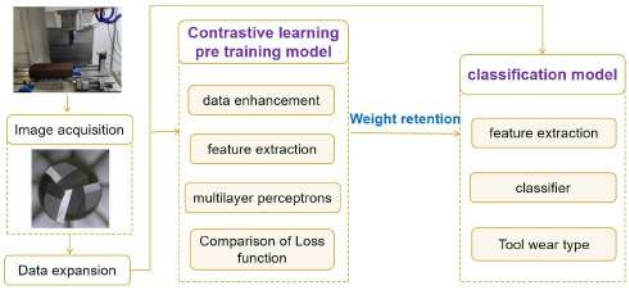

Fig. 1 The flow of fault image classification method based on contrastive learning

The fault vibration signal collected by the sensor has the characteristics of non -linear, non -stability and non -periodic, and cannot intuitively reflect the operating status of mechanical equipment. Therefore, in order to better extract the key features of faults, this study establishes an optimized method based on wavelet transform and Gramian Angular Field-Modify(GAF), as shown in Figure 2. Artificial extraction features to indicate status features, and can directly extract deep features from the conversion 2-D images.

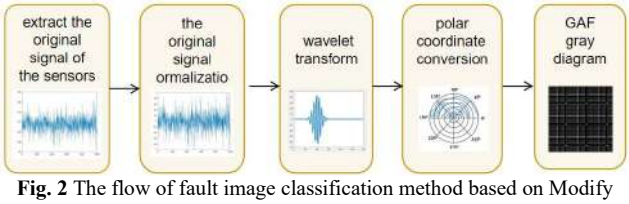

Fig. 2 The flow of fault image classification method based on Modify Gramian Angular Field

This study validates an optimized Multi-scale Permutation Entropy (MPE) algorithm, as shown in Figure 3. This method demonstrates promising results across various rotating machinery fault diagnosis tasks, exhibiting a degree of universality.

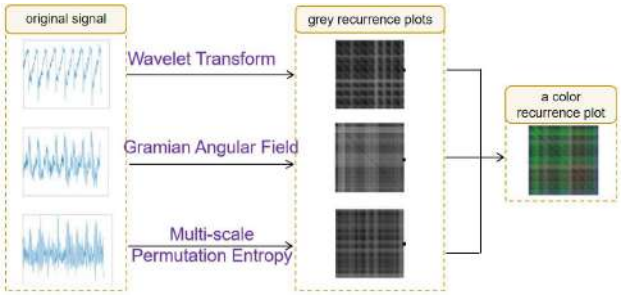

Fig. 3 The flow of fault image classification method based on Multi-scale Permutation Entropy

RESULTS AND DISCUSSION

Taking the example of tool wear image classification based on CL.

In a tool milling experiment, a total of 138 labeled images were obtained, categorized into five types of tool wear. The dataset was augmented (180x), and 200 images from each of the five classes were selected as the test set, with the remainder used as the pre-training dataset. The pre-training data, with labels removed, was input into a CL pre-training model. From the pre-training set, datasets containing 50, 100, 150, and 200 images per class were selected for training, along with the original 200-image test set per class, creating T-50, T-100, T-150, and T-200 datasets. These datasets were then evaluated using CL, ImageNet, and ResNet18 networks. Ten repeated experiments were performed by 4 sample data sets, and the results were taken as shown in Table 1.

Table 1. Results of 3 methods with four sample size datasets

Methods	T-50	T-100	T-150	T-200
CL	**68.62%**	**76.02%**	**80.05%**	**81.30%**
IM	55.12%	63.37%	70.88%	74.54%
Resnet18	48.40%	56.98%	64.69%	69.41%

It can be seen that with the increase of the number of samples, the accuracy of the three methods is increasing. Compared with the other two methods, the CL pre - training method has better classification performance on tool wear image.

CONCLUSION

This study uses rotating machinery as a research object, and is studied with experimental data of tools, gear boxes, and bearings. The CL as the main body of the research has three types of rotating mechanical failure diagnosis methods to solve the fault diagnosis recognition accuracy under the small sample data set. The label samples under the difference and large samples accounted for a relatively low data set. Under the problem that a large number of labels were not applied to improve accuracy. These methods have achieved good results in specific experiments that have low signaling and high - signal -to -noise -ratio, and the wear image data of the experimental failure type. Finally, it is good to propose an optimized MPE algorithm that demonstrates promising results across various rotating machinery fault diagnosis tasks, exhibiting a degree of universality.

ACKNOWLEDGEMENT

The authors would like to acknowledge the financial support from Universiti Kebangsaan Malaysia (GUP-2021-016) and the European Unions's Horizon 2020 research and innovation programme under the Marie Sklodowska-Curie grant agreement No 730888.

REFERENCES

Cheng, Y., Zhu, H., Wu, J., Or, S.W., & Shao, X 2021. Remaining useful life prognosis based on ensemble long short-term memory neural network. IEEE Transactions on Instrumentation and Measurement, 70, 3503912.

Song H.Z., Li L., Yang X.K., et al. Review on Fault Diagnosis and Remaining Life Prediction of High Speed Locomotive Bearings [J]. Bearings, 2020, 3: 61-67.

Li X, Cheng J, Shao H, et al. A fusion CWSMM-based framework for rotating machinery fault diagnosis under strong interference and imbalanced case[J]. IEEE Transactions on Industrial Informatics, 2021, 18(8): 5180-5189.

Wang H.C., Sun W., Sun W.F., et al. A novel tool condition monitoring based on Gramian angular field and comparative learning. International Journal of Hydromechatronics, 2023, 6(2): 93-107.

Thermal shock behavior of ceramics - description using constitutively informed particle dynamics

Mahendaran Uchimali[c,*], Venkatesh Ananchaperumal[a], Srikanth Vedantam[b]
[a]Department of Mechanical Engineering, Clemson University, Clemson, SC, 29631, USA
[b]Department of Engineering Design, Indian Institute of Technology Madras, Chennai, India 600036
[c]School of Mechanical Sciences, Indian Institute of Technology Bhubaneshwar, India
***Corresponding author: mahendaran@iitbbs.ac.in**

ABSTRACT

A coupled thermo-elastic discrete model (Constitutively informed Particle Dynamics (CPD)) is proposed and used to describe the thermal shock behavior of a brittle material. The CPD model is based on a novel multibody interaction which directly incorporates the continuum constitutive response. The initiation and propagation of cracks in quenched ceramic specimens were simulated and the model is able to faithfully reproduce the crack patterns similar to experiments. The resulting crack patterns show a periodical and hierarchical characteristic which is the unique feature of the thermal shock behavior of a brittle material. The present study focuses on the development of the thermo-elastic CPD model and application to thermal shock behavior of ceramic.

Keywords: Discrete Element Model, Constitutively informed particle dynamics, Thermal Crack, Brittle Crack.

INTRODUCTION

Due to excellent thermo-mechanical characteristics, anti-oxidation, and corrosion resistance, ceramics are used in many industries. Brittleness and limited thermal shock resistance make these ceramics susceptible to damage. Given the challenging nature of fracturing processes under thermal shocks, thus theoretical and numerical approaches offer various tools to study thermal crack dynamics over experiments. Classical continuum mechanics, which uses partial differential equations, cannot handle spatial discontinuities. Thus, standard techniques cannot study crack behaviors without adding features to eliminate spatial derivatives.

In contrast, discrete models describe the body as a collection of particles that interact, making discontinuities easy to describe. The primary objective of this work is to develop a discrete model for thermo-elastic behavior through a top-down methodology that effectively tackles the aforementioned constraints, such as limited constitutive behaviors and mesh dependent behaviors. The application of Constitutively Informed Particle Dynamics (CPD) has been utilized to examine the characteristics of shape memory alloys [Uchimali 2022], in which the interactions between particles are determined based on continuum constitutive models. This article proposes a discrete element framework to describe the coupled thermo-elastic behaviors of materials. The proposed model integrates the existing CPD model with a new discrete transient heat transfer model. This study aims to use the developed model to analyze thermal shock behavior of brittle material such as Al_2O_3.

Constitutively informed Particle Dynamics (CPD)

This section provides a concise overview of the top down discrete particle approach for the sake of comprehensiveness.

CPD model for elasticity

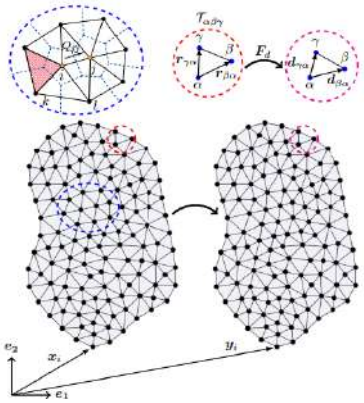

Figure 1 Particles in reference and current configuration. Insets (denoted with same color circles) shows specific triangle in respective configurations and heat flex transfer between Voronoi tile is represented as transfer between particles i and j. Shaded triangle is treated as failed and the particles interaction force is **f** *= 0 zero*

In the CPD model, the initial domain is regarded as a collection of particles that interact with each other. The material contained within the Voronoi tile, which is depicted as an inset with a blue dashed circle in Fig. 1, is considered to be aggregated within a particle denoted as *i*. The equations that govern the motion of the discretized particle i within the given domain is,

$$m_i \frac{\partial^2 \boldsymbol{y}_i}{\partial t^2} + C \frac{\partial \boldsymbol{y}_i}{\partial t} = \boldsymbol{f}_i^{\square} +$$

In the given equation, c denotes the damping coefficient, m_i, y_i and f_i represents the mass, position vector and the interaction force exerted on the particle *i* respectively. The interparticle interaction f_i is defined as the negative gradient of the total energy of the body.

Thermo-elastic model

Thermo-elastic material can be characterized by the free energy in the form ψ(F, θ). Multiplicative decomposition of the deformation gradient is employed to incorporate thermo-mechanical coupling ($F = F_e F_\theta$). The CPD model establishes the discrete deformation tensor (F^d) for particles using triangles. Similarly, the thermal deformation tensor for an isotropic material can be defined for triangles as, $F_\theta^d = \vartheta(\theta)I$, where ϑ is the thermal stretch ratio in any material direction. The temperature of the domain at any instance is evaluated using the heat conduction model. The intermediate particle positions are obtained using the F_θ^d and these intermediate positions are considered to be a reference position for calculations of elastic deformations.

Heat conduction

The heat conduction between the material contained in two adjacent Voronoi tiles is deemed by the CPD to be equivalent to the heat conduction between two particles. Thus heat flux transmitted between particles i and j represents the heat flux between the material in the Voronoi tiles. The heat flux can be obtained from Fourier's law of heat conduction $Q_{ij} = -KA_{ij}(\theta_i - \theta_j)/r_{ij}$, where θ_i and θ_j are the temperature of the particles *i* and *j* respectively, K thermal conductivity of the material, r_{ij} distance between the particles, and A_{ij} is cross sectional area. The time dependent temperature of particles can be obtained from the heat equation,

Results and discussion

Validation - 2D transient heat transfer problem

In this section we perform the heat conduction response only, without considering elastic behavior of the material. A rectangular domain is discretized with 15000 particles is considered at an initial temperature of θ(y, 0) = θ1 = 25◦C and suddenly the temperature of the particles at y = L is increased to θ(L, t) : θ2 = 100◦C. The temperature distribution obtained from simulation agrees well with analytical solutions as shown in Fig.2.

Thermal shock simulation

To simulate the thermal shock event, the temperature of the domain is increased to θ_{high} in small steps and then temperature on the outer boundary is reduced to 25◦C. Other than temperature, the boundary particles are free. Figure 3 illustrates the crack pattern from simulation and experiment. The pattern obtained qualitatively very similar to the experimental observation.

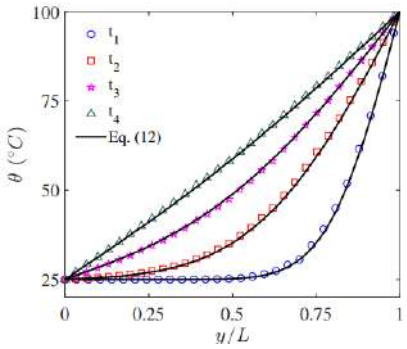

Figure 2 Comparison of the temperature in the domain at four different time instances between analytical and discrete simulation.

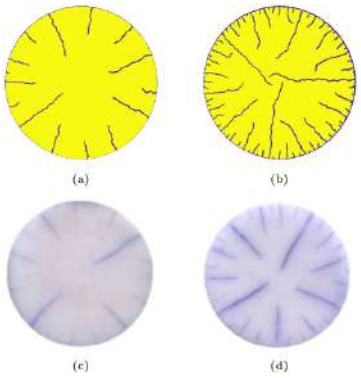

Figure 3 Figure 3: Crack shock crack patterns obtained from simulations (a-d) and experiments (e-h) [Liu 2015] at various temperatures.

Summary

A thermo-elastic coupled model based on the CPD discrete description is developed and applied to simulate the hierarchical crack pattern in a thermal shock response of the brittle material. A numerical scheme is proposed and implemented to solve a transient heat transfer model and approximate the temperature field at every instance. The temperature field was subsequently used in the elastic CPD model to evaluate the strain and stress and it is used to simulate the corresponding crack patterns using brittle failure criteria based on strain energy density. Thermal and elastic properties corresponding to alumina (Al_2O_3) is used in the simulations

REFERENCES

Uchimali, M., Vedantam S., 2022. Modeling stress–strain response of shape memory alloys during reorientation of self-accommodated martensites with different morphologies, Mechanics of Advanced Materials and Structures 29, 6948--6956.

Liu, Y., Wu, X., Guo, Q., Jiang, C., Song, F., Li, J., 2015. Experiments and numerical simulations of thermal shock crack patterns in thin circular ceramic specimens. Ceramics International 41, 1107–1114

Miter Gate Inspired Structure for Anti-Intrusion Beam in Side Collisions

Kho Jia Chyn[1], Wan Fathul Hakim W Zamri[1,*], Fauziana Lamin[2]
[1]Department of Mechanical and Manufacturing Engineering, Faculty of Engineering and Built Environment, Universiti Kebangsaan Malaysia, 43600 Bangi Malaysia.
[2]Vehicle Safety and Biomechanics Research Centre, Malaysian Institute of Road Safety Research, 43000 Kajang, Selangor, Malaysia
*Tel: +60139718837 Email: *wfathul.hakim@ukm.edu.my*

ABSTRACT

Anti-intrusion beam is a passive safety device installed in cars and is mounted on the door panels to protect the passengers during side collision. An arched door beam has been proven to reduce the bending moment by the axial load in the longitudinal direction generated during the deformation to increase the load in the lateral direction. A traditional miter gate structure has a load transfer structure similar to the arched door beam and is anticipated to outperform straight beam structure. Different geometrical variations of miter gate-inspired anti-intrusion beams have been created and simulated in a three-point bending simulation to determine the relationship between different geometrical variations and the reaction force generated. A final design was selected based on reaction force, weight, manufacturing process, and other factors to compare with a traditional straight square beam with similar weight using a drop-weight cylinder pole in a three-point bending setting.

Keywords: Anti-intrusion beam, Crashworthiness, Side collision, Side impact beam, Side impact.

INTRODUCTION

According to Fatality Facts 2021, side collision is the second most prevalent type of vehicle accident death (22%) after frontal collision (59%). In order to reduce the intrusion displacement of the side door into the passenger car, an anti-intrusion beam is installed inside the door panel to absorb the impact energy and reduce the penetration of impacting objects into the passenger compartment during side impact. Hasegawa et al. (2023) developed an arched door beam to reduce the bending moment by the axial load in the longitudinal direction generated during the deformation and to increase the load in the lateral direction. A full car simulation was performed in accordance with the new IIHS MDB test standards, and the results showed that the arched structure can increase the load gradient and reduce body deformation and spine acceleration (Hasegawa et al., 2023). Miter gate is used as navigation lock gates and comprise two rotating leaves with vertical hinge axes, located in the lock chamber walls. In the closed position, the leaves meet at the centre of the lock, supporting one another on the free ends. The angled edges of the gate will form a V-shape joint that will withstand the pressure of the water and form a tight joint. Due to this, the miter gate design motivation was utilized.

Fig. 1 Design of miter gate-inspired beam of 2mm thickness, 2 ribs, and 15° mating angle

A traditional square straight beam with beam length of 900mm, and cross-sectional area of 40mm × 40mm was designed as shown in **Fig 1**. Several geometrical variations such as thickness, the number of ribs, and mating angle were made and the relationship between reaction force generated was investigated using three-point bending simulations.

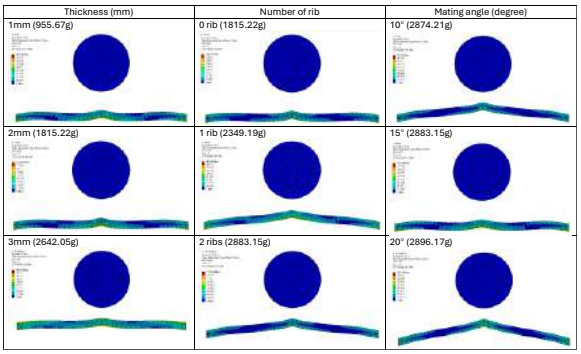

Fig. 2 Von Mises Stress contour of the miter gate-inspired beam with different geometrical variation

The simulation result in **Fig 2** showed that the reaction force increases with increased thickness, the number of ribs, and mating angle. A final design of 2mm thickness, 0 number of ribs, and 15° mating angle was chosen based on reaction force generated, weight, manufacturing difficulty, and other factors.

In a standard side pole impact test, the test vehicle is propelled sideways into the rigid pole at an angle of 75° at 32 km/h. To save the computational time and

resources required, drop weight cylinder impact simulation was conducted on a traditional square beam and miter gate-inspired anti-intrusion beam (Ben et al., 2010 & Erzen et al., 2002). End-clamping was designed for the square beam as it will affect the reaction force generated (Erzen et al., 2002). The mass of the traditional square beam and miter gate-inspired beam are 1851.73g and 1815.22g respectively. The drop height was set as 5000mm with an impact velocity of 7670.7mm/s.

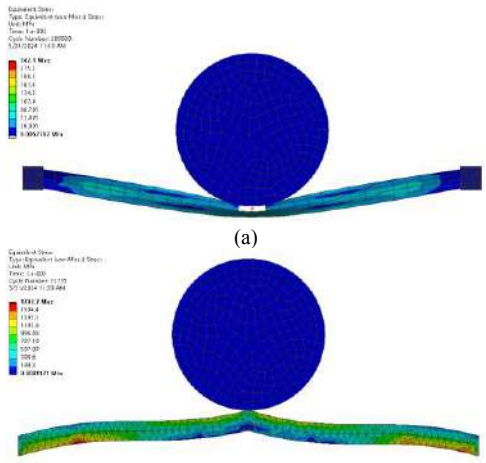

(a)

(b)

Fig. 3 Von Mises stress contour of the beam in cylinder drop weight impact simulations of: (a) traditional square straight beam, (b) miter gate-inspired beam

RESULTS AND DISCUSSION

The reaction force generated in the square beam was 12,475N whereas in the miter gate-inspired beam it was 165,750N. The reaction force generated in the miter gate-beam was almost 13 times higher than that of the square beam. The plastic hinge was formed at the centre of the square beam at the early stage of the drop weight pole impact, followed by a decrease in load sustainability capacity (Pedro Rebelo, 2016). Whereas in the case of a miter gate-inspired beam, no visible plastic hinge was formed. The displacement in the bending direction of the miter gate-inspired beam was 70.75mm, 17% smaller than the 85.61mm displacement for the traditional square beam. According to Baroutaji et al. (2017), under the bending moment, the deformation of a thin-walled structure begins with a local indentation at the point of loading. This was followed by the global bending of the tube, caused by a significant in the cross-sectional area at the loading point, this explains the weaker bending load in the square straight beam. Whereas in a miter gate-inspired beam, part of the bending load at the centre was transformed into axial load towards the two ends. Since the axial load yield 5 times greater mean crush force than the bending load (Baroutaji et al., 2017), this explained for the much greater reaction force that can be generated in the miter gate-inspired beam.

CONCLUSION

In terms of reaction force generated and intrusion displacement of the beam when subjected to a dropped cylinder at the centre, the miter gate-inspired beam performed better than the square beam by 1230% and 17% respectively. However, the extraordinary performance of the anti-intrusion beam comes at the expense of weaker performance under off-center loading conditions.

REFERENCES

Atsushi Hasegawa, Yasuhisa Egawa, Takuro Nisida, Kengo Kishida, Yoshihiro Fujimura, Ryotaro Takeuchi, Hitomi Yamada, Takayuki Fujii & Yumi Saito (2023) New load transfer structure to reduce body deformation in side collisions, Traffic Injury Prevention, 24:sup1, S68- S74.

Baroutaji, Ahmad & Sajjia, Mustafa & Olabi, Abdul Ghani. 2017. On the crashworthiness performance of thin-walled energy absorbers: Recent advances and future developments. Thin-Walled Structures. 118. 137-163.

Ben, Goichi & Sugimoto, Nao & Aoki, Yoshio. (2010). Development of Simulation Technology for Impact Behavior of CFRP/Al Alloy Hybrid Beams in Side Collision of Automobiles. Advanced Composite Materials - ADV COMPOS MATER. 19. 363-379.

Erzen S., Ren Z. & Anzel I. 2002. Analysis of FRP side-door impact beam. In Proceedings of the 2nd IMechE Automobile Division Southern Centre Conference on Total Vehicle Technology, How Do We Get The Innovation Back Into Vehicle Design? (pp. 109–120).

Fatality Facts 2021 Passenger vehicle occupants. Insurance Institute for Highway Safety (IIHS). Passenger vehicle occupants.

Pedro Mota Rebelo. 2016. Design Study of a Side Intrusion Beam for Automotive Safety.

ACKNOWLEDGEMENT

The authors would like to thank the Ministry of Higher Education (MOHE) of Malaysia for supporting this study through the Fundamental Research Grant Scheme (FRGS), No. FRGS/1/2022/TK09/UKM/02/31

K-Means Clustering of Road Surface Conditions using Wavelet-based Vibration Parameters

C.H. Chin[1, 2, *], S. Abdullah[1, 2], A.K. Ariffin[1, 2], S. S. K. Singh[1, 2]
[1] Department of Mechanical and Manufacturing Engineering, Faculty of Engineering & Built Environment, Universiti Kebangsaan Malaysia, 43600 UKM Bangi, Selangor, Malaysia.
[2] Computational and Experimental Mechanics (CEM) Research Group, Universiti Kebangsaan Malaysia, 43600 UKM Bangi, Selangor, Malaysia.
Tel: +60389118406 Email: chuinhaochin@ukm.edu.my

ABSTRACT

This study presents a clustering method for wavelet-based vibration parameters of a car suspension system to classify road surface conditions. Various vibration signals from the suspension system were collected under different road conditions. The wavelet transform was applied to determine the multifractality and low-frequency singularity spectral energy of the vibration data. Next, the K-means clustering method was employed to classify road conditions using the wavelet-based vibration parameters. The results show that the vibration parameters of rural roads exhibited distinctive wavelet parameters, with very high multifractality and spectral energy values. In contrast, highways with smooth surface profiles showed much lower values of these vibration parameters. The K-means clustering method segregated the data points into three clusters. Cluster 1, which represents a smooth surface profile, is mainly composed of data points from highways. All data points from rural roads are included in Cluster 2, representing rough surface profiles. Most data points from industrial and campus roads fall within Cluster 3 because these roads exhibited similar vibration behaviours. It can be concluded that K-means clustering is effective for classifying road conditions based on the vibration parameters.

Keywords: K-means clustering, Vibration signal, Multifractality, Spectral Energy, Wavelet transform

INTRODUCTION

Random road excitations significantly contribute to the fatigue failure of suspension components in ground vehicles, such as coil springs and lower control arms. The vibrations experienced by the suspension system are highly influenced by the road surface conditions. Researchers have focused on profiling road surfaces to classify these conditions and assess the resulting fatigue damage. However, this profiling often requires expensive equipment and extensive experimentation time. Therefore, a more convenient method for characterizing road surface conditions is necessary (Tomiyama et al. 2022).

In the study by Chin et al. (2023), the continuous wavelet transform (CWT) was used to extract singularities from the vibration loading histories of coil springs. It was found that the low-frequency features represented by these singularities significantly contribute to high fatigue damage. The wavelet theory is also suitable for integration with multifractal analysis. The wavelet leaders (WL) method is a new multifractal analysis technique developed from the discrete wavelet transform (DWT) that offers high computational efficiency compared to other multifractal analyses (Komorska & Puchalski 2021). In signal processing, multifractality often relates to the complexity of a signal composed of different fractals with various scaling properties. For automotive applications, road surface profiles naturally exhibit multifractal properties depending on their condition. Thus, the multifractal properties of road excitations are used as a parameter for predicting the durability of suspension components.

This study proposes characterising road surface conditions using wavelet-based singularity spectral energy and the multifractal properties of vibration signals. The methodology includes acquiring signals via road tests, Hölder singularity spectral energy analysis of the vibration signals, wavelet leader multifractal analysis, and k-means clustering of the wavelet-based vibration properties. This study contributes to classification of the road conditions based on the multifractal properties and spectral energy of road excitations.

RESULTS AND DISCUSSION

In this study, road tests were conducted on various road conditions, including an industrial area, a university campus, a highway, and a rural area, to obtain the vibration signals of the suspension system caused by road excitations. Fig. 1 illustrates examples of vibration signals under different road conditions. Among these conditions, the rural road had the highest amplitude cycles due to its rough surface profile. In contrast, the highway had a smoother surface profile and thus the vibration is relatively low. The university campus and industrial roads had some bump events, which caused some spikes in the vibration signals.

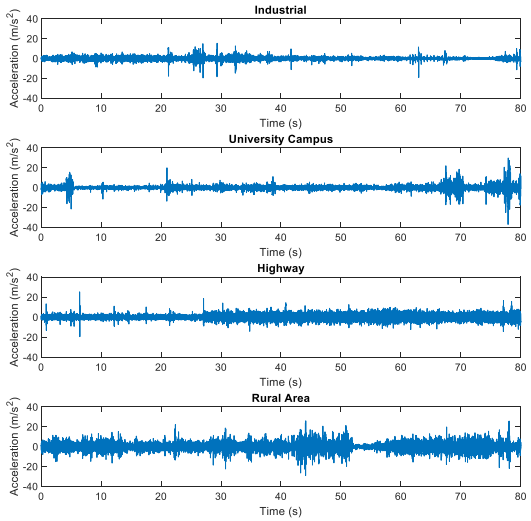

Fig. 1 Vibration signals obtained from various road conditions: (a) Industrial area, (b) University campus, (c) Highway, (d) Rural area

Fig. 2 shows the data scattering of the vibration parameters for different road conditions. The K-means clustering method was used to segregate the wavelet-based vibration parameters, including singularity spectral energy and multifractality. The data from the rural area exhibited distinctive behaviours with very high values of multifractality and spectral energy, due to the rough surface profile of the rural roads. Meanwhile, the highway data points are characterised by low values of multifractality and spectral energy.

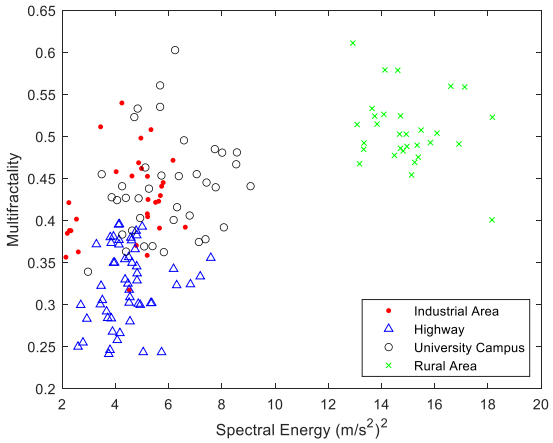

Fig. 2 Data scattering of multifractality and singularity spectral energy of different road conditions.

Fig. 3 shows the clusters of the vibration parameters obtained using the K-means clustering method. It was found that the rural area data points formed Cluster 2 due to their distinctive behaviours, thus representing a rough surface profile. Cluster 1, which represents a smooth surface, is mainly composed of data points from the highway. The roads of the university campus and industrial area did not exhibit significant differences in their surface behaviours, and their data points fall under Cluster 3. The K-means clustering method is found to be an effective approach for classifying road conditions based on vibration parameters.

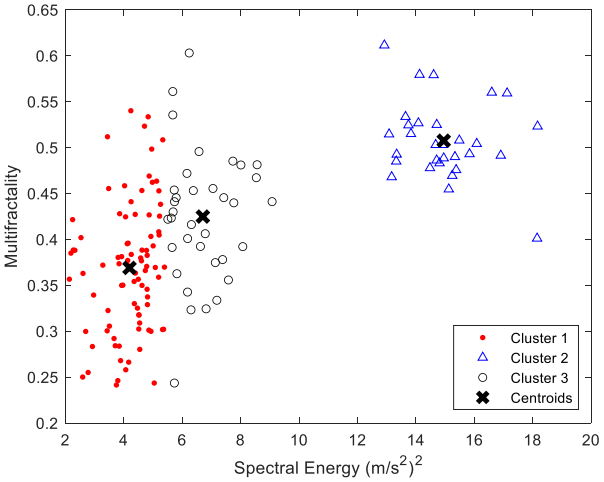

Fig. 3 Clustering of vibration parameters under different road conditions

CONCLUSION

This study utilised the K-means clustering method to classify road conditions using the wavelet-based vibration parameters. The wavelet analysis was performed to determine the multifractality and singularity spectral energy of vibration signals acquired from different roads. It was found that the data points were separated into three clusters representing smooth, intermediate, and rough road surface profiles. This demonstrates that the K-means clustering method is an effective and convenient tool for classifying different types of roads.

REFERENCES

Chin, C.H., Abdullah, S., Singh, S.S.K., Ariffin, A.K. & Schramm, D. 2023. Fatigue Life Modelling of Steel Suspension Coil Springs Based on Wavelet Vibration Features Using Neuro-Fuzzy Methods. *Materials* 16(6).

Komorska, I. & Puchalski, A. 2021. Rotating Machinery Diagnosing in Non-Stationary Conditions with Empirical Mode Decomposition-Based Wavelet Leaders Multifractal Spectra. *Sensors* 21(22).

Tomiyama, K., Yamaguchi, Y., Moriishi, K. & Kotani, Y. 2022. Development of a validation technique for road surface profile applicable to point cloud data. *Journal of Road Engineering* 2(2): 114–123.

ACKNOWLEDGEMENT

The authors would like to acknowledge the financial support from Ministry of Higher Education Malaysia and Universiti Kebangsaan Malaysia through the research grant no. FRGS/1/2023/TK10/UKM/01/3; and the European Unions's Horizon 2020 research and innovation programme under the Marie Sklodowska-Curie grant agreement No 730888.

Numerical study of back-to-back gapped built-up cold-formed steel of C-channel with long bolted connection in trusses system

Muhammad Khairuddin Zulkifli, Shahrizan Baharom
Civil Engineering Department, Faculty of Engineering & Built Environment, Universiti Kebangsaan Malaysia, Postal code: 43600 Malaysia
Tel: +60138536523 Email: mkhairuddinz1295@gmail.com

ABSTRACT

Back-to-back gapped built-up cold-formed steel (CFS) trusses subjected to a three-point bending experiment were investigated in this study through comprehensive finite element analysis (FEA) using ABAQUS. The results of the analysis demonstrated that the validated model was in close agreement with the experimental data, showing moment-capacity ratios between the experimental and finite analysis data ranging between 1.00 and 1.06. The findings from the parametric studies emphasized that increasing the bolt diameter from M12 to M20 resulted in a reduction in deflection by 7-13% without significantly impacting the moment capacity. Additionally, it was observed that incorporating long bolts within the diagonal members to prevent early buckling led to an improved performance. Specifically, the addition of one bolt resulted in a 1.6% increase in the moment capacity, whereas the addition of two bolts led to a 13.2% improvement. However, the inclusion of a third bolt did not yield any further benefit. These observations underscore the pivotal role that bolt and diagonal member configurations play in enhancing the structural performance of CFS trusses.

Keywords: ABAQUS, Back-to-back gapped built-up, Cold-formed steel, Long bolted, C-spacer

.

INTRODUCTION

Cold-formed steel (CFS) sections are being chosen more frequently for construction since these section offer the benefits of being lightweight, formability in design and high strength which makes it appropriate for use as roof trusses, joists and columns for light to medium load bearing applications. Their slender nature, however, also makes them susceptible to buckling and therefore it is necessary that they are extensively investigated for studying their performance under various loading conditions and with different configurations. This study focuses on the buckling strength, ultimate capacity, and overall behavior of built-up CFS columns, particularly those configured in back-to-back lipped channel sections made from multiple C-profiles. Existing design codes often fall short in addressing the complex buckling behavior of these sections.

Previous studies have explored various aspects of these back-to-back gapped built-up columns. Crisan et al. (2014) calibrated design formulas for buckling strength and validated numerical models with experimental data. Vijayanand and Anbarasu (2017) examined the effect of spacers on the ultimate strength using finite element analysis (FEA) to compare their findings with the Direct Strength Method (DSM) and Effective Width Method (EWM). Dubina D. and Zaharia (1997) investigated the nonlinear behavior and axial capacity of gapped built-up CFS channel sections, while Anbarasu et al. (2020) and Roy et al. (2020) studied the axial and flexural capacities of these columns with spacers and web stiffeners, respectively.

These studies employed advanced numerical simulations and parametric analyses to evaluate factors such as slenderness ratio, connector spacing, and cross-sectional dimensions, providing valuable insights into the structural efficiency and safety of built-up CFS columns.

RESULTS AND DISCUSSION

The finite element (FE) model using ABAQUS 2020 was validated against experimental results for back-to-back gapped built-up cold-formed steel (CFS) trusses under three-point bending, showing good agreement with experimental tests (Figure 1). A parametric study was conducted with the validated FE model to examine the effects of varying bolt diameters and the inclusion of long bolts in diagonal members on moment capacity and deflection.

The parameter study on bolt sizes from M12 to M20 had minimal impact on moment capacity as shown in Figure 2 (a). However, increasing bolt diameter reduced deflection at the ultimate moment by 7% to 13%, enhancing structural stiffness without improving load-bearing capacity.

The FE analysis shown in Figure 2 (b) of long bolts in diagonal members assessed configurations with one, two, and three long bolts. Adding one long bolt increased moment capacity by 1.6%, while two long bolts significantly boosted it by 13.2%. A third bolt did not further enhance capacity, indicating two bolts were sufficient to prevent local buckling (Figure 3).

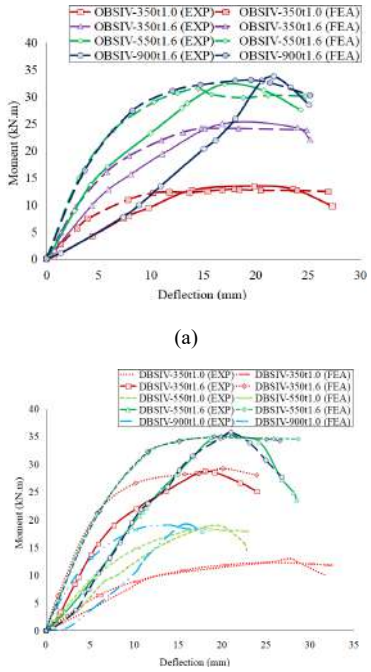

(a)

(b)

Fig. 1 Moment-deflection curve validation: (a) One bolt system truss, (b) Two bolt system truss

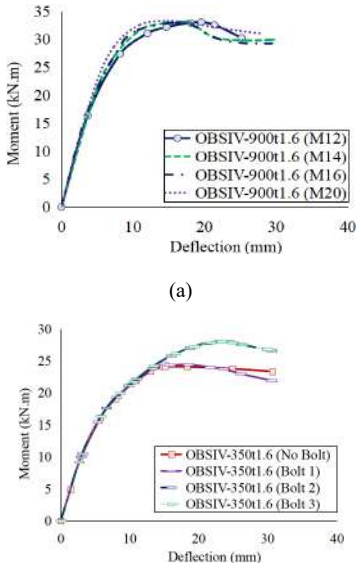

(a)

(b)

Fig. 2 Moment-deflection curve of truss with parameter: (a) Bolt size, (b) Bolted connection at truss diagonal member

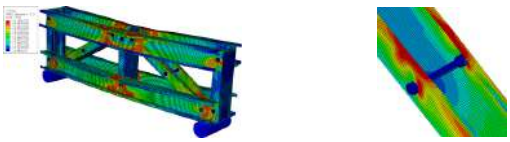

(a)

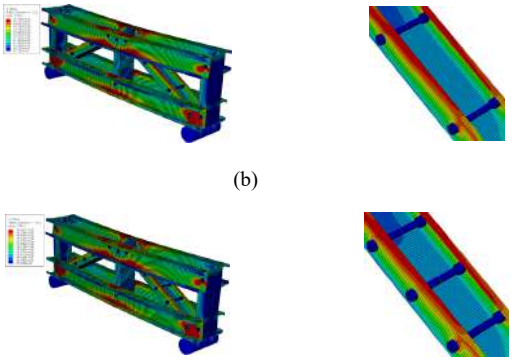

(b)

(c)

Fig. 3 Failure mode finite analysis of truss OBSIV-350t1.6: (a) Bolt 1, (b) Bolt 2, (c) Bolt 3

CONCLUSION

The finite element analysis validated against experimental results, demonstrated that the FE model reliably predicts the behavior of back-to-back gapped built-up CFS trusses under three-point bending. The parametric study revealed that increasing bolt diameter reduces deflection, while adding long bolts to diagonal members significantly enhances moment capacity up to a certain point. This insight can guide the design and optimization of CFS trusses for improved structural performance.

REFERENCES

Anbarasu, M. and Dar, M.A., 2020. Axial capacity of CFS built-up columns comprising of lipped channels with spacers: Nonlinear response and design. Engineering Structures, 213, p.110559.

Dubina, D. and Zaharia, R., 1997. Cold-formed steel trusses with semi-rigid joints. *Thin-Walled Structures*, 29(1-4), pp.273-287.

Roy, K., Lau, H.H., Ting, T.C.H., Chen, B. and Lim, J.B., 2020. Flexural capacity of gapped built-up cold-formed steel channel sections including web stiffeners. *Journal of Constructional Steel Research*, 172, p.106154.

Vijayanand, S. and Anbarasu, M., 2017. Effect of spacers on ultimate strength and behavior of cold-formed steel built-up columns. *Procedia engineering*, 173, pp.1423-1430.

ACKNOWLEDGEMENT

The author sincerely thanks the Ministry of Higher Education of Malaysia and Universiti Kebangsaan Malaysia for their financial support through grants DIP-2021-010 and TAP-K012430. Additionally, the author appreciates Ajiya Berhad, Malaysia, for providing the test specimens.

Experimental and Modeling of Tribological Behavior of Rare Earth Oxide Mediated Mg nanocomposites

Surja Deka[a*], Farzin Mozafari[b], Ashis Maliick[a]
[a]Department of Mechanical Engineering, IIT (ISM) Dhanbad, Jharkhand, 826004, India
[b]Department of Mechanical Engineering, Abdullah Gül University, Kayseri, 38080, Turkey

Tel: +919127581202 Email: surjadeka@gmail.com

ABSTRACT

Magnesium-based materials have experienced increased utilization in the automotive, aviation, and marine industries due to their lightweight attributes, possessing high specific strength, and exhibiting resilience to impact and wear. This study aims to examine the impact of rare earth oxide nanoparticles (CeO_2) on the tribological characteristics of pure magnesium. The Mg/CeO_2 nanocomposites were synthesized by an in-situ hot extrusion-based powder metallurgy process. Reciprocating wear tests were conducted on the nanocomposites under different loads of 5, 9, and 13N on a universal tribometer. The findings revealed that the incorporation of reinforcement has significantly enhanced the wear resistance of the nanocomposites. The wear rates of Mg/0.5CeO_2, Mg/1.0CeO_2, and Mg/1.5CeO_2 decreased by 9.65%, 18.22%, and 27.45%, respectively, in comparison to pure Mg at 5N. In order to comprehend this enhancement, an examination of the wear mechanisms of the worn-out surface was conducted using FESEM analysis. Furthermore, a machine learning framework based on a feedforward neural network has been developed to characterize the wear characteristics of nanocomposites. The trained network successfully replicates the wear behavior of nanocomposites with high accuracy.

Keywords: Mg nanocomposite, Wear, Machine Learning.

INTRODUCTION

Magnesium alloys possess a distinctive blend of characteristics, including a high strength-to-weight ratio, outstanding machinability, excellent vibration dampening, ease of recyclability, and high dimensional stability. Nevertheless, these alloys suffer from inadequate mechanical qualities, such as low hardness, and limited wear resistance, which restrict their application Bharathi et al. (2022). Studies have shown that Mg-based metal matrix nanocomposites when reinforced with various nano-particles, can have mechanical and tribological capabilities that are equal to or even better than Mg alloys or similar composites that have higher amounts of micron-sized reinforcements. For instance, Raghav et al. (2018) conducted a study where they studied the effect of nano reinforcement on the wear behavior of Mg and reported that CO nanoparticles offer improved wear behavior of Mg. Lim et al. (2005) investigated the dry sliding wear behavior of pure magnesium that was strengthened with nano-sized alumina particles at a volume fraction of up to 1.11%. The nanocomposites showed enhanced wear resistance as the volume % of reinforcement increased. Machine learning (ML) techniques have recently become progressively important in tribology research, providing valuable insights into wear behavior and the ability to estimate tribological characteristics. Machine Learning (ML), a subdivision of artificial intelligence, empowers machines to acquire knowledge from data, identify patterns, and provide forecasts without the need for explicit programming. A recent study conducted by Aydin et al. (2023) showed the effectiveness of machine learning (ML) on a limited dataset consisting of 60 experimental data points. Their investigation demonstrated the reasonable accuracy of various machine learning regression models in forecasting the rate of wear.

This work aims to enhance our understanding of the elements that influence the tribological properties of the Mg/CeO_2 nanocomposite. This will enable us to provide an analytical foundation for assessing the wear behavior and mechanisms under various wear circumstances. In addition, machine learning algorithms were created to predict the wear performance of the samples.

RESULT AND DISCUSSION

The tribological features of Mg/CeO_2 nanocomposites with different reinforcement concentrations were evaluated using a reciprocating wear test. The test was conducted under applied loads of 5, 9, and 13 N. Fig. 1 illustrates the worn track's 3D profilometer imaging and FESEM micrographs at 5N load. The wear rates of all the samples are tabulated in Table 1. According to the data in Table 1, it is evident that higher levels of reinforcing content in the nanocomposites led to a decrease in the wear rate identified in the samples. This effect arises as a result of the existence of reinforcing particles in the Mg matrix, as well as their proper bonding and distribution.

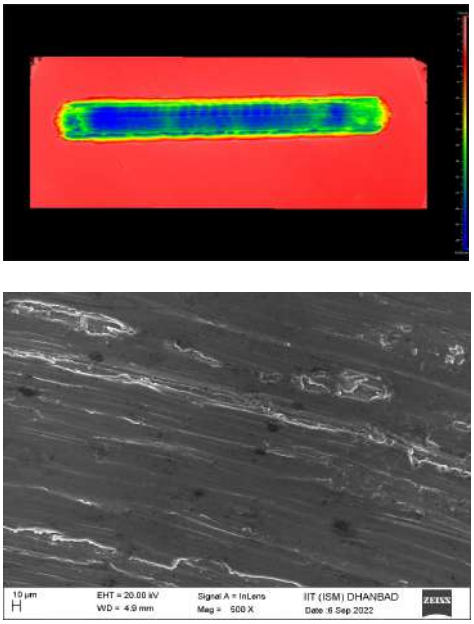

Fig. 1 3D profilometer image and FESEM micrographs of the worn track of pure Mg at 5N.

Table 1: Wear rate values of pure Mg, and Mg/CeO_2 nanocomposites

	Wear rate * 10^{-3} (mm^3/m)			
Load	Pure Mg	Mg/0.5CeO_2	Mg/1.0CeO_2	Mg/1.5CeO_2
5	9.45	8.49	8.42	7.61
9	12.46	12.34	11.97	11.62
13	16.68	15.07	13.64	12.10

Wear modeling of Mg/CeO_2 nanocomposites:

A machine learning (ML) framework has been built that utilizes feedforward neural networks to accurately predict the wear behavior of Mg/CeO_2 nanocomposites (Fig. 2). An imputation technique was employed to estimate and fill in missing data since it helps to increase the sample size, reduces bias, preserves the connections between variables, consequently, allows thorough analysis, and improves interpretability. It's crucial to emphasize that wear experiments have shown that the applied load and volume fraction significantly affect the wear properties of Ultrafine Mg/CeO_2. To address this sensitivity, a feedforward network includes a single input layer with two independent input features. The network has two hidden layers, each with 10 perceptrons using the hyperbolic tangent sigmoid transfer function, which provides non-linearity and smooth activation. The output layer, with a single cell, uses a linear transfer function to produce the normalized wear rate.

Table 2 illustrates the successful prediction of the wear rate of Mg/CeO_2 by the proposed feedforward network. This prediction is based on the input properties of applied load and CeO_2 nanoparticle volume fraction. The network has undergone training using a comprehensive dataset, which has allowed it to comprehend the complex connections between these characteristics and the related rates of wear.

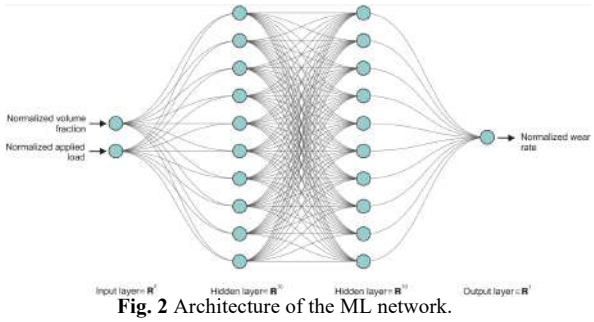

Fig. 2 Architecture of the ML network.

Table 2: Comparison of wear rates between experimental and ML approach. EXP means experiment.

Wear rate * 10-3 (mm3/m)								
Load	Pure Mg		Mg/0.5CeO2		Mg/1.0CeO2		Mg/1.5CeO2	
	EXP	ML	EXP	ML	EXP	ML	EXP	ML
5	9.45	9.85	8.49	9.24	8.42	9.15	7.61	8.40
9	12.46	13.02	12.34	12.11	11.97	11.46	11.62	10.55
13	16.68	16.17	15.07	14.98	13.64	13.77	12.10	12.70

CONCLUSION

This work examined the tribological characteristics of ceria-reinforced Mg nanocomposites developed utilizing the powder metallurgy approach. The results showed that nanocomposites had significantly higher wear resistance than monolithic Mg. Furthermore, feedforward neural networks were able to accurately anticipate the wear behavior of nanocomposites.

REFERENCES

Bharathi, M.L., Rag, S.A., Chitra, L., Ashick, R.M., Tripathi, V., Kumar, S.S., Al Obaid, S., Alfarraj, S., Murugesan, M. & Raghavan, I.K. 2022. Investigation on wear characteristics of AZ91D/nanoalumina composites. *Journal of Nanomaterials*, 1: 2158516.

Raghav, G.R., Balaji, A.N., Muthukrishnan, D., Sruthi, V. & Sajith, E. 2018. An experimental investigation on wear and corrosion characteristics of Mg-Co nanocomposites. *Materials Research Express*, *5:*066523.

Lim, C.Y.H., Leo, D.K., Ang, J.J.S. & Gupta, M. 2005. Wear of magnesium composites reinforced with nano-sized alumina particulates. *Wear*, *259*: 620-625.

Aydin, F., Durgut, R., Mustu, M. & Demir, B. 2023. Prediction of wear performance of ZK60/CeO2 composites using machine learning models. *Tribology International*, *177*: 107945.

Comparison on axial compressive behavior of different types of cementitious mortars incorporated with silica fume

S. M. Priok Rashid[a], Hassan Amer Algaifi[b], Shahrizan Baharom[a,*], A.B.M.A. Kaish[a]
[a]*Department of Civil Engineering, Universiti Kebangsaan Malaysia (UKM), Bangi 43600, Selangor, Malaysia*
[b]*Institute of Energy Infrastructure (IEI), Universiti Tenaga Nasional, Jalan IKRAM-UNITEN, Kajang 43000, Malaysia*
Tel: +60123689016 Email: shahrizan@ukm.edu.my

ABSTRACT

Concrete, being the most commonly used building material has been seriously affected by high cost of ingredient materials. Concrete is a highly complex, heavy and heterogeneous composite material. In contrast, mortar is better than concrete for applications requiring good workability, proper bonding, lightweight, and flexibility etc. At present, researchers from all over the world are conducting their research with different types of mortar because it is found to be more sustainable cementitious system than concrete. The compressive strength of cement mortar plays a fundamental role in the design and construction of the structures. The objective of this research was to develop economical, structurally effective, and practically applicable mortar which could be applied in different building structures such as beams, columns, wall panels etc. Three different types of mortars were prepared to compare their effectiveness on various kind of structures. Control mortar, rubberized mortar and steel fiber reinforced mortar was used in this research to evaluate their axial compressive behavior. The target strength was 35 MPa for 28 days for all types of mortars. Total 18 cubes (100×100×100 mm) were prepared to examine their compressive strength at 7 and 28 days. Results showed that steel fiber reinforced mortar had higher compressive strength while comparing with control and rubberized mortar. Neglecting the self-weight of steel fiber reinforced mortar, it was found to be more practical to use in the building structures.

Keywords: Compressive strength, Mortar, Crumb rubber, Steel fiber, Silica fume.

INTRODUCTION

For the manufacturing of concrete and mortar, Portland cement (PC) is still the primary binder material. As a result, enormous amounts of cement were produced each year. Unfortunately, cement manufacture is caused by high CO_2 emissions and high material and energy consumption. Each year, the cement industry uses 12–15 percent of all global industrial energy resources. The primary cause of global warming, which essentially affects climate change, is increased CO_2 emissions. By 2050, CO_2 levels in the atmosphere may reach 450–550 parts per million, resulting in hazardous droughts, wildfires, a rise in sea level, and an increase in the global average temperature of 1.4–5.8 °C food shortages for millions of people. The cement industry emits not only CO_2 but also NO_x and SO_3, which contribute to acid rain and health problems. Blended cement or non-Portland cement can be utilized to solve the challenges caused by the PC industry (Kaplan et al. 2021).

Cementitious mortars with exceptional specifications could be achieved by the use of a low water-binder ratio (w/b), incorporation of silica fume (SF) for its positive pozzolanic reactions and improvement in packing between cement particles, the addition of high-range water-reducing admixtures to facilitate flow, and the application of heat treatment. Because high strength is accompanied by an increase in brittleness, the use of steel fiber leads to enhancement in ductility of these materials.1-4 In fact, the addition of steel fibers to these types of steel fiber reinforced mortars (SFRMs) can make an essential contribution to ensure mechanical adhesion after crack initiation and decrease the microcrack development due to autogenous shrinkage. High-strength SFRM with superior properties could be used in many structural applications, such as prestressed and precast concrete members exposed to high loading conditions, highway bridges, rehabilitation and retrofitting of some concrete structures, and structures exposed to harsh environments such as marine and sewage (Noori et al. 2015).

Algaifi et al. (2023) experimented with rubberised cementitious material which has gained significant attention within the civil engineering community. Focusing on green concrete, rubberised concrete is one of the environmentally friendly materials that were investigated in this present literature. Compared to conventional concrete, it contains crumb rubber, as the partial replacement of either fine or coarse aggregate. Indeed, the reputation of rubberised concrete is rapidly increasing in the civil engineering community in recent years. This is attributed to the fact that reusing discarded rubber in concrete does not only provides an alternative aggregate source, but reduces landfill and tackles the associated health problems induced by burning rubber (Mhaya et al. 2021)

A brief overview of existing literature indicates that there is a lack of studies comparing the effects of same strength with different materials on performance of mortars especially on the compressive strength characteristics with and without silica fume. In this study, the behavior of SFRM and rubberized mortar made by steel fibers and crumb rubber under compression is investigated, and results are compared with a common control mortar.

MATERIALS AND METHOD

Locally available Tasek Ordinary Portland cement (OPC) CEM I 42.5 N was used. Normal coarse sand was used as fine aggregate. Silica fume was used as pozzolanic material to increase the strength. RPF RAPIDCAST was used as superplasticizer to improve the workability of the mortar.

Hook end steel fibers were used in this research. It's length and diameter were 60 mm and 0.75 mm. Crumb rubber was collected from recycled waste tires after end-of-life service. Both shredders and shearing instruments were used to cut the discarded tyres into small fragments, followed by granular production using the micro-mill process. The maximum size of the crumb rubber particle was found to be 1.0 mm.

Three different types of mortars such as control mortar, rubberized mortar, and steel fiber reinforced mortar was prepared to achieve the desire strength. The target strength was 35 MPa for 28 days for all type of mortars. 18 cubes were prepared. The cubes were tested under Universal testing machine as shown in Fig. 1.

Fig. 1. Testing of the cubes

RESULTS AND DISCUSSION

The compressive strength of Control mortar, rubberized mortar and steel fiber reinforced mortar for 7 days is presented in Table 1.

Table 1. Compressive strength of the mortars

Mortar	Compressive strength (MPa)
Control mortar	20.5
Rubberized mortar	21.03
SFRM	22.47

CONCLUSION

The results were found to be satisfactory aligning with the objective of this research. SFRM showed better performance among all different types of mortars. The construction of structures using SFRM could improve their service life with minimal maintenance requirements. SFRM seems to be a promising material in the construction of bridges, offshore structures, prestressed concrete, and the structural elements subjected to lateral forces such as wind and earthquakes.

REFERENCES

Algaifi, H.A., Syamsir, A., Baharom, S., Alyami, M., Al-Fakih, A.M. and Anggraini, V., 2023. Development of rubberised cementitious material incorporating graphene nanoplatelets and silica fume. *Case Studies in Construction Materials*, *19*, p.e02567.

Kaplan, G., Bayraktar, O.Y. and Memis, S., 2021. Effect of high volume fly ash and micro-steel fiber on flexural toughness and durability properties in self-compacting lightweight mortar (SCLM). *Construction and Building Materials*, *307*, p.124877.

Mhaya, A.M., Huseien, G.F., Faridmehr, I., Abidin, A.R.Z., Alyousef, R. and Ismail, M., 2021. Evaluating mechanical properties and impact resistance of modified concrete containing ground Blast Furnace slag and discarded rubber tire crumbs. *Construction and Building Materials*, *295*, p.123603.

Noori, A., Shekarchi, M., Moradian, M. and Moosavi, M., 2015. Behavior of steel fiber-reinforced cementitious mortar and high-performance concrete in triaxial loading. *ACI Materials Journal*, *112*(1), p.95.

ACKNOWLEDGEMENT

The authors would like to express their gratitude and thanks to Universiti Kebangsaan Malaysia for funding this research under the Young Researchers Grant Scheme (Please include the project code).

Numerical Simulation and Experimental Study of Mechanical Properties of Aluminum Foam at High Strain Rate Using Split Hopkinson Pressure Bar

Afdhal[1], Leonardo Gunawan[2], Ahmad F. Muzammil[1], Sigit P. Santosa[1]
[1]*Solid Mechanics and Lightweight Structures Research Group*
[2]*Dynamics and Control Research Group*
Faculty of Mechanical and Aerospace Engineering, Institut Teknologi Bandung
Jl. Ganesha 10, Bandung 40132, Indonesia
Email: l.gunawan@itb.ac.id

ABSTRACT

Aluminum foam is a material with a large energy absorption capability, making it suitable for many engineering applications. The use of aluminum foam has increased in recent years due to its advantages, particularly in structural design for crashworthiness and blastworthiness. Evaluating its energy absorption capability requires understanding its mechanical properties, especially at high strain rates. In this work, the mechanical properties of aluminum foam are modeled using results from Split Hopkinson Pressure Bar (SHPB) tests. Curve fitting of the stress-strain relationship obtained from SHPB tests was performed to derive material parameters for numerical simulations. Geometry models developed by Santosa et al., including solid cylinder and cruciform shapes, were used, while Deshpande-Fleck Foam and Linear Piecewise Plasticity were used as material models. The results were then compared to experimental results to identify the best model. It was shown that the Deshpande-Fleck Foam model with the solid cylinder geometry provided the best results compared to other models.

Keywords: Aluminum foam, SHPB, Numerical simulation, Energy absorption.

INTRODUCTION

Aluminum foam is a type of metal foam widely used in automotive, aerospace, and many other applications. It has good energy absorption characteristics because it can be plastically deformed on a large scale due to a fairly long plateau stress, as shown in Fig. 1. Its low density, with cavities at certain porosity levels, makes aluminum foam lighter. Additionally, this material is easy to recycle, making it more environmentally friendly.

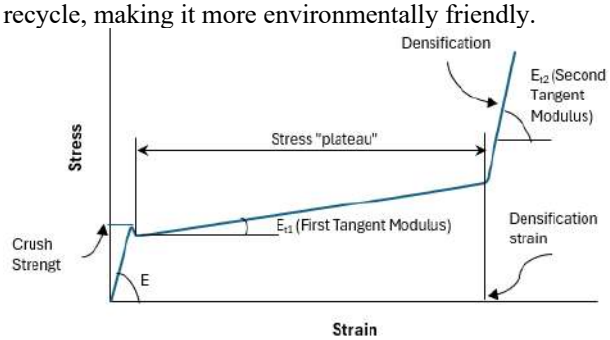

Fig. 1 Mechanical response of aluminum foam for compressive load (Ashby, MF et al., 2000)

The use of aluminum foam has increased in recent years due to its advantages, particularly in structural design for crashworthiness and blastworthiness to reduce fatalities. The Lightweight Structures Laboratory has been using aluminum foam in crash box foam-filled for crashworthiness applications (Dirgantara, T. et al. 2018). Information about material properties at high strain rates (500 – 10^4/s) is needed to support the design of structures that experience high strain rate loading.

In this work, experiments to obtain the mechanical properties of aluminum foam at high strain rates were conducted using a split-Hopkinson Pressure Bar (SHPB) designed for soft materials. The stress-strain curves obtained were then used in numerical simulations using FEM. Cylindrical solid and cruciform geometries were used as models for the aluminum foam, while piecewise linear plasticity and Deshpande-Fleck were used as material models. Several simulations were conducted by combining these two geometrical models and two material models to obtain the most representative aluminum foam models with results closest to the experimental work. Additionally, computational time was recorded and compared to provide further considerations in determining the best model of aluminum foam.

RESULTS AND DISCUSSION

This section is divided into two parts: a comparison of experimental and numerical results at a strain rate of 2000/s, and a strain rate sensitivity study for both experimental and numerical results. The first part evaluates the numerical model's conformity to experimental data, while the second examines strain rate sensitivity in aluminum foam. Details of the simulated cases are provided in Table 1.

Table 1 Numerical simulation cases

No	Model Name	Geometrical Model	Material Model
1	Model-A	Cylindrical Solid	Deshpande-Fleck
2	Model-B	Cruciform Mid Surface	Piecewise Linier Plasticity
3	Model-C	Cruciform Solid	Piecewise Linier Plasticity
4	Model-D	Cylindrical Solid	Piecewise Linier Plasticity

Fig. 2(a) compares experimental and numerical results for Model-A, showing a 31% difference in strain values, which affects strain rates. This discrepancy is due to the specimen experiencing crumble failure during testing, which the numerical simulation without failure criteria cannot capture, leading to continued strain hardening in the model. The stress value difference is acceptable at 7.5%. Thus, the model better captures stress than strain for the aluminum foam specimen. Fig. 2(d) presents the final stress-strain results for this model.

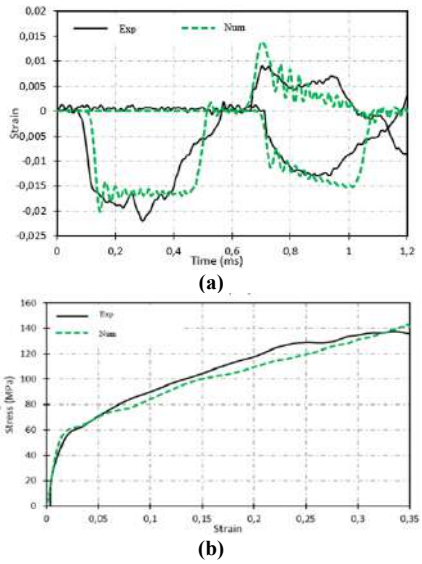

Fig. 2 Experimental and numerical comparison for Model-A, (a) strain wave, (b) stress-strain curve

Table 2 Summary of the results comparison

Model Name	Strain diff. (%)	Stress diff. (%)	Computational time
Model-A	31	**7.5**	**15 minutes**
Model-B	**8.2**	24	2.5 hours
Model-C	23	15.4	33 hours
Model-D	66	9.2	15 minutes

Table 2 summarizes the results of the four cases. Model-A shows the smallest difference in stress values among the models. It is the only model using the Deshpande-Fleck material model, specifically developed for aluminum foam, which captures its behavior more accurately. This results in the best stress value accuracy for Model-A compared to the other models using the more general Piecewise Linear Plasticity model, which is simpler but less precise for aluminum foam.

Experimental results for strain rates effect on aluminum foam is shown in Fig. 3. It can be seen that the difference in stress flow for different strain rate value is not significant. Aluminum foam is found to be insensitive to the strain rates follows general types of aluminum material. Especially for this type if aluminum foam with composition as shown in pervious section, at strain rates 3000/s the specimen experienced earlier failure at strain 0.23 compared to another lower strain rate values.

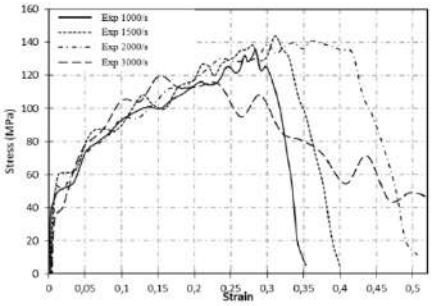

Fig. 3 Experimental results for various strain rate values

CONCLUSION

Experimental works using SHPB to determine the mechanical properties of aluminum foam at various strain rates were successfully conducted. Numerical simulations with four models were also performed. Comparisons between numerical and experimental results show that Model-A and Model-D effectively capture the aluminum foam's behavior. Strain rate sensitivity studies were conducted in both experimental and numerical simulations, revealing that aluminum foam is strain rate insensitive. Three of the four numerical models confirmed this, except for Model-D.

REFERENCES

Ashby, MF et al. 2000. Metal Foam: A Design Guide. Butterworth Heinemann. MA.

Afdhal, Gunawan L, Santosa SP, Putra IS, Huh H. 2014. Development of numerical simulations of Split Hopkinson Pressure Bar. *ARPN Journal of Engineering and Applied Sciences* 11(10): 6657-6662.

Santosa SP, Wierzbicki T. 1998. On The Modeling of Crush Behavior of A sClosed-Cell Aluminum Foam Structure. *Journal Mechanic Physic and Solids* 46, No. 4: 645-660.

Deshpande VS, Fleck NA. 1999. High Strain Rate Compressive Behaviour of Aluminum Alloy Foams. *International Journal of Impact Engineering* 24: 277-298.

ACKNOWLEDGEMENT

Thank you to Faculty of Mechanical and Aerosapce Engineering for supporting this research.

Finite Element Analysis on Residual Compression Strength After Various Low-Velocity Impact Loading of Composite Sandwich Laminate

Joseph Bernard[1], Muhamad Giri Suada[2,*],Hendri Syamsudin[2]
[1]Graduate Study, Aeronautics and Astronautics Department
[2]Solid Mechanics and Lightweight Structures Research Group
Faculty of Mechanical and Aerospace Engineering, Institut Teknologi Bandung
Jl. Ganesha 10, Bandung 40132, Indonesia
**Email: mgsuada@itb.ac.id*

ABSTRACT

It is widely known that low-velocity impact creates barely visible impact damage (BVID) in delamination, significantly reducing its compression strength. The present paper elaborates on applying finite element analysis to investigate residual compression strength after various low-velocity impact loading of composite sandwich laminate. Carbon/epoxy laminates were selected for the present study. The finite element modeling is based on Hashim-Roten for intra-laminar damage modeling of face-sheet, B-K model, and cohesive element to model inter-laminar damage model. For compression load, the core of the sandwich itself was made of foam and modeled following crushable foam, including its hardening entity. In tension loading, an ideal perfect-plastic model is used. After showing that the face-sheet is much stiffer than the core, compression strength of the composite sandwich panel is dominantly controlled by face-sheet behavior. Face-sheet laminate experiences delamination and matrix damage, leading to a significant reduction of compression strength. Also, the present study concludes a linear relationship between LVI loading and delamination size and an exponential relation between LVI loading and residual compression strength, which agrees with most of the experiment results.

Keywords: Composite Sandwich laminate, Finite Element, Low-Velocity Impact, Residual Strength after Impact

INTRODUCTION

Sandwich structures are a type of structural composite. They provide greater bending rigidity without significant weight penalty. Thus, the potential of sandwich structures is substantial, both in the aerospace and aviation industry and in other fields [1]. Some current applications of the sandwich structure in the aerospace industry include helicopter blades, optical benches in spacecraft, the skin of the control surfaces of large passenger aircraft, control surfaces (i.e., the all-moving horizontal tailplane) on fighter aircraft, and the principal structural elements on general aviation aircrafts such as the wing's spar cap and stiffened skin structure [1], [2].The present study aims to numerically investigate and predict the residual compression strength after various low-velocity impact loading on composite sandwich panels.

FINITE ELEMENT MODEL

The specimen model was meshed with a combination of several different element types. The face sheet is each made of 8 layers 0^0 unidirectional carbon/epoxy. The face sheets were meshed using 8-node quadrilateral continuum shell elements with reduced integration (SC8R). The foam core was meshed using 8-node linear brick (solid) elements with reduced integration (C3D8R). The interlaminar cohesive element was meshed using 8-node three-dimensional elements (COH3D8). ASTM D7167/D7136M was adopted to perform Low-Velocity Impact loading, adopting the standard of ASTM D8287/D8287M

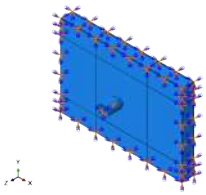

Figure 1 Low-velocity impact model boundary conditions.

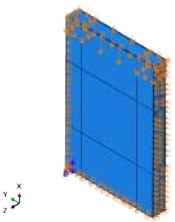

Figure 2. *Compression-after-impact model boundary conditions on specimen*

Impact loading is varied from 2 J to 22 J, and face sheets made from carbon-fiber/epoxy prepreg of TR 50S12L and ROHACELL® 71 IG-F foam core, which is closed-cell rigid foam plastic based on PMI (polymethacrylimide). The damage model adopted for intra-laminar is Hashin-Rotem, for inter-laminar is quadratic stress criterion for initiating damage and B-K model for delamination growth.

FINITE ELEMENT MODEL VALIDATION

The proposed model is validated by experimental results carried out by Mohmed [18]. The result is as follows:
Table 1. LVI Model Validation Results

Variable	*FEM*	*Experimental Result [18]*	*Error*
Peak Force [N]	*1797.40*	*1800.00*	*-0.14%*
Maximum Displacement [mm]	*14.61*	*14.30*	*2.17%*
Energy Absorbed [J]	*14.08*	*16.51*	*-9.72%*

The error for the energy absorbed between the LVI simulation and the experimental result is rather large, close to 10%. As Mohmmed [18] having the same experiences.

RESULTS AND DISCUSSION

The relation between impact energy and delamination area is depicted in the following figure.

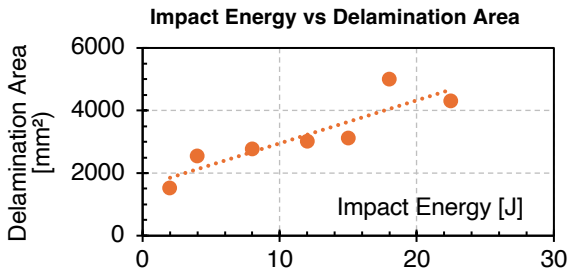

Figure 3 *Impact Energy vs Delamination Area*

Delamination occurred at every impact energy level. The delamination shape is relatively elliptical or circular and centered around the impact area. Only the top face sheet experienced delamination, while the bottom face sheet experienced negligible delamination at higher energy levels (15 J, 18 J). The relationship between the impact energy and the (projected) delamination area is plotted in Figure 3. The stress-strain profiles at compression loading are as follows:

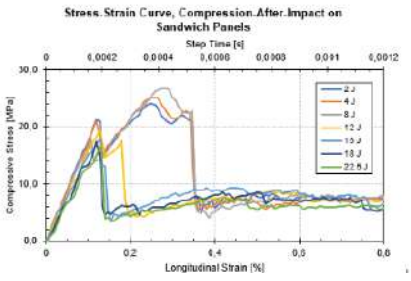

Figure 4. Stress-strain curve of the impacted sandwich composite panel with various impact energies.

From the stress-strain curves of the sandwich panels impacted with energies of 2 J up to 12 J, the stress-strain behavior shows a sudden drop of stiffness to slightly less than the original stiffness. This phenomenon happened after a relatively linear-elastic behavior. Then, the stress-strain response is again linear-elastic with a slope less than previous. In the 2 J, 4 J, and 8 J cases, this response continued until a certain point, in which the stiffness was slightly reduced before the final failure, in which the panel lost all stiffness. In the 12 J case, the panel lost all stiffness when this linear-elastic response reached a point.

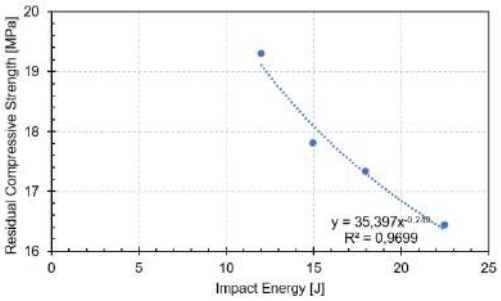

Figure 5 Residual compression strength vs impact energy

CONCLUSION

The reduction of the compressive strength of composite sandwich panels subjected to low-velocity impact is very significant, with a reduction of about 58% up to 75%, as shown in this research. The residual compressive strength of the composite sandwich panels subjected to various low-velocity impact energy levels is shown in Figure 5. After undergoing low-velocity impact, the composite sandwich panels have shown signs of damage in their fibers, matrix, and adhesives. Low-velocity impact causes delamination and especially significant matrix failure in the top face sheet of the composite sandwich panel. From the compression-after-impact test, it was found that matrix damage together with delamination are still the dominant failure mode during compression testing.

REFERENCES

[1] Tolerance for Composite Sandwich Airframe Structures', Washington, D.C., Aug. 1999. [Online]. Available: https://www.tc.faa.gov/its/worldpac/techrpt/ar99-49.pdf

[2] M. C. Y. Niu, Composite Airframe Structures: Practical Design Information and Data. Hong Kong: Conmilit Press, Ltd., 1992.

[3] B. Vijaya Ramnath, K. Alagarraja, and C. Elanchezhian, 'Review on Sandwich Composite and their Applications,' in Materials Today: Proceedings, 2019, pp. 859–864. doi: 10.1016/j.matpr.2019.05.169.

[4] W. D. Callister and D. G. Rethwisch, Materials Science and Engineering: An Introduction, 9th ed. Hoboken, New Jersey: John Wiley & Sons, Inc., 2014.

[5] R. Bai, J. Guo, Z. Lei, D. Liu, Y. Ma, and C. Yan, 'Compression after impact behavior of composite foam-core sandwich panels,' Compos Struct, vol. 225, Oct. 2019, doi: 10.1016/j.compstruct.2019.111181.

[6] S. N. A. Safri, M. T. H. Sultan, N. Yidris, and F. Mustapha, 'Low Velocity and High Velocity Impact Test on Composite Materials - A review', The International Journal Of Engineering And Science (IJES), vol. 3, no. 9, pp. 50–60, 2014.

[7] M. O. W. Richardson and M. J. Wisheart, 'Review of low-velocity impact properties of composite materials', Compos Part A Appl Sci Manuf, vol. 27, no. 12, pp. 1123–1131, 1996, doi: 10.1016/1359-835X(96)00074-7.

Bone Implant Design with Lattice Structures for Additive Manufacturing

Nurul Hannani Abdul Hadi, Abdul Hadi Azman

Department of Mechanical and Manufacturing Engineering,
Faculty of Engineering and Built Environment, Universiti Kebangsaan Malaysia

Tel: +60389118405 Email: hadi.azman@ukm.edu.my

ABSTRACT

Additive manufacturing (AM) enables the production of parts with complex geometries with topology optimization. Topology optimization (TO) is an effective approach for creating lightweight and unique configuration of additively manufactured products that are difficult to obtain via conventional method. By integrating TO with additive layer manufacturing and, employing architectured material such as lattice structure, it is feasible to produce intricate three-dimensional geometries befitting the biomedical industry. However, there are presently some major setbacks in the use of implants due to wear and progressive loss of osseointegration of implants. Hence, this study is aimed to optimize the hip implant design through integration of lattice structure and TO for AM. In this paper, a 3D model of a hip implant with different design space, integrating with lattice structure, topology optimization and lattice optimization are examined through Finite Element Analysis (FEA). The results indicates that the pore size for osseointegration was successfully attained with a target length of lattice structure 3 mm and a minimum and maximum diameter of 0.3 to 0.6 mm. In conclusion, by combining topology optimization and lattice structure, also known as lattice optimization method can significantly reduce the weight of a bone implant for fabrication with additive manufacturing.

Keywords: Additive Manufacturing, Lattice Structures, Topology Optimisation

INTRODUCTION

Additive manufacturing (AM), commonly known as 3D printing, is a technique that creates 3D objects by printing materials layer-by-layer. AM allows the production of not only prototypes but also fully functional components for the automobile, aerospace, and medical industries. Given the layer-by-layer manufacturing method, complex-shaped components can be created without any additional tooling or joins. In fact, selective laser melting (SLM), one of the most fundamental AM techniques in the medical industry, is capable of achieving the fine details needed across the porous geometry for optimal connection between the implant and the bone, supporting long-term implant stability (Popovich et al. 2016).

Rapid prototyping addresses the problem of rising implant demand, which is frequently caused by prosthetic failure or wear, as well as an ageing population. This, in turn, has a positive impact on the worldwide demand for hip implants. Several studies have revealed a sharp increase in the number of younger individuals undergoing hip surgery. Thus, there is an urgent requirement to extend the lifespan of implants to at least 30 years. However, despite the rising demand for hip replacement surgeries, 10 to 20% of patients may require revision surgery due to prosthesis failure, which is mainly caused by stress shielding. Many difficult issues may inevitably arise during revision surgery, with osseous defects being the most intractable situation (Chen et al. 2020). The operation might be more difficult, especially for senior patients, and bone resorption can raise the risk of fractures.

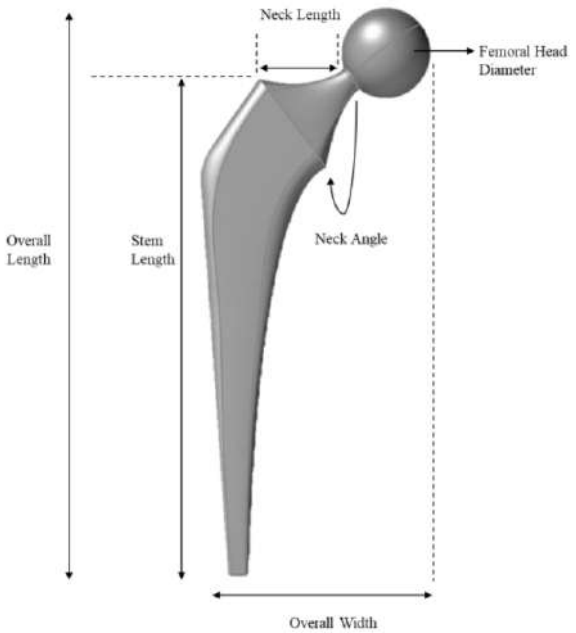

Fig. 1 Bone implant dimensions

Thus, several studies have attempted to solve the stress shielding issue. Ridzwan and Shuib proposed a topology-optimized hip implant stem to reduce stress shielding (He et al. 2018) by minimising compliance with different stem volume fraction constraints and chose the topologies that were feasible to interpret and manufacture. Compared to a non-optimized implant, a 17% reduction in stress shielding was achieved. However, their optimization setup produced the stiffest design within the specified amount of material, which was not ideal for reducing stiffness.

RESULTS AND DISCUSSION

Under static in vivo conditions, finite element analysis (FEA) was used to model each hip implant design using different design spaces. This FEA was conducted for each implant to examine the impact of the loading pattern on mechanical parameters such as strain, yield point, safety factor estimation, von Mises stress, and deformation.

Four biocompatible titanium alloys were analyzed using finite element analysis. Of these, three implants demonstrated excellent biocompatibility, corrosion resistance, and high fracture toughness, being linear isotropic and homogeneous in nature. The implants analyzed included a solid structure implant, an integrated lattice structure implant, and a combination of lattice and topology-optimized implants.

The results showed that the maximum stresses for all four implants occurred at the femoral head, decreasing towards the middle of the implant and reaching a minimum at the support part of the implant. This stress distribution is due to the maximum load applied to the femoral head's surface at the y-direction angle. The simulation results indicated that the maximum von Mises stress was 989.7 MPa, while the minimum was 329.3 MPa for RB3 and RB4, respectively.

The analysis demonstrated that factors such as von Mises stress, maximum deformation, and the safety factor of a model are influenced by volume space and surface area

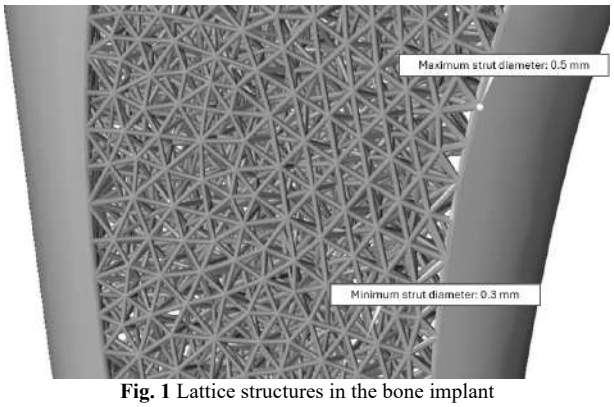

Fig. 1 Lattice structures in the bone implant

CONCLUSION

In conclusion, the study demonstrates that by optimizing the topology and lattice structure, the tensile strength of the hip implant can be increased while reducing its mass.

REFERENCES

Chen, Z., Yan, X., Yin, S., Liu, L., Liu, X., Zhao, G., Ma, W., et al. 2020. Influence of the pore size and porosity of selective laser melted Ti6Al4V ELI porous scaffold on cell proliferation, osteogenesis and bone ingrowth. *Materials Science and Engineering C* 106(February 2019): 110289. doi:10.1016/j.msec.2019.110289

He, Y., Burkhalter, D., Durocher, D. & Gilbert, J. M. 2018. Solid-Lattice Hip Prosthesis Design: Applying Topology and Lattice Optimization to Reduce Stress Shielding From Hip Implants 6–10. doi:10.1115/dmd2018-6804

Popovich, A., Sufiiarov, V., Polozov, I., Borisov, E. & Masaylo, D. 2016. Additive manufacturing of individual implants from titanium alloy. METAL 2016 - 25th Anniversary International Conference on Metallurgy and Materials, Conference Proceedings (February 2017): 1504–1508.

ACKNOWLEDGEMENT

The authors would like to express their gratitude and thanks to the Ministry of Higher Education for the support of this research project under the research grant FRGS/1/2023/TK10/UKM/02/4

Acknowledgment

The success of the 3rd Virtual Conference on Computational and Experimental Mechanics would not have been possible without the dedicated efforts and contributions of many individuals. The organising committee would like to acknowledge the contributions of the following personnel and organisations:

Prof. Dr. T. Prakash G. Thamburaja
Prof. Ir. Dr. Ahmad Kamal Ariffin
Prof. Ir. Dr. Shahrum Abdullah
Prof. Dr. Ir. Tatacipta Dirgantara
Assoc. Prof. Dr. Shahrizan Baharom
Dr. Salvinder Singh Karam Singh
Dr. Muhamad Alias Bin Md. Jedi
Dr. Abdul Hadi Bin Azman
Dr. Azli bin Arifin
Dr.-Ing. Chin Chuin Hao
Dr. Lam Meng Chun
Dr Afdhal

We also extend our gratitude to the authors for their valuable contributions, and to the reviewers for their diligent work in evaluating the submissions. Their scholarly efforts have ensured the high quality of the papers included in these proceedings.

Our sincere thanks go to the keynote speakers, session chairs, and all participants for their active engagement and insightful discussions, which have greatly enriched the conference experience.

Finally, we thank all the attendees for their participation and interest in the 3rd Virtual Conference on Computational and Experimental Mechanics. We hope that the knowledge shared and connections made during this conference will inspire future research and collaborations in the fields of computational and experimental mechanics.

3rd VIRTUAL CONFERENCE ON COMPUTATIONAL AND EXPERIMENTAL MECHANICS (VCCEM 2024)

UNIVERSITI KEBANGSAAN MALAYSIA
The National University of Malaysia

INSTITUT TEKNOLOGI BANDUNG 1920

NARATIF BAHARU UKM
UNIVERSITI WATAN KITA

FKAB
FAKULTI KEJURUTERAAN DAN ALAM BINA
Faculty of Engineering & Built Environment

e ISBN 978-629-96532-6-4

PENERBIT FAKULTI KEJURUTERAAN & ALAM BINA